UNIVERSIDAD POLITÉCNICA DE MADRID
Escuela Técnica Superior de Ingenieros en Topografía, Geodesia y Cartografía

Applications of multitemporal interferometry SAR (MT-InSAR) in the management of natural and induced geological risks

DOCTORAL THESIS

Submitted for the degree of Doctor by:

Carlos García Lanchares
M. Sc. Estrategias y Tecnologías para el Desarrollo

Madrid, 2024

UNIVERSIDAD POLITÉCNICA DE MADRID
Escuela Técnica Superior de Ingenieros en
Topografía, Geodesia y Cartografía

Doctoral Degree in Geomatic Engineering

Applications of multitemporal interferometry SAR (MT-InSAR) in the management of natural and induced geological risks

DOCTORAL THESIS

Submitted for the degree of Doctor by:

Carlos García Lanchares
M.Sc. Estrategias y tecnologías para el Desarrollo

Under the supervision of:
Dr. Miguel Marchamalo Sacristán
Dr. Luis Cueto-Felgueroso Landeira

Madrid, 2024

Title: Applications of multitemporal interferometry SAR (MT-InSAR) in the management of natural and induced geological risks

Author: Carlos García Lanchares

Doctoral Programme: Doctoral Degree in Geomatic Engineering

Thesis Supervision:

Dr. Miguel Marchamalo Sacristán

Dr. Luis Cueto-Felgueroso Landeira

External Reviewers:

Dr. Alfredo Fernández-Landa

Dra. Vrinda Krishnakumar

Thesis Defense Committee:

Thesis Defense Date:

Tribunal nombrado por el Magfco. y Excmo. Sr. rector de la Universidad Politécnica de Madrid, el día ……de……de……de…….

Presidente/a D/Dª …….

Vocal D/Dª ……..

Vocal D/Dª ……..

Vocal D/Dª …….

Secretario/a D/Dª ……..

Suplente D/Dª ……

Suplente D/Dª ……

Realizado el acto de defensa y lectura de la Tesis el día …….. de ……. de ……. en la Escuela Técnica Superior de Ingenieros en Topografía, Geodesia y Cartografía de la Universidad Politécnica de Madrid.

Calificación……

PRESIDENTE/A VOCALES

SECRETARIO/A

This thesis has received public funds from Comunidad de Madrid, Industrial doctorates program (IND2020/TIC-17528), the KUK-AHPAN Project, Grant RTI2018-094827- 417B-C21/C22 funded by MCIN/AEI/10.13039/501100011033 and by "ERDF A way of making Europe" and Detektia.

The map that leads to you…

Acknowledgement

Este trabajo ha sido todo un viaje que he podido disfrutar con muchos compañeros y compañeras, que han hecho de ello toda una experiencia. Me gustaría referirme a algunos de ellos. Adelanto que no voy a poder hacer justicia a todos ellos.

Primeramente, mis padres y mi hermano, que han estado allí en todo momento para bien o para mal; volver a casa siempre sienta bien si están ellos.

A mis amigos de toda la vida, que, aunque nos encontremos en momentos vitales muy diversos, siempre escuchan, dan su opinión y enriquecen cada opinión y guían cada decisión.

A mis compañeros del Club Natación Alcobendas, con los que podía escaparme todos los días para disfrutar de entrenamientos, competiciones, cocidos y otros momentos.

A todos los compañeros del equipo Kuk Ahpán, especialmente a Belén, Maribel y Orlando, que me han abierto las puertas de una nueva y genial disciplina y hemos podido aunar maneras de trabajar consiguiendo muy buenos resultados.

A todos los compañeros de Detektia, que me han dado la oportunidad de trabajar con ellos y que espero que tengan una larga trayectoria industrial.

Al equipo del Laboratorio de Topografía de la escuela de Caminos, espero poder seguir trabajando en muchas más ocasiones con vosotros.

A todas las instituciones que se han visto implicadas por el camino, Tragsatec, IGME, IGN, Empagua, Universidad de Costa Rica, Universidad de Leeds y equipo de Comet.

A Jose Luis Armayor, Luis Cueto, Vrinda, Amanda Vázquez, Pedro Ruano, Raquel Morales, Juan José Durán y otros muchos.

Y sobre todo a mi tutor Miguel Marchamalo, que el primer día me dijo que tenía que dejar de ser adicto al control, porque los dos no podíamos serlo, la tesis no hubiera podido salir adelante sin él.

Abstract

The thesis presents a detailed analysis of the use of Multi-temporal Synthetic Aperture Radar Interferometry (MT-InSAR) technology in the management of geological risks in various urban areas of Central America, focusing on three specific cases: Guatemala City, La Palma, and San José. Each of these areas faces unique challenges due to their geology and human activity, making MT-InSAR an indispensable tool for risk assessment and mitigation.

In Guatemala City, the study focuses on ground subsidence caused by excessive groundwater extraction. This densely populated and constantly expanding region faces a significant geological risk due to the overexploitation of aquifers, resulting in sinkholes and potential ground collapses. MT-InSAR allows for precise monitoring of these deformations, providing crucial data for urban planning and the implementation of sustainable water management policies.

In La Palma, the focus is directed towards recent volcanic activity, particularly along the Cumbre Vieja, has been critically examined. The 2021 eruption, linked to previous volcanic events, highlights the ongoing geological dynamism of La Palma. MT-InSAR technology is used to detect and analyze past and present deformations, facilitating the implementation of prevention measures and early warning systems.

Finally, in San José, the research addresses both ground subsidence and seismic activity. Given the location of San José in a high tectonic activity zone, the risks of earthquakes and the consequent ground deformation are of particular concern. The use of MT-InSAR helps to identify potential risk areas and to monitor the structural integrity of the urban environment, improving the disaster response capability.

These three case studies demonstrate the versatility and effectiveness of MT-InSAR technology in identifying and managing different types of geological risks. By integrating this technology into risk management policies, authorities can significantly improve the resilience and safety of vulnerable urban areas in Central America.

Resumen

La tesis presenta un análisis detallado del uso de la tecnología de Interferometría de Radar de Apertura Sintética Multitemporal (MT-InSAR) en la gestión de riesgos geológicos en varias áreas urbanas de Centroamérica, enfocándose en tres casos específicos: Ciudad de Guatemala, La Palma y San José. Cada una de estas áreas enfrenta desafíos únicos debido a su geología y actividad humana, haciendo de MT-InSAR una herramienta indispensable para la evaluación y mitigación de riesgos.

En Ciudad de Guatemala, el estudio se centra en la subsidencia del suelo causada por la extracción excesiva de agua subterránea. Esta región densamente poblada y en constante expansión enfrenta un riesgo geológico significativo debido a la sobreexplotación de los acuíferos, lo que resulta en la formación de sumideros y posibles colapsos del suelo. MT-InSAR permite un monitoreo preciso de estas deformaciones, proporcionando datos cruciales para la planificación urbana y la implementación de políticas sostenibles de gestión del agua.

En La Palma, el enfoque está dirigido hacia la reciente actividad volcánica, particularmente a lo largo de Cumbre Vieja, que ha sido críticamente examinada. La erupción de 2021, vinculada a eventos volcánicos anteriores, resalta el dinamismo geológico continuo de La Palma. La tecnología MT-InSAR se utiliza para detectar y analizar deformaciones pasadas y presentes, facilitando la implementación de medidas de prevención y sistemas de alerta temprana.

Finalmente, en San José, la investigación aborda tanto la subsidencia del suelo como la actividad sísmica. Dada la ubicación de San José en una zona de alta actividad tectónica, los riesgos de terremotos y la consecuente deformación del suelo son de particular preocupación. El uso de MT-InSAR ayuda a identificar áreas de riesgo potencial y a monitorear la integridad estructural del entorno urbano, mejorando la capacidad de respuesta ante desastres.

Estos tres estudios de caso demuestran la versatilidad y efectividad de la tecnología MT-InSAR en la identificación y gestión de diferentes tipos de riesgos geológicos. Al integrar esta tecnología en las políticas de gestión de riesgos, las autoridades pueden mejorar significativamente la resiliencia y seguridad de las áreas urbanas vulnerables en Centroamérica.

Table of Contents

List of Figures

List of Tables

Abbreviations and Acronyms

UPM	Universidad Politécnica de Madrid
MT-InSAR	Multi Temporal Interferometry Synthetic Aperture Radar
SAR	Synthetic Aperture Radar
SNAP	SeNtinel Application Platform
PSI	Persistent Scatterer Interferometry
SBAS	Small Baseline Subset
ESA	European Space Agency
IGME	Instituto Geológico y Minero de España
RMG	Región Metropolitana de Guatemala
JAXA	Japan Aerospace Exploration Agency
NASA	National Aeronautics Space Administration
AECID	Agencia Española de Cooperación Internacional para el Desarrollo

1. Introduction and framework

1.1. Introduction and Objective

This doctoral thesis aims to advance the understanding and monitoring of deformation processes in areas with high geological risk, as in most of Central America and volcanic islands such as La Palma, across various scales. This collaborative work is supported by three case studies which involves the collaboration of several actors (academic and managers) and the use innovative tools. Throughout this project, the scope of analysis has taken into consieration the natural and induced geological processes that can help to explain observed deformation patterns, including volcanic, tectonic and aquifer management activities at different scales.

This thesis materializes the collaboration between the technological startup Detektia and the Universidad Politécnica de Madrid in the form of Industrial Doctorate to advance geological risk mitigation technologies in vulnerable areas through Multi-Temporal Synthetic Aperture Radar (MT-InSAR). This initiative, integral to the KUK-APHÁN project targeting seismic risk reduction in Central America (2019-2023), involves partnerships with governments and academic entities across El Salvador, Guatemala, Honduras, and Costa Rica. It aims to globally market the developed technologies to public administrations, construction companies, and risk reduction consultants in Central America and the Caribbean. This strategic dissemination seeks to enhance public safety and infrastructure resilience, showcasing significant European advancements in sustainable urban development and infrastructure maintenance. Detektia has emerged in response to an international demand, given that its technology, which only requires spatial information with no need for ground instrumentation, can be utilized globally.

The current lack of competition underscores the importance of rapidly scaling the product to become a market leader in the coming years. This proposal is crucial for Detektia's internationalization, occurring within an international R&D project that will introduce EYERADAR, the platform used to communicate the products to the managers or other potential clients, marking a significant step in broadening its global footprint and market presence.

The Laboratory of Topography and Geomatics at the Civil Engineer School of Madrid is dedicated to teaching, research, and technology transfer in the fields of Cartographic Engineering, Geodesy, Photogrammetry, and Terrain Engineering. Located within the School of Roads, it boasts computer classrooms, topographic equipment, and skilled personnel. The Laboratory aims to bridge the gap between

research in Topography, Geomatics, and applied civil engineering, driving R&D and technology transfer in monitoring, GIS, and Remote Sensing in collaboration with engineering firms. This effort enriches its teaching approach, integrating computing and preparing future engineers for professional practice.

This proposal promotes the research and technology transfer activities of the UPM's Laboratory of Topography and Geomatics, focusing on internationalizing its operations. It emphasizes the direct positive impact on sustainability, contributing to achieving environmental, social, and economic Sustainable Development Goals, which are particularly pertinent currently.

The direct positive impact on sustainability associated with this proposal should be highlighted, aiding in the achievement of the Sustainable Development Goals that are of environmental, social, and economic importance today.

Implementing preventative and effective control of infrastructure can significantly reduce greenhouse gas emissions by avoiding collapses and irreversible damage, thereby reducing the need for new construction and subsequently lowering GHG emissions. Furthermore, the selection of the company by the European accelerator Parsec, the only accelerator in the EU using Earth Observation data to innovate in critical sectors like energy and food during the COVID-19 pandemic, highlights the environmental importance of this approach.

From a social perspective, technology significantly impacts societal safety and resilience. The development of technological surveillance solutions can minimize the risk of disasters caused by natural or technological hazards. By analyzing changes at a millimetric level, we aim to reduce infrastructure vulnerability, a critical factor in preventing collapses. This approach not only enhances public safety but also strengthens the overall resilience of communities against potential disasters. Economically, infrastructure monitoring using satellite radar technology leads to significant savings. It reduces personnel expenses associated with on-site measurements as well as the costs associated with preventive maintenance. Additionally, it is vital to recognize the economic benefits of avoiding potential collapses or irreversible failures in infrastructure, which can mean substantial financial savings for governments and organizations, thereby contributing to more efficient and economically sustainable infrastructure management practices.

The MT-InSAR technique dates back several decades, but it is only today, thanks to the efforts of the international community (governments, space agencies, universities, etc.), which have promoted the launch of numerous satellites equipped

with radar sensors, and the development of computer equipment and algorithms, that the processing of such a vast amount of information has been made possible.

The need to establish quality metrics for MT-InSAR products has emerged as a central theme, given their importance in assessing the reliability and usefulness of these products. The proposed metrics include coherence, phase variance, precision, accuracy, and uncertainty, among others, all of which are essential to ensure the quality of the information provided by MT-InSAR.

As regards the challenge in defining the quality, the discussion on MT-InSAR products highlights the fact that quality is determined more by the decisions of the MT-InSAR engineer than by the data itself. This underscores the importance of applying appropriate thresholds to reveal or hide information depending on the intended application, leading to a more application-oriented understanding of MT-InSAR data quality.

Hanssen (2023) proposes a classification system to support this characterization or intention of MT-InSAR products. This system categorizes products from Opportunistic (O-products) to Advanced Application-Aligned (AAA-products), based on the specificity of their application and the quality of control and assurance.

- **Opportunistic Products (O-products):** These are defined as those calculated without a specific objective, problem, or application in mind. These products are not validated by certified experts and, therefore, may lack the precision needed for specific applications.
- **Accepted Products (A-products):** These are not defined a priori for a specific application but are accepted by certified experts. Although they can be useful, they are not necessarily optimized for particular problems.
- **Application-Agnostic Products (AA-products):** These are approved by certified experts and may include minimal contextual information. While they are of higher quality than A-products, they are still not aligned with specific problems.
- **Advanced Application-Aligned Products (AAA-products):** Represent the highest category, designed after defining a specific problem by an identified end-user. They utilize contextual data and are intended to solve concrete problems, making them optimal for very specific applications. The quality of these products is ultimately defined by the end-user's satisfaction, and their effectiveness can be precisely evaluated and validated.

This classification emphasizes the importance of aligning MT-InSAR products with the specific needs of end-users, ensuring that the data is not only technically proficient but also relevant to the real-world problems being addressed.

In the context of the high quality and choice of MT-InSAR products currently available; the Copernicus Ground Motion Service, despite its relevance and applicability across a wide range of geological and infrastructure monitoring contexts, would be classified as an AA (Application-Agnostic) product according to the taxonomy proposed by Ramon Hanssen (2023). This is because, although it provides high-quality data on ground movement at continental level, it is not designed or tailored for specific deformation problems, nor has it been reviewed by experts in particular fields such as landslides in order to be considered an AAA product (Hanssen ,2023)

The research delves into the use of MT-InSAR technology for the study of geological risks. The goal is to thoroughly explore how geological alterations can be located and characterized at different scales, with the aim of developing more effective methods for risk prevention and mitigation in the Central American region and La Palma. Additionally, it seeks to promote the use of these technological tools at an international level, establishing a new standard in geological risk management.

The initial objectives set out in the research, along with an explanation of how and why they have been adapted to better meet the needs of the project are detailed below:

1. **Validate the Use of MT-InSAR Technology for the Prevention of Geological Risks in Central America's Urban areas:** The objective of creating risk scenarios is aimed at minimizing future damages caused by adverse events. To accomplish this, it is essential to focus on several key areas: increasing public awareness about risks, enhancing building codes to lower vulnerability, improving emergency response strategies, and calculating potential losses for the insurance industry.
2. **Contrast the MT-InSAR deformation results in different case studies with information from other disciplines used to analyze geological risks**: Integrate and compare the data obtained through MT-InSAR with information from other disciplines such as geology, geotechnics, and hydrogeology to validate and enrich the results.

3. **Determine the scope or correlation between contemporary piezometric data and MT-InSAR results for the case study of Guatemala City:** Analyze and correlate the available piezometric data with the deformation results detected by MT-InSAR to better understand the causes and patterns of ground deformation.
4. **Establish how MT-InSAR provides a basis for integration into an infrastructure monitoring system**: Evaluate and propose the integration of MT-InSAR data and methodologies into urban and interurban infrastructure monitoring systems, providing a solid foundation for the management and prevention of geological risks.

1.2. Thesis structure and roadmap

This document, organized into 8 chapters (Figure 1.1), embarks on a comprehensive exploration of ground deformation phenomena through the lens of advanced satellite technology, setting the stage for an in-depth investigation across various geographical locales.

- Chapters 1, 2, and 3 introduce and contextualize the work, outline the objectives, synthesize the state of the art, and describe the study areas where all analyses and discussions have been developed; it also provides a an overall perspective about MT-InSAR, the basics and different algorithms of processing that exist as Persistent Scatterers Interferometry (PSI) or small baseline subset interferometric synthetic aperture radar (SBAS).

- Chapter 4 presents an in-depth analysis of land deformation within the Metropolitan Area of Guatemala City, utilizing Persistent Scatterer Interferometry (PSI) techniques. A significant amount of SAR images from Sentinel-1 satellites were processed to characterize deformation patterns over urbanized surfaces. A key finding was the identification of areas experiencing significant subsidence. This chapter highlights the utility of MT-InSAR technology in urban planning and risk management, offering a foundational approach for mitigating potential risks associated with land subsidence.

- Chapter 5 focuses on correlating MT-InSAR data with hydrogeological observations to understand the impact of groundwater management on land subsidence in Guatemala City. By integrating MT-InSAR analysis with piezometric data, the research reveals patterns of subsidence closely related to groundwater extraction activities. The findings emphasize the critical need for sustainable

groundwater management practices aimed at avoiding the exacerbation of subsidence rates and advocates the incorporation of MT-InSAR data into hydrogeological studies to improve the understanding and management of subsidence phenomena.

- Chapter 6 explores the application of MT-InSAR technology to study seismic and volcanic risks in Central America, with a focus on San José de Costa Rica and La Palma in the Canary Islands. It presents detailed case studies where MT-InSAR data has been utilized to monitor and analyze deformation patterns related to seismic activities and volcanic eruptions. This chapter underlines the effectiveness of MT-InSAR in detecting and characterizing ground deformations, providing valuable insights for disaster preparedness and risk reduction strategies. It stresses the role of MT-InSAR in enhancing the understanding of seismic and volcanic processes, aiding in better hazard assessment and mitigation efforts in vulnerable areas.

- Chapter 7 brings together the ideas from the previous chapters and relates them to the degree of achievement of the proposed objectives, ultimately leading to the conclusions in chapter 8.

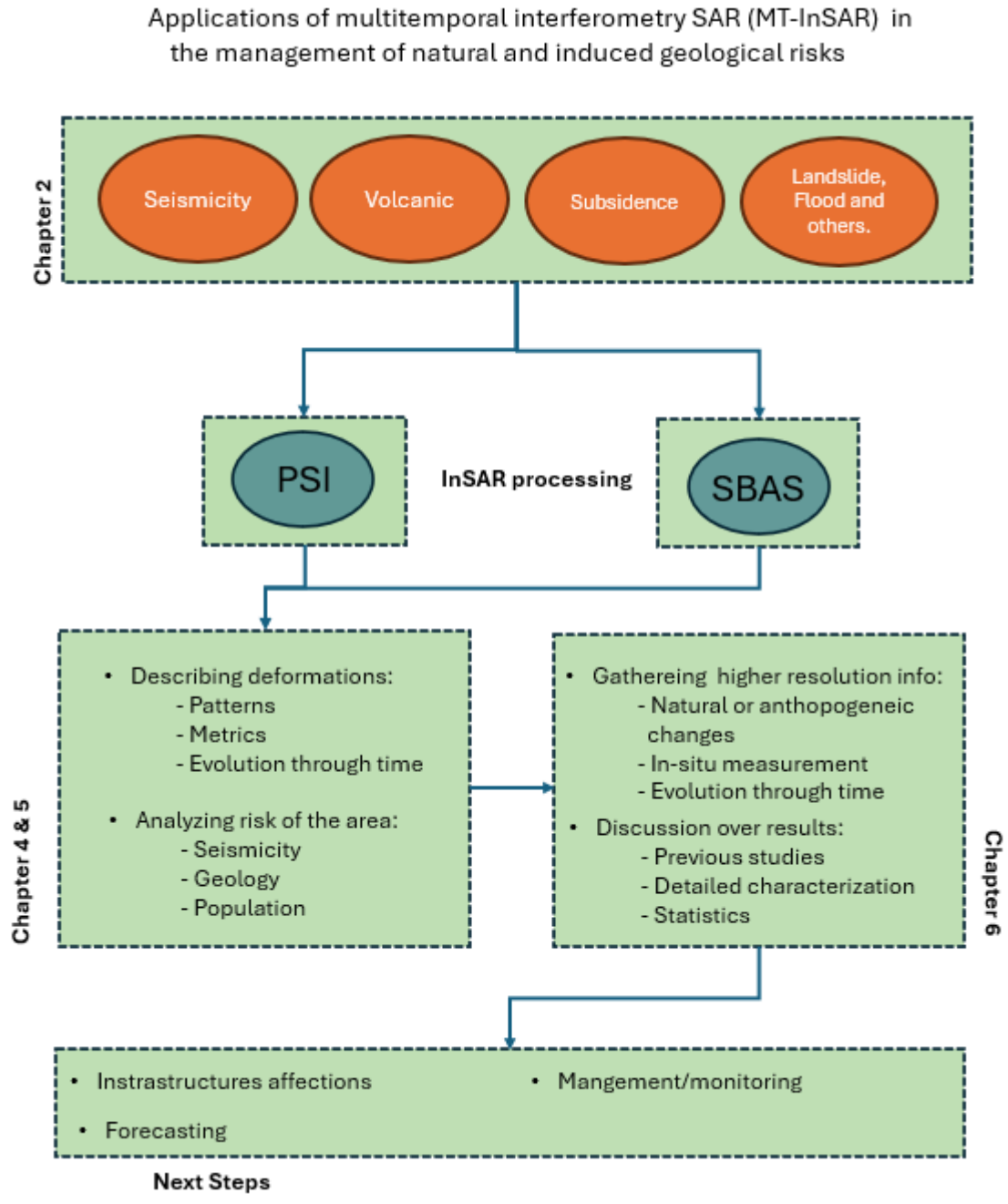

Figure 1.1: General scheme giving an overview of the thesis

1.3. Thesis outcomes

During the three-year course of this doctoral thesis, several pieces of research have been conducted and published, contributing significantly to the field of study. These publications, encompassing a diverse range of topics within the scope of the thesis, highlight the ongoing efforts and scholarly contributions made throughout the research period:

- García-Lanchares, C.; Marchamalo, M.; Sancho, C. (2021). Descripción del proyecto de tesis doctoral: aplicación de la tecnología MT-InSAR a la prevención de los riesgos geológicos naturales e inducidos en ciudades e infraestructuras prioritarias de Centroamérica. En Proceedings 3rd Congress in Geomatics Engineering. Editorial Universitat Politècnica de València. 170-176
- Benito, M. B., Alvarado, G. E., Marchamalo, M., Rejas, J. G., Murphy, P., Franco, R.; Sanchez, J. (2023). Temporal and spatial evolution of the 2021 eruption in the Tajogaite volcano (Cumbre Vieja rift zone, La Palma, Canary Islands)
- García-Lanchares, C., Marchamalo-Sacristán, M., Fernández-Landa, A., Sancho, C., Krishnakumar, V., & Benito, B. (2023). Analysis of Deformation Dynamics in Guatemala City Metropolitan Area Using Persistent Scatterer Interferometry. Remote Sensing, 15(17), 4207.
- García-Lanchares, C., Marchamalo-Sacristán, M., Fernández-Landa, A., (2024). Use of MT-InSAR in the analysis of the influence of groundwater management on land subsidence in the Metropolitan Area of Guatemala City (Under development)
- Benito M.B., Arroyo-Solorzano, M., Climent, A., Montero, W., Alvarado, G., Lopez, A., García-Lanchares, C., Marchamalo,M., Ornelas, A., Hernández, Rubio O., Quirós, L.E.; 2023; Seismic Hazard Scenarios for the City of San Jose, Costa Rica: Evaluation of Critical Ruptures on Nearby Faults

Furthermore, the following publications were presented in different conferences:

- Ornelas Agrela, A. F., Benito Oterino, B., Blanco, R. F., García Lanchares, C., Marchamalo Sacristan, M., Alvarado, G., Schmidt, V. (2022,May). Deterministic scenarios for seismic hazard assessment in the metropolitan

area of San Jose, Costa Rica. First results of the Kuk-Ahpán Project. In EGU General Assembly Conference Abstracts (pp. EGU22-604).

- García-Lanchares C., Marchamalo M., Benito M.B., Sancho C., Fernández-Landa A., Ornelas A., Franco R., Hernández O, Montero W., Arroyo M. 2022. An analysis of the contribution of MT-InSAR interferometry for seismic hazard management. A study case: San José (Costa Rica) Living Planet 2022 Symposium, Bonn, Germany, 23-2 May, 2022
- García-Lanchares C., Marchamalo M., Benito M.B., Sancho C., Fernández-Landa A., Ornelas A., Franco R., Hernández O., Gamboa C. 2022. Análisis de la dinámica de deformación en área urbana en el área metropolitana de Ciudad de Guatemala con metodología MT-InSAR y datos Sentinel-1. Memorial del XIV Congreso Geológico de América Central y VII Congreso Geológico Nacional. Colegio de Geólogos de Costa Rica. ISBN 978-9930-9769-0-6. San José, Costa Rica
- García-Lanchares C., Marchamalo M., Benito M.B., Sancho C., Fernández-Landa A., Ornelas A., Hernández O., Montero W., Arroyo M. 2022. Aplicaciones de la interferometría SAR en los estudios de riesgo sísmico y volcánico. 10ª Asamblea Hispano Portuguesa de Geodesia y Geofísica - Toledo, noviembre de 2022
- García-Lanchares, C., Marchamalo-Sacristán, M., Fernández-Landa, A., Sancho, C., Krishnakumar, V., & Benito, B. (2023). MT-InSAR for Land Deformation Analysis in Guatemala City; Fringe 2023; Leeds (England)

1.4. Theoretical background

1.4.1. Risk assessment and Remote sensing

The analysis of generic risk is crucial for assessing and understanding the vulnerability of a region or community to various hazards (Figure 1.2), thereby facilitating the implementation of effective mitigation and preparedness measures. This analysis is essential for informing strategic decisions in areas such as urban planning, the design of resilient infrastructures, and the development of response and recovery strategies for potential adverse events.

To conduct an effective risk analysis the United Nations International Strategy for Disaster Reduction (UNISDR, 2009) among other authors (UNISDR, 2015; Ward

et al., 2019) consider it essential to construct a risk framework around the following criteria :

- **Risk:** Losses that a society or community can suffer depending on the product of the hazard and the vulnerability associated with its conditions (social, economic, political, cultural, technical and environmental)
- **Hazard:** Refers to the probability of an adverse event occurring,this being an essential component in risk evaluation. Hazard can vary depending on the type of risk considered (natural, technological, health, etc.) and is based on the likelihood of such an event occurring in a specific region.
- **Cost:** Related to the economic losses associated with an adverse event. This includes damage to properties, infrastructure, resources, and the costs of recovery and reconstruction. This aspect is considered by multiplying the potential losses by the probability of event occurrence in order to evaluate the risk.
- **Vulnerability:** Indicates the susceptibility of a region or community to suffer damage or losses due to an adverse event. In the context of risk analysis, it considers the ability of structures, infrastructure, and the population to withstand and recover from the effects of the event (UNISDR, 2015).

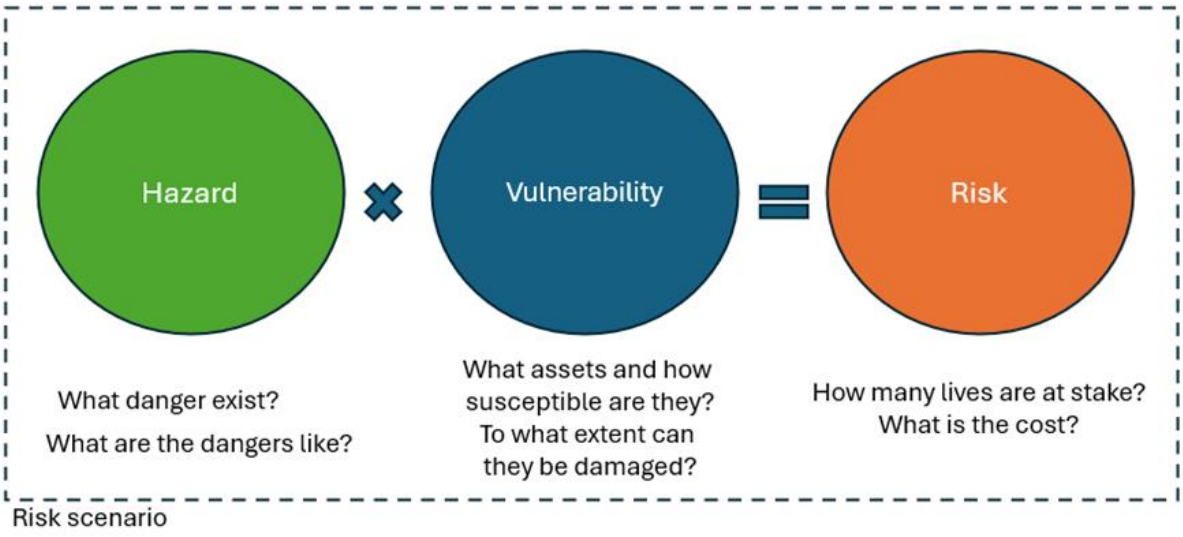

Figure 1.2:Components of a Risk study

In a review by Ward et al. (2019) , natural hazards are categorized into hydrological, climatological, meteorological, and geological types, aiding the understanding of their diversity and assessment methodologies. Focusing on geological hazards,

(Ward et al. 2019) highlight the challenges posed by volcanic eruptions, land subsidence, and earthquakes due to their unpredictability and the potential devastation, emphasizing factors such as tectonic movements and human-induced changes. The review emphasizes adaptation and mitigation strategies, particularly noting the vulnerability of resource-constrained regions, where the inability to implement effective disaster risk (DRR) reduction exacerbates challenges, especially with geological hazards and their sudden onset, impacting unprepared communities significantly.

The risk posed by natural hazards is extremely high and is increasing. Since 1990, reported disasters have led to over 1.6 million fatalities globally, and economic losses are estimated at an average of around $260-310 billion per year. The need to reduce the risk associated with natural hazards is recognized by the international community, and is at the heart of the Sendai Framework for Disaster Risk Reduction (UNDRR 2015).

Coy (2010) focus on risk from the engineering perspective, stressing the importance of understanding natural processes, correlations, and frequency of events in specific locations. Geological threats such as earthquakes, landslides and subsidence are analyzed in accordance with their distinct characteristics and regional recurrence, while vulnerability is assessed through social, economic, and infrastructural lenses, considering factors such as population density, construction quality and urban policies. The evaluation of geological risk emphasizes the interplay between threat and vulnerability, with technologies like MT-InSAR enhancing accuracy. Research undertaken by Coy M. underscores the increasing ecological and socio-economic risks in Latin America, noting that between 1972 and 2001, natural disasters claimed an estimated 84,000 lives and affected 13 million people, with events like the 1976 Guatemala City earthquake resulting in approximately 23,000 fatalities. These risks are compounded by societal disparities, unequal power dynamics, and access imbalances, shaping the ongoing relationship between society and nature in Latin American countries.

1.4.2. Contribution of remote sensing to risk analysis

Remote sensing techniques play a crucial role in hazard studies, providing valuable data for disaster management and risk analysis (Oštir et al., 2003). These techniques have been successfully applied in various hazard studies, including tsunami vulnerability analysis (Römer et al., 2012), glacial terrain analysis (Allen

et al., 2008) and glacier and permafrost hazard assessment (Kääb et al., 2005). Publications by different authors have highlighted the advantages afforded by the use of remote sensing and Geographical Information systems in nature-hazard monitoring (Joyce et al., 2009; Oštir et al., 2003):

- Comprehensive Hazard Analysis: Integrating diverse data types, such as satellite imagery, topographical maps, and demographic statistics, into a single platform, enhances the accuracy and comprehensiveness of hazard analysis, offering a holistic view of potential risks.
- Precise Identification and Risk Assessment: Utilizes detailed spatial analysis to identify susceptible areas, assess vulnerability, and evaluate risk levels, facilitating targeted interventions.
- Enhanced Decision-Making Support: Assists in developing informed preparedness strategies and response plans by simulating and predicting natural hazard impacts, thus saving lives, and reducing economic losses.
- Effective Communication: Offers powerful visualization capabilities, including mapping and 3D modelling, for disseminating hazard information among emergency responders, decision-makers, and the public.
- Optimized Resource Allocation and Planning: Aids in the strategic allocation of emergency response resources and the planning of evacuation routes, optimizing disaster response efforts.

1.4.3. Remote sensing: From SAR to MT-InSAR

Remote sensing systems based on electronic radiation detectors are obviously not image-generating systems; the result is not an image but rather a set of numbers stored in a computer-compatible format. These systems are divided into two groups according to different technical solutions. Passive remote sensing systems measure existing radiation, such as the solar radiation reflected from the earth's surface. Active remote sensing systems emit radiation at the studied object and measures the amount of reflected radiation. Sensors measures the average reflection in a selected wavelength band (Figure 1.3) (Mårtensson, 2024)

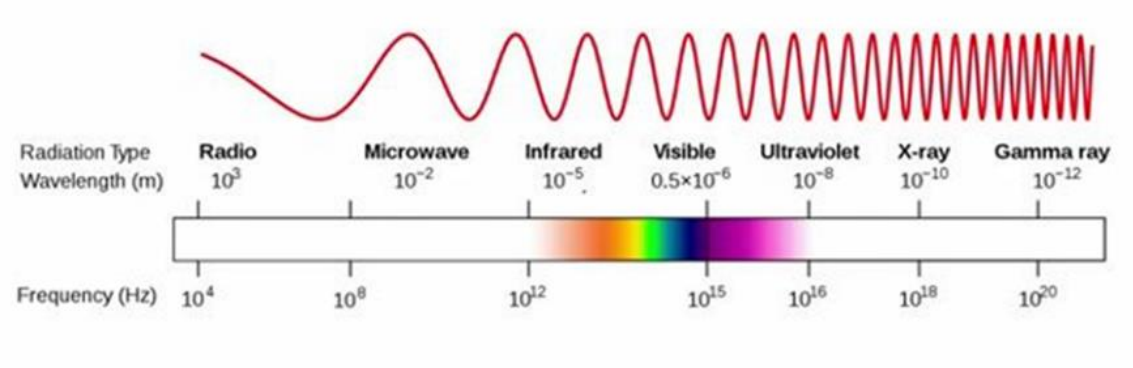

Figure 1.3: Electromagnetic Spectrum (Patruno, 2024)

The result is recorded as an image element on the scan line termed a pixel. A pixel is usually square, and when discussing the ground resolution of a particular sensor system, the pixel size is cited; for example, an 80 m pixel size means that the smallest image element records the average reflection from an area of 80 by 80 m (6400 m²) (Figure 1.4.) (Mårtensson, 2024).

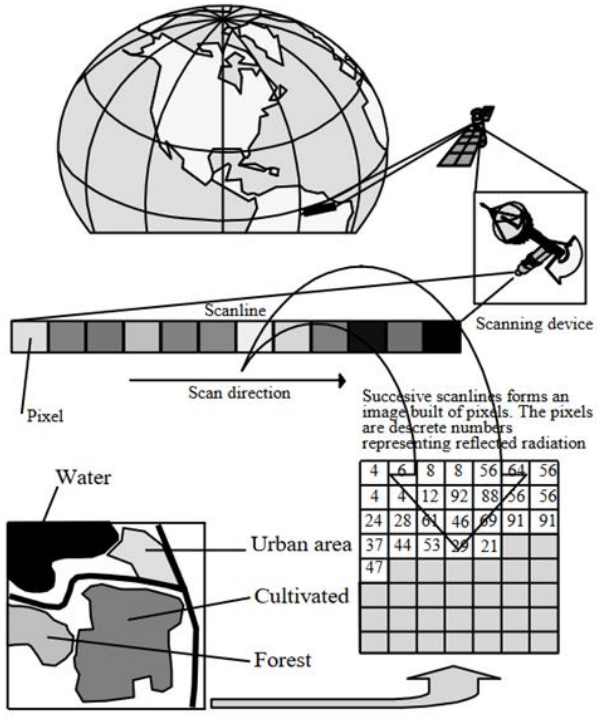

Figure 1.4: Scheme of the transformation of sensed radiation into the pixels of an image (Mårtensson, U, 2024).

Basics of SAR

Synthetic Aperture Radar (SAR) (Figure 1.5) is a cutting-edge radar sensor technology, adept at capturing high-resolution imagery from significant distances. Its application in remote sensing is typically observed in space-based platforms, deployed aboard aircraft or satellites, facilitating the acquisition of high-resolution images of the Earth's surface, sensitive to the microwave region of the electromagnetic spectrum. SAR is an active sensor system which operates day and night, by emitting electromagnetic waves in one of the specific frequency bands, namely the X band (3 cm), C band (6 cm), and L band (24 cm) and P band (64 cm). The penetration capabilities of SAR ensures minimal signal degradation and facilitates imaging under clouds and all-weather conditions. This aspect is particularly advantageous over optical imaging techniques, offering consistent monitoring capabilities for dynamic events or for surveying areas commonly covered by clouds (Massonnet & Feigl, 1998).

The data acquired using coherent radar systems resembles a hologram, rather than a traditional image, requiring significant signal processing to develop the final imagery. The conversion of raw SAR data into an intelligible image format is a complex inverse problem, involving detailed processing to accurately represent the features on the Earth's surface (Bamler & Hartl, 1998).

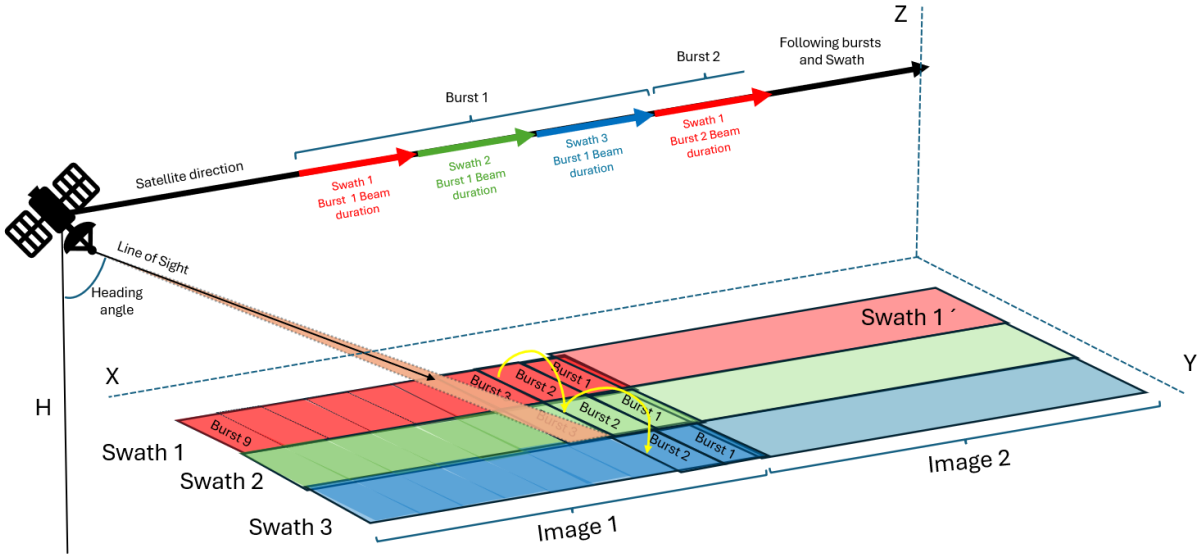

Figure 1.5: illustrates the geometry involved in Synthetic Aperture Radar (SAR) imaging.

In the context of Synthetic Aperture Radar (SAR) as described by Bamler & Hartl (1998) SAR system employs a side-looking geometry to illuminate the Earth's

surface. As the sensor traverses its path at a height H, it emits microwave pulses downward onto its footprint a specified area of the Earth's surface covered by the radar's illumination. These pulses are emitted at a consistent rate, defined by the pulse repetition frequency (PRF), and the SAR system captures the scattered echoes from the Earth's surface in response to each pulse.

The reception of these echoes is coherent, meaning the SAR system preserves the phase information of the received signals. The echoes are then organized into a two-dimensional matrix based on the 'two-way signal delay time' and the 'pulse number.' The 'pulse number' is directly related to the position of the satellite along its path, while the 'delay time' corresponds to the slant range distance from the SAR sensor to the target on the ground (Bamler & Hartl, 1998).

Scatterers located at varying distances from the radar (across different slant ranges) cause different delays between the emission and reception of the radiation. Given the almost purely sinusoidal nature of the transmitted signal, this delay, denoted as τ, results in a phase shift, φ, between the transmitted and received signals. Consequently, the phase shift is proportionally related to the total round-trip distance of the radiation, 2R, divided by the wavelength λ of the transmitted signal. This principle is depicted in Figure 1.6 (Ferretti et al., 2007).

To elaborate further, the assumption made about the ensemble of scatterers that they are temporarily stationary and reside in the far-field of the SAR antenna is critical for SAR imaging. This means that the scatterers, which could be any feature on the Earth's surface that reflects the radar signal back to the antenna, are unchanging during the short time span of radar signal emission and reception. The assumptions concerning the scatterers' ensemble in Synthetic Aperture Radar (SAR) imaging namely, their temporary stationarity and far-field placement are pivotal. They presume that scatterers, reflecting radar signals back to the antenna, remain unchanged during signal emission and reception, which is essential for simplifying signal interpretation by avoiding additional phase complexities due to movement. The 'far-field' assumption ensures that scatterers are at a distance where radar waves become parallel, enabling SAR systems to treat wavefronts as planar, simplifying image formation by recording phase and amplitude without near-field curvature complexities. These assumptions are foundational to SAR system design and operation, facilitating the creation of precise Earth surface representations vital for diverse applications such us surveillance, environmental monitoring, and deformation analysis.

These assumptions help to ensure that the radar signals can be processed and interpreted to create a clear and accurate representation of the Earth's surface. They are fundamental to the design and operation of SAR systems (Figure 1.6 and equation 1.1).

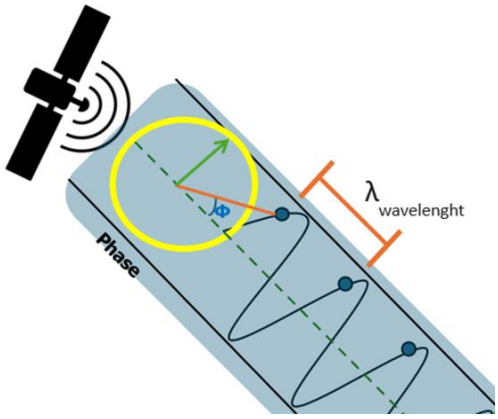

Figure 1.6: Relation of sinusoidal function with SAR functioning

$$\phi = \frac{2\pi}{\lambda} = \frac{4\pi}{\lambda} R \qquad (1.1)$$

ϕ : The phase shift measured in radians.

λ : The wavelength of the SAR signal.

R: The one-way slant range distance from the SAR system to the target.

Equation 1.1: The formula depicted is a mathematical representation of the phase shift (ϕ) observed in a Synthetic Aperture Radar (SAR) signal due to the round-trip travel of the radar waves to and from a target.

A complex SAR (Synthetic Aperture Radar) image is a type of data representation used in SAR imaging systems, characterized by each pixel in the image containing both amplitude and phase information. This is distinct from traditional optical or radar images, which typically only provide amplitude information (i.e., the intensity or brightness of the returned signal) (Ferretti et al., 2007).

- **Amplitude:** Represents the strength or intensity of the radar signal that is backscattered from the surface features to the SAR antenna. The amplitude in a SAR image can give insights into the material properties and texture of the Earth's surface. For example, areas with high backscatter (bright areas

in the image) might indicate metallic objects or rough terrain, while low backscatter (dark areas) might indicate smooth surfaces like water bodies.

- **Phase:** Encodes the position of the scatterer relative to the radar system, based on the phase of the returned signal. The phase is a measure of the time delay between the radar signal's emission and its reception after bouncing off the target. In SAR imaging, this delay is converted into a phase angle within the complex number associated with each image pixel.

In Synthetic Aperture Radar (SAR) imagery, the detected signal is typically represented in varying shades of grey to depict different levels of backscattered radiation (Figure 1.7). In such images, bright pixels indicate regions where the radar signal is strongly reflected to the sensor, which is characteristic of areas with structures or materials that have a high radar reflectivity, like urban environments with buildings and concrete surfaces. Conversely, dark pixels are indicative of areas with low radar reflectivity, such as calm water bodies, where the smooth surface results in the radar signal being scattered away from the sensor, leading to minimal backscatter. This method of visualization allows for the differentiation of surface features based on their radar reflectivity properties.

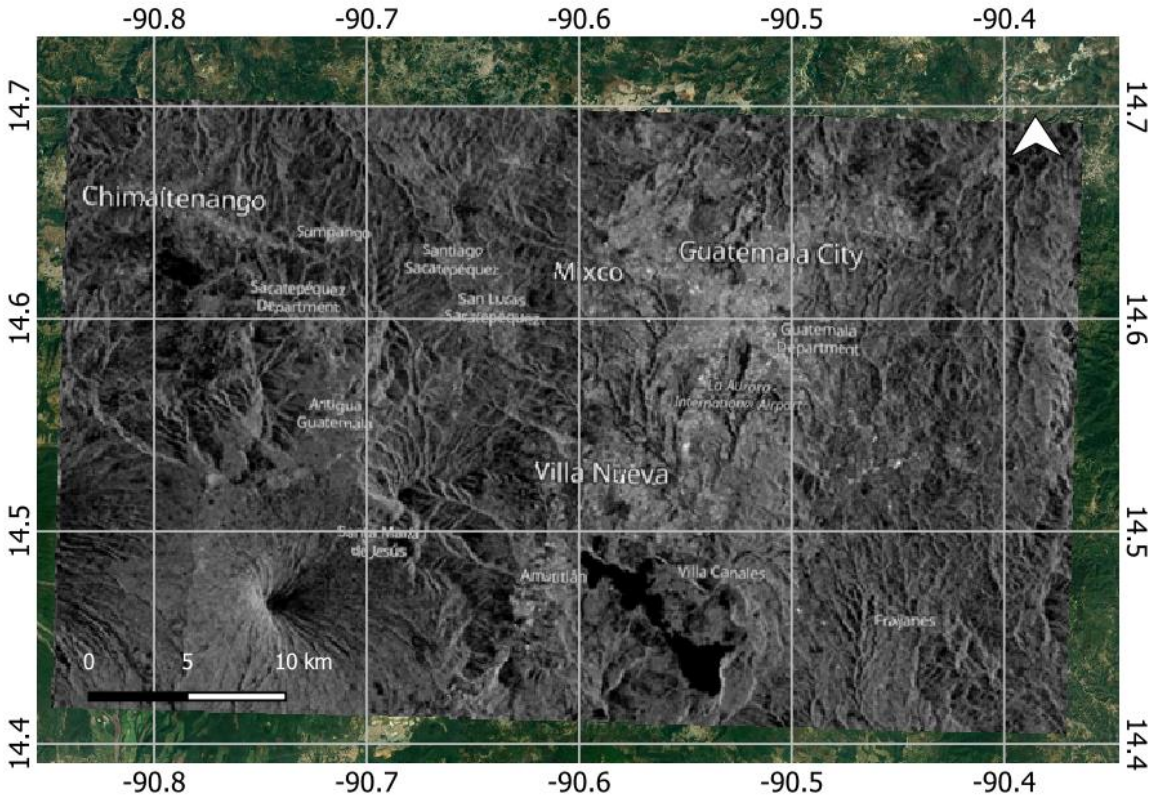

Figure 1.7: Shows a SAR image over Ciudad de Guatemala, SAR sensor in Sentinel 1 satellite. (Source: Sentinel-hub)

SAR sensors

Synthetic Aperture Radar (SAR) sensors have undergone significant evolution since the launch of the first SAR satellite, Seasat, in 1978. This evolution has been marked by the development and continuous improvement of technologies, which have greatly expanded the capabilities and applications of space SAR systems. The differentiation of these systems according to the frequency bands in which they operate - X, L, and C - has allowed for specialization and adaptation to specific Earth observation needs (Moreira, 2014).

- **X-band:** The TerraSAR-X and TanDEM-X satellites represent outstanding examples of the evolution of SAR sensors in the X-band. Launched in June 2007, TerraSAR-X marked a milestone by providing high-resolution radar images for commercial and scientific applications. Its "twin," TanDEM-X, launched in June 2010, joined TerraSAR-X in a closely controlled flight formation, a first for a space-based radar interferometer. Together, they have generated a global Digital Elevation Model (DEM) of the Earth's surface with unprecedented accuracy, which has been fundamental for scientific research and a wide range of commercial applications.
- **L-band:** The Tandem-L mission proposal illustrates the innovative potential of L-band SAR sensors for the systematic monitoring of dynamic processes on the Earth's surface. Tandem-L aims to use an L-band radar interferometric instrument to provide a unique dataset for research on climate and the environment, geodynamics, hydrology, and oceanography. This approach promises to revolutionize our ability to inventory the height and biomass of forests globally, measure Earth's deformation due to tectonic processes and/or anthropogenic factors, and monitor soil moisture and ocean surface currents, among other applications.
- **C-band:** Sentinel-1a, the first satellite of the ESA/EU Copernicus program, launched on April 3, 2014, exemplifies the evolution of SAR sensors in the C-band. Equipped with a C-band SAR instrument, Sentinel-1a was designed with a focus on emergency services, the marine environment, and land use mapping, in addition to contributing to climate change research. Its main acquisition mode, the Interferometric Wide Swath (IW) mode, utilizes the beam steering concept in azimuth known as TOPS (Terrain Observation by Progressive Scans), achieving improved image performance. Sentinel-1a's ability to provide high-resolution images and its contribution to Earth

observation under all weather conditions and at any time of day underline the vital role that C-band SAR sensors play in global monitoring and disaster management.

The evolution of space-based SAR sensors continues to mark a golden era for Earth observation, with each frequency band offering unique capabilities that open new possibilities for science and society. Innovations in technologies such as digital beamforming and waveform diversity, along with the use of large reflector antennas, promise to elevate these capabilities to unprecedented levels, allowing for detailed and frequent observation of our planet.

Recent advancements in spaceborne Synthetic Aperture Radar (SAR) technology have led to the launch of several satellites with SAR sensors. The Indian Space Research Organisation (ISRO) launched the RISAT-1 in 2012, providing multi-mode, multi-polarization SAR data (Chakraborty et al., 2013). Similarly, the KOMPSAT-5, launched by Korea, and the HJ-1-C, launched by China, have enhanced SAR capabilities for applications such as disaster monitoring and environmental management (Deng et al., 2014; Kwag, 2013). These satellites have significantly improved the imaging capacity of SAR systems, providing high-resolution, all-weather, and day-and-night images (Moreira, 2014). The potential of SAR technology for applications such as traffic monitoring and ship detection has also been highlighted (Wang et al., 2019).

SAR Interferometry

Generating interferograms involves comparing multiple SAR images captured at the same geographical point but at distinct moments in time. This comparison yields maps that can accurately track changes, movements, or alterations in the Earth's surface. Such data is invaluable for numerous practical applications, offering critical insights into surface dynamics. InSAR phase measurements can detect variations between two SAR image captures, commonly designated as the master and the slave images. Figure 1.4 exemplifies the primary phase component observable in a standard InSAR assessment. In a straightforward scenario, the phase response from an isolated point scatterer is defined as (Bamler et al., 1999; Guarnieri & Prati, 1996). The equation depicted is used to calculate the phase (ϕ). It is defined as in equation 1.2.

$$\phi = \frac{2Rp*2\pi}{\lambda} + \phi scat \qquad (1.2)$$

- Rp is the slant range, which is the straight-line distance between the radar antenna and the point on the ground.
- λ is the wavelength of the radar signal.
- ϕ_{scat} represents the phase contribution from the scattering properties of the target, which depends on its electrical characteristics.

Equation 1.2: Interferometric phase

This formula encapsulates the total phase as a combination of the distance-dependent phase shift and the target's scattering properties. The first term accounts for the phase change due to the signal's round-trip travel time, and the second term ϕ_{scat} accounts for the phase shift introduced by the interaction of the radar signal with the scattering characteristics of the target's surface.

Importance on coherence

In the intricate process of InSAR, coherence stands as a pivotal element, directly influencing the quality and reliability of the resulting interferograms. Coherence is a measure of the similarity in phase characteristics between pairs of SAR images, crucial for the accuracy of the phenomena being monitored. When selecting SAR images for interferogram generation, a meticulous approach must be taken, factoring in the view angle, which significantly impacts the resulting image geometry. SAR satellites capturing data on both ascending and descending passes offer differing viewpoints of the terrain, each with its unique geometrical considerations.

The geometrical baseline the spatial separation between the satellite's positions across distinct passes also plays a critical role, dictating the interferogram's sensitivity to the Earth's topographical nuances and its overall coherence. A profound understanding of these spatial factors is necessary to ensure that topographic features are accurately represented, and the integrity of the phase information is maintained across the images.

Temporal dynamics are equally consequential. The temporal baseline, denoting the time span between image acquisitions, must be carefully calibrated to mitigate decorrelation effects that can obscure or distort the image, such as those induced by

alterations in the landscape, yet it should be sufficiently extended to capture the subtleties of gradual geological shifts. The timing of acquisitions is further nuanced by factors such as natural lighting and seasonal changes, which can affect image clarity and coherence.

Importantly, the coherence of certain terrains is inherently variable; areas subjected to foreshortening—where the terrain slope faces the radar—tend to lose coherence rapidly when the perpendicular baseline exceeds a minimal threshold. This effect is particularly pronounced in challenging environments such as dense forests or water bodies, where the complex interaction with radar signals often results in low coherence. Conversely, terrains with opposing slopes generally exhibit higher coherence, provided they are not obscured by shadows, benefiting from enhanced spatial resolution and a greater effective critical baseline compared to flat areas (Ferretti et al., 2011).

Importantly, the coherence of certain terrains is inherently variable; areas subjected to foreshortening where the terrain slope faces the radar tend to lose coherence rapidly when the perpendicular baseline exceeds a minimal threshold. This effect is particularly pronounced in challenging environments such as dense forests or water bodies, where the complex interaction with radar signals often results in low coherence. Conversely, terrains with opposing slopes generally exhibit higher coherence, provided they are not obscured by shadows, benefiting from enhanced spatial resolution and a greater effective critical baseline compared to flat areas (Ferretti et al., 2007).

InSAR

Interferograms are a key output of Synthetic Aperture Radar (SAR) interferometry, a technique used for topographic mapping and surface change monitoring (Guarnieri; 1996; Bamler, 1999). An interferogram can be created by using two SAR images, and it can be defined as the phase increment between both images, taken over the same area but in different moments.

The creation of an interferogram using Synthetic Aperture Radar (SAR) imagery is a methodical process (see figure 1.8) that begins with the acquisition of the primary datasets known as the master and slave images. These images, often in the form of Single Look Complex (SLC) files, contain comprehensive amplitude and phase information necessary for the subsequent steps of interferometric analysis (Ferretti et al., 2007).

The interferometric phase measured in InSAR, as depicted in Equation 1.3, encapsulates the cumulative effects of various geophysical and atmospheric factors that influence the SAR signal. Each component in the equation represents a different source of phase change (Osmanoğlu et al., 2011):

$$\Delta\phi=\phi_{flat}+\phi_{topo}+\phi_{orbit}+\phi_{defo}+\phi_{tropo}+\phi_{iono}+\phi_{scat}+\phi_{noise} \quad (1.3)$$

Equation 1.3: Total interferometric phase

- ϕ_{flat}: The flat earth phase, which accounts for the phase shift due to the assumption of a flat Earth in the SAR processing.(DEOS, 2008)
- ϕ_{topo}: The topographic phase contribution, representing the phase change due to the Earth's topography (Bamler et al., 1999).
- ϕ_{defo}: The phase contribution related to actual ground deformation between the SAR image acquisitions.
- ϕ_{orbit}: The phase error introduced by inaccuracies in the satellite's orbital information.
- ϕ_{tropo}: The tropospheric phase contribution, which accounts for the phase delay caused by the radar signal's interaction with the troposphere.
- ϕ_{iono}: The ionospheric phase contribution, which reflects the phase shift introduced by the ionosphere (Hanssen, 1996; Zebker et al., 1997).
- ϕ_{scat}: The phase contribution related to the electrical properties of the scatterers on the ground.
- ϕ_{noise}: The interferometric phase noise term (ϕnoise) can be linked to coherence and is composed of four distinct decorrelation factors.

As Ferretti et al. (2007) and Colesanti et al. (2003) suggest, InSAR phase measurements are sensitive to these various components. Depending on the specific application, some of these factors may be considered noise. For instance, when the goal is to generate a Digital Elevation Model (DEM), ground deformation is treated as noise since it is not relevant to the elevation data being sought. Conversely, when studying ground motion, the stable topographic phase (which would form the DEM) needs to be removed to isolate and analyze the deformation signal.

As we delve into the realm of InSAR, we transition from the broader overview of this advanced remote sensing technique into a more detailed examination of the algorithms that underpin its functionality. MT-InSAR, standing for Multi-temporal Interferometric Synthetic Aperture Radar, harnesses a series of SAR images taken over time to accurately track ground deformation.

MT-InSAR

MT-InSAR, or Multi-temporal Interferometric Synthetic Aperture Radar, is a powerful remote sensing technique for monitoring ground deformation. It overcomes the limitations of conventional InSAR, such as phase decorrelation and atmospheric artifacts, by using multiple time series of SAR images (Bamler et al., 1999; Even & Schulz, 2018; Massonnet & Feigl, 1998; Rosen et al., 2000; Singh Virk et al., 2018).

A range of MT-InSAR algorithms have been developed, each with its own strengths and limitations (Singh Virk et al., 2018)

- **PSInSAR (Persistent Scatterer Interferometry):** The PSInSAR technique, perfected by Ferretti et al., shines in urban settings where numerous stable scatterers are present. This method's strength lies in its precision, capable of pinpointing surface movements to within millimeters. It adeptly forms interferograms, sidestepping the baseline decorrelation problems often seen in conventional MT-InSAR methods. However, its prowess diminishes outside of urban landscapes due to a scarcity of persistent scatterers. It may also stumble when faced with phases that are inconsistent or lack coherence, despite the presence of stable amplitudes (Hooper et al., 2004)
- **Stable Point Network (SPN):** SPN excels at processing expansive datasets of radar imagery, enabling the measurement of ground deformation with millimetric accuracy. It effectively minimizes geometric decorrelation, a common hurdle in selecting Persistent Scatterers. Nevertheless, a substantial collection of images is necessary to pinpoint electromagnetically stable points, which could be a challenge in regions with infrequent satellite coverage (Crosetto et al., 2008)
- **Persistent Scatterer Pair (PSP):** Designed by Costantini et al. (2021), the PSP method adeptly tackles the complications posed by atmospheric disturbances and orbital inaccuracies without relying on filtering. It has the advantage of pinpointing Persistent Scatterers within full-resolution SAR images, paving the way for intricate analyses. However, the extensive computational effort

required due to the numerous potential connections between Persistent Scatterers can be taxing.

- **Small Baseline Subset (SBAS):** The SBAS method, introduced by Lanari et al. (2004), specifically targets slow-moving deformations, providing highly accurate measurements. It achieves this by utilizing interferograms with minimal spatial and temporal baselines, which helps in reducing the effects of decorrelation and topography. The intricacy of processing and analyzing a dataset divided into numerous small subsets is, however, a notable challenge.
- **Coherent Pixels Technique (CPT):** CPT is a PSI technique that isolates complete deformation evolution, DEM error, and atmospheric artifacts from a stack of interferograms, an approach detailed by Mora et al. This method is particularly advantageous as it allows for the isolation of deformation signals. The multi-looking step required for coherence estimation, which might reduce spatial resolution, is a limitation to consider (Mora et al., 2003).
- **SqueeSAR:** developed by (Ferretti et al., 2011), increases interferometric coherence using statistical approaches and is particularly effective in non-urban areas. It manages to improve coherence over distributed targets and offers an increased coverage of ground points. Vegetation can, however, interfere with the identification of radar targets, affecting the deformation detection process. Moreover, the precision and quality of deformation measurements can diminish with increasing distance from the reference point.
- **IPTA:** Interferometric Point Target Analysis is applied on selected point targets that exhibit persistent scattering behavior over a prolonged observation period (Werner et al., 2003). Errors resulting from atmospheric artifacts in SAR scenes separated by large baselines are reduced through the use of multiple scenes of the site and higher measurement accuracy can be achieved. Several manmade structures over urban areas, infrastructures or exposed rocks outside the cities showing visible scattering are helpful in achieving estimates of the progressive terrain deformation in millimeters (C.-T. Chen et al., 2007).

MT-InSAR software's

MT-InSAR data is being processed by different open source and commercial tools listed below; Open-Source Research Packages: ISCE, ROI-PAC, DORIS, GMTSAR,

StaMPS and SNAP Commercial Packages: Gamma, GEOMETICA, ENVI SARScape, ERDAS IMAGINE, SARPROZ and DI-APASON. Some of the recent trends being followed using StaMPS, SARPROZ (copyright(c) 2009 Daniele Perissin) and G-POD services of ESA for land surface deformation monitoring are discussed as bellow.

- **Stanford Method for Persistent Scatterers** (StaMPS): StaMPS a MATLAB based software developed at Stanford University and subsequently upgraded at the University of Iceland, Delft University of Technology and the University of Leeds. The package is equipped with persistent scatterer and small baseline methods and with an option to combine them. It is developed for PSI processing to work well in barren terrain in nonurban areas undergoing nonlinear deformation having no man-made structures. It uses amplitude and phase information of individual pixels to determine the probability of being a permanent scatterer (PS). StaMPS like PSI utilizes amplitude scattering values for initial PS selection, includes the SBAS (Small Baseline Subset) method to identify those scatterers that dominates in scattering from the resolution cell and the pixels whose phase decorrelates little for short time periods during filtering called slowly decorrelation filtered phase (SDFP). First PS selection based on amplitude scattering values is carried out and then it is refined in an iterative manner by performing phase analysis in space and time. Utilization of these techniques enables a deformation signal with greater coverage to be extracted. Both PS and SDFP selections are combined and deformation is then extracted using the phase unwrapping algorithm (Ab Latip et al., 2015; Sousa et al., 2010).
- **SARPROZ**: designed by Daniele Perissin of Purdue University Netherlands, which is capable of processing different sets of interferograms by different techniques running in the software background. Parameter estimation can be done by PSI algorithm, Capable of estimating APS through different algorithms for graph inversion. Acquired SLC Image data is first converted into a format which SAPROZ recognizes. Then various steps such as computation of data statistics, precise orbital application, retrieving weather data from each scene, creating a subset of the area of interest etc. are performed using GUI (Graphical User Interface). SARPROZ automatically downloads the metrological data during the day of acquisition. Master and Slave Images are extracted from the data set, co-registered and the offset between master and slave images is predicted. Each slave image is aligned to

the master image in such a way that each pixel belonging to a portion of the imaged terrain in the slave image is exactly under the corresponding pixel in the master image. Amplitude Stability Index is calculated by generating the co-registered stack, reflectivity map, temporal average of the intensity values of the image datasets etc. (Bakon et al., 2016). Coarse points are selected and DEM assisted geocoding is performed. Selection of the good tie points depends upon the resolution of the data available. Bright pixels identifiable in the reflectivity map are selected manually as Ground control points (GCPs). DEM is then converted to SAR coordinates to support PSI processing. A phase to height and phase to flat constants conversion process is then carried out. Amplitude stability index threshold is applied to create PS candidates to estimate preliminary parameters and Atmospheric Phase Screen (APS) (Lazecky et al., 2015).

- **GAMMA:** developed by Grenerczy & Wegmüller (2011) , is distinguished in the realm of MT-InSAR processing tools by its comprehensive capabilities for the analysis of SAR, MT-InSAR, and PSI data, especially with its complete integration of Sentinel-1 SAR data.nThis method is instrumental in maintaining the continuity of phase information across bursts in Sentinel-1 data, thus preventing the occurrence of phase jumps which can significantly compromise the accuracy of MT-InSAR analysis. GAMMA's robust processing capabilities extend to phase filtering, unwrapping, and coherence estimation, each being a vital step in the generation of reliable MT-InSAR results. The software's Interferometric Point Target Analysis (IPTA) component supports methodologies like SBAS and PSI, enabling the derivation of deformation time series.
- **LiCSBAS:** It is a distinctive open-source tool created by Yu Morishita, offering a specialized approach to MT-InSAR time series analysis. As elucidated in the "LiCSBAS Tutorial" (Morishita et al., 2020), this software operates within a Python3 setting and is engineered to analyze interferograms sourced directly from LiCSAR, a service providing pre-processed interferograms generated using the GAMMA software. The integration between LiCSBAS and LiCSAR showcases an end-to-end processing capability, streamlining the journey from raw data acquisition to detailed geophysical interpretation.

In the realm of ground deformation detection and analysis, MT-InSAR techniques, specifically PSI via SNAP-StaMPS and SBAS within the LiCSBAS framework, have emerged as crucial methodologies. This study leverages these approaches to assess

their efficacy in detecting deformations. The accuracy of both the SNAP-StaMPS and LiCSBAS techniques is set within 2 mm/yr as evidenced in the literature (Mancini et al., 2021; Morishita et al., 2020).

Sang-Wan (2010) compared PSInSAR and SBAS, noting that while both techniques are capable of identifying ground deformations, PSInSAR excels at detecting local deformations, whereas SBAS is more effective in areas with minimal unwrapping error. This underscores the necessity of choosing the appropriate method based on the study area's specific characteristics and the deformation type.

Bouraoui (2014) and Goel (2014) both discussed the use of SBAS and PSInSAR in time-series analysis, with Goel emphasizing the need for increased spatial density of measured points and Bouraoui highlighting the potential of combining the two methods. Ferretti et al. (2011)proposed a new algorithm, SqueeSAR, for processing interferometric data-stacks. Even & Schulz (2018) discussed the use of distributed scatterers in MT-InSAR, reviewing the use of DS in PS algorithms.

2. Study areas

This introduction sets the stage for a detailed exploration of the chosen study areas, highlighting the reasons behind their selection and the significance of their inclusion in this work. Each of these regions offers a unique setting to better understand the geological processes at play and their impacts on human society. Furthermore, analyzing these areas significantly contributes to our understanding of how different communities and risk management systems respond to the threat of natural disasters.

The selection of the study areas for this work reflects the needs of the stakeholders within the framework of the industrial doctorate. Primarily, the areas studied in the kuk-Áhpàn project include Central America and Murcia, with the addition of La Palma following the event in September 2021. All these study areas share a common geological risk that characterizes them due to their geographical location. Furthermore, these areas also tie in with the industrial interests of Detektia, which involve the monitoring of large infrastructures or urban areas with fervent development, where the technology developed is required for appropriate maintenance and planning to achieve sustainable development.

Finally, the choice of areas in the study also facilitates the learning process and meets the requirements of the Geomatics Engineering doctoral program, such as the publication of scientific articles and the preparation of materials to participate in scientific conferences. Taking into consideration the abovementioned factors, combined with the fact that local contacts were able to provide information to validate the MT-InSAR results, the most suitable locations for the development of this Industrial Doctorate research were San José, Costa Rica, Guatemala City, and La Palma.

Figure 2.1 serves as a visual starting point for this discussion, illustrating the geographical locations and key characteristics of the study areas. Throughout this section, we aim not only to document the geological peculiarities and associated risks of each region, but also to reflect on the lessons learned and mitigation strategies applicable on a global scale. By delving into the study of these areas, our aim is to contribute towards a more resilient future, one in which we are more prepared for the challenges presented by natural disasters.

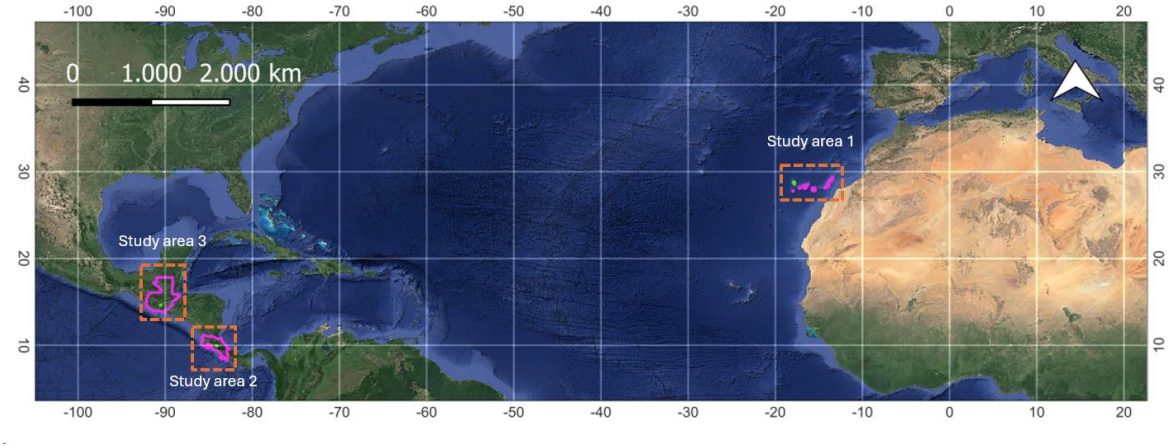

Figure 2.1:Global vision of the location for the three study areas. Geographical Reference system WGS84

Through this section, we aim not only to document the geological peculiarities and associated risks of each region but also to reflect on the lessons learned and mitigation strategies applicable on a global scale. By delving into the study of these areas, we commit ourselves to the goal of advancing towards a more resilient future, prepared to face the challenges that natural disasters present.

2.1. La Palma

La Palma, situated at coordinates 28° 36′ 46″ N and 17° 51′ 58″ W, along with the adjacent island of El Hierro, are the most westerly islands of the Canary archipelago. They form a chain extending east to west, lying between 97 and 403–516 km to the west of Africa's passive continental margin as depicted in Figure 2.2. Both islands are active volcanic sites. El Hierro's last eruption was in 2011, while La Palma has had numerous documented historic eruptions, including a recent one in 2021 (Carracedo et al. 2001; Klügel et al. 1999, 2005) . La Palma is the archipelago's second youngest and historically most active island, accounting for the majority of the archipelago's historic eruptions in the past 600 years, with all eruptive activity occurring along the southern Cumbre Vieja rift. The island's prior eruption in 1971 is known as the Teneguía eruption, named after a local aboriginal site. The 2021 Tajogaite eruption, named after the location of its first vent, is significant locally as it links the current magma plumbing system with those that fueled the 1971, 1949, and earlier eruptions. This connection allows for the tracking of the seismic evolution of the magma plumbing system beneath La Palma (Benito et al., 2023).

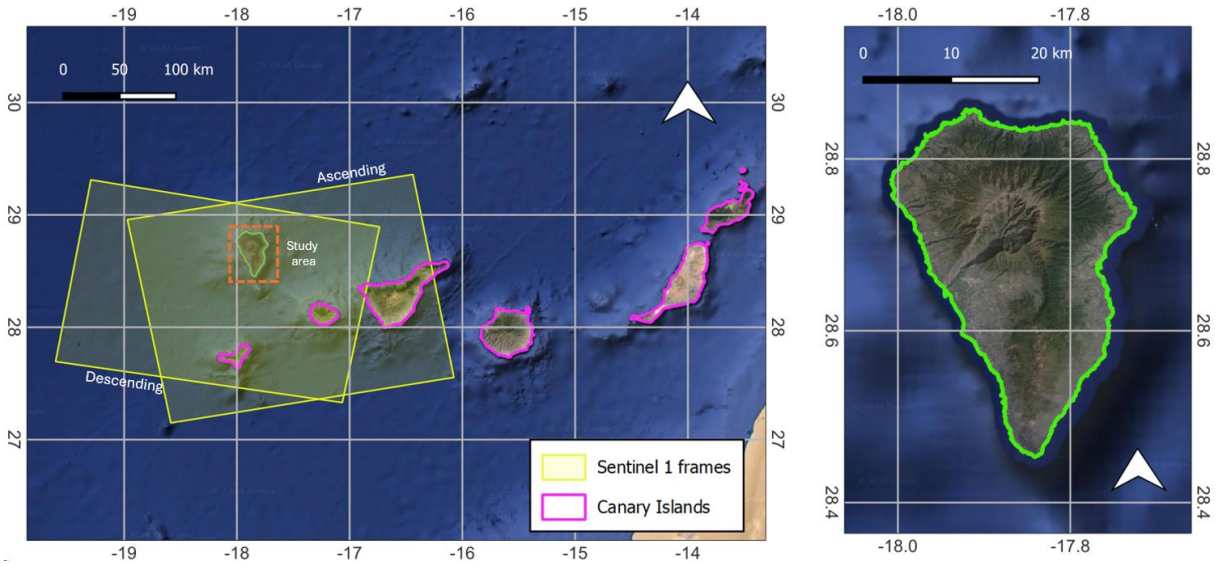

Figure 2.2: Study area in La Palma. Geographical Reference system WGS84

2.2. Central America

These studies collectively underscore the importance of understanding the general deformation caused by seismic and volcanic activity, and the need for comprehensive risk and vulnerability assessments in these areas.

2.2.1. San José de Costa Rica

Central America is a complex mosaic of landscape dynamics, shaped by a wide range of terrestrial processes. Few other regions on Earth exhibit such a magnitude of geomorphological diversity. Throughout the Central American isthmus, there is a great diversity of tectonics, lithology, and climatic domains concentrated in 0.4% of the Earth's surface. The physiography is primarily defined by the northwest-southeast orientation of the Mesoamerican trench and the volcanic front. These morphotectonic components were formed in the Cenozoic era, through the subduction process of the Cocos oceanic plate beneath the Farallon plate, along the western edge of the Caribbean plate.

Throughout the Cenozoic, this first-order contrast in basement lithology has been overlaid by a diverse collection of rock formations generated in a variety of tectonic environments, including volcanic mountain ranges, fore-arc and trench-slope basins, alluvial plains and deltas, intra-arc rift valleys, fold-and-thrust belts, high plateaus, and carbonate platforms.

In the north, the Motagua Polochic fault system cuts across central Guatemala, accommodating sinistral shearing between the North American and Caribbean plate (Samsonov et al., 2013; Zheng et al., 2018).

Central America spans an area of 500,000 km² and is home to around 40 million people. It is situated on a narrow strip of land that separates the Pacific Ocean from the Caribbean Sea, connecting the vast continental lands of South and North America. Central America consists of seven countries. The Quaternary volcanic belt is one of the most notable geotectonic features of the region. Among the most characteristic geotectonic characteristics of the region is the 1100km Quaternary volcanic front, which stretches from the Mexican-Guatemalan border to the central part of Costa Rica and embraces 40 major volcanoes. (Denyer, n.d.)

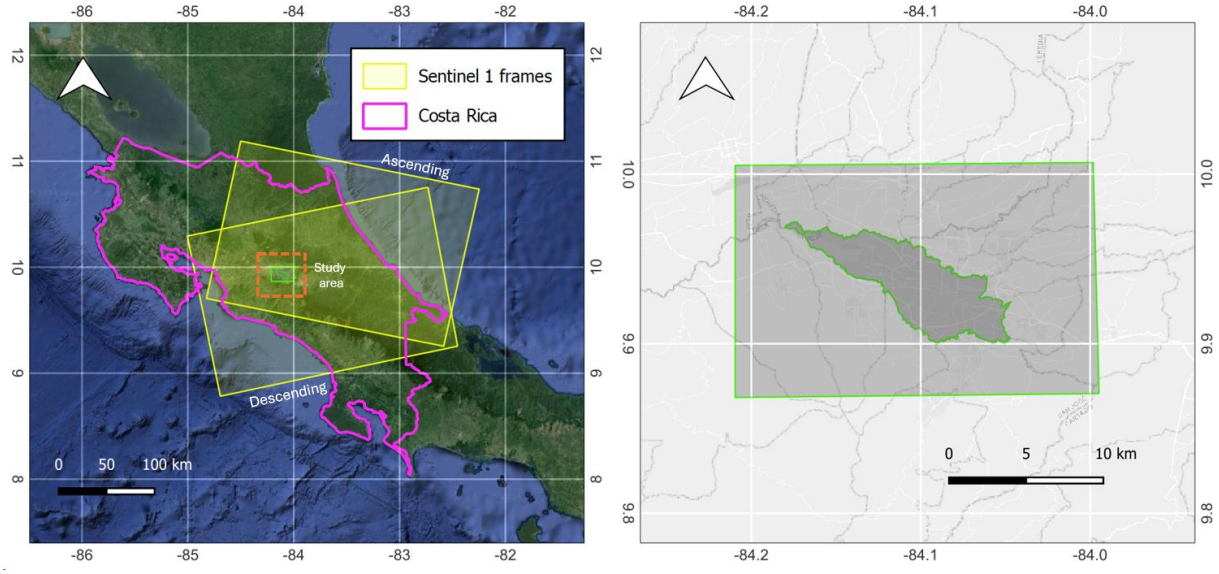

Figure 2.3: Study area in Costa Rica. Geographical Reference system WGS84

2.2.2. Guatemala City

DRR plays a crucial role in promoting social and economic growth and ensuring a sustainable future. Central American urban areas are geologically young volcanic areas. The physiographic architecture of Central America is primarily determined by the northwestern course of the Central American trench and the Central American volcanic front, which were formed by Cenozoic subduction. Soils in the region, combined with heavy rainfall, topographic complexity, and a seismically active area, can be prone to great instability during earthquakes and heavy precipitation (Bommer & Rodríguez, 2002). The Population Census XII and the Housing Census VII reveal that 14,901,286 people reside in Guatemala, with a

yearly population growth rate of 1.8% between 2002 and 2018. The Guatemala Department, which includes Guatemala City and 16 other municipalities, houses the most significant percentage of the country's population, 20.2% of the total (Instituto Nacional de Estadística Guatemala, 2019) . This population growth has resulted in increased infrastructure development and exploitation of natural resources, such as underground water. Between 2017 and 2019, 2–3 million square meters of construction was authorized, with the municipality of Guatemala accounting for 45% of these new construction areas. Housing projects make up a large proportion of these projects, with an increase of 1,363,777 buildings between 2002 and 2018 (UNISDR, 2009). Construction and urban growth must be conducted within the framework provided by risk assessments, with a focus on disaster risk reduction. Land use sensitive to disaster risks, urban planning, safe construction, and sound infrastructure will not only contribute to water management, but will also protect lives and properties, and thus benefit entire cities (UNISDR, 2009).

Using PS InSAR, this study analyzes the deformation dynamics of part of the Metropolitan Region of Guatemala, known officially as Región Metropolitana de Guatemala (RMG) (Figure 2.4). This area includes Guatemala city (comprising 22 zones) and four adjacent cities: Santa Catarina de Pinula, Petapa, Villanueva, and Mixco. The RMG is influenced by natural factors, such as geological features, extreme climate with intense precipitation, and socio-demographic factors, which makes it an interesting case study.

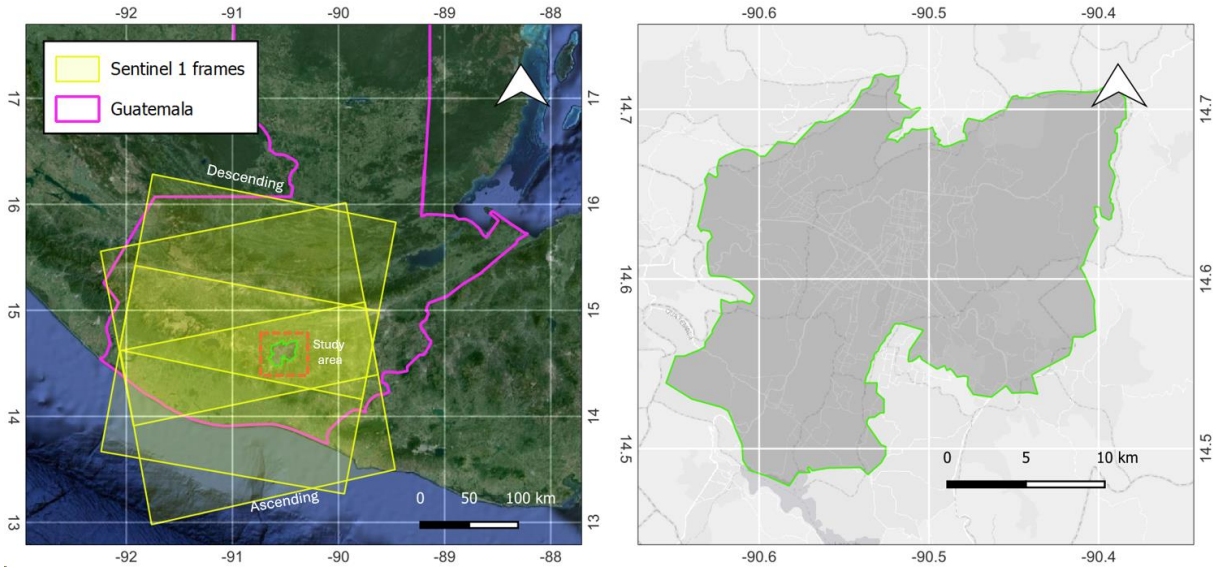

Figure 2.4: Study area in Guatemala. Geographical Reference system WGS84

3. MT-InSAR applied to the prevention of geological hazards of tectonic and volcanic origin: San José (Costa Rica) and La Palma (Spain)

This chapter is partially published in the following publications…

Benito M.B., Arroyo-Solorzano, M., Climent, A., Montero, W., Alvarado, G., Lopez, A., García-Lanchares, C., Marchamalo,M., Ornelas, A., Hernández, Rubio O., Quirós, L.E.; 2023; Seismic Hazard Scenarios for the City of San Jose, Costa Rica: Evaluation of Critical Ruptures on Nearby Faults

Benito, M. B., Alvarado, G. E., Marchamalo, M., Rejas, J. G., Murphy, P., Franco, R.; Sánchez, J. (2023). Temporal and spatial evolution of the 2021 eruption in the Tajogaite volcán (Cumbre Vieja rift zone, La Palma, Canary Islands)

3.1. Application of MT-InSAR in the development of seismic threat scenarios in the city of San José (CR)

3.1.1. Introduction

Costa Rica is characterized by high seismicity of intermediate moment magnitude Mw < 7.7, with earthquakes generated both in the subduction zone of the Cocos plate beneath the Caribbean, and in faults of the volcanic chain. The most significant recent seismic activity in the country is centered on the earthquakes of April 22, 1991, in the Limón area, with Mw 7.7 and intensity IMM X and DE January 8, 2009, in the Cinchona area, both caused significant human and economic losses (Barquero & Rojas, 2010). The capital of the country: San José, is located in the complex fault system of the Central Valley, which has been affected by numerous destructive earthquakes throughout its history (Benito et al., 2023). In this research we use satellite technology to analyze and describe the dynamics of deformation in the city of San José and the most important seismic structures in the area, for which images are obtained from Sentinel-1, the ESA constellation equipped with C band radar sensors (Figure 3.1).

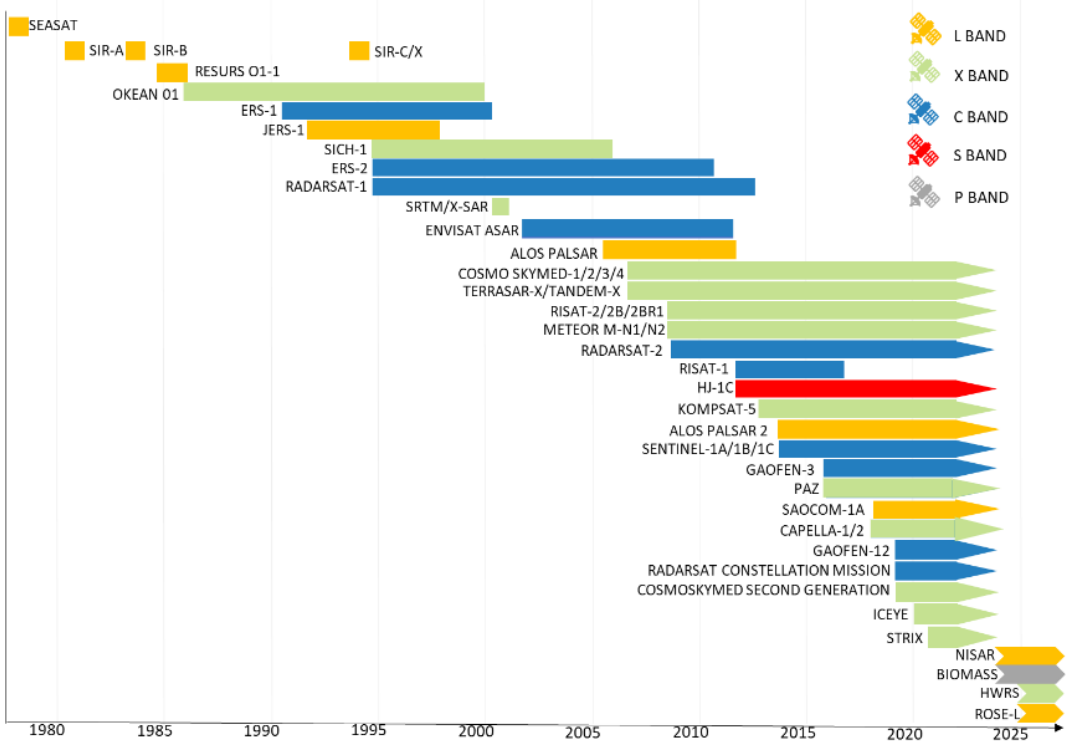

Figure 3.1: SAR missions

3.1.2. Data and methods

Study area

The designated study area in the thesis encompasses the Central Canton of San Jose, specifically focusing on three key faults - Cipreses, Belo Horizonte, and Río Azul - as identified by the Kuk-Ahpan project (Ornelas Agrela et al. 2022). This area, primarily flat and heavily urbanized, includes the entire canton and extends to regions adjacent to these faults. The spatial parameters were set based on the influence of these significant geological structures on San José.

Data & Analysis

In the deformation analysis of San José's Central Canton, data from Sentinel-1 A/B, provided by COMET (2021), were utilized. The analysis included two frames, 092A_08036_141719 and 084D_08033_121612; these two references stand for the codes used by Comet on its LiCSAR service where interferograms are accessible (Morishita et al., 2020), comprising 947 interferograms collected between March 2017 and January 2022. These interferograms were derived from a total of 253 Sentinel-1 images, with 116 from the ascending track and 137 from the descending track, as detailed by (Morishita et al., 2020).

SBAS was used for image processing in this study.The SBAS approach processed COMET-provided interferograms using LiCSBAS software, a technique detailed by COMET (Morishita et al. 2020) to generate deformation time series and velocity data. This dual-method approach provided comprehensive insights into the studied geological phenomena. LICSBAS (Morishita et al. 2020) is an open-source MT-InSAR time series analysis package that integrates with LiCSAR (Gonzalez et al. 2016; Lazecky et al. 2020), developed by the Centre for Observation and Modelling of Earthquakes, Volcanoes and Tectonics (COMET) at the University of Leeds.

In the MT-InSAR analysis for this study, LiCSBAS software was used to select a reference point based on high coherence (greater than 0.95) and stability throughout the time series. This point is located at the coordinates 9.965° latitude and -84.108° longitude (WGS84). The deformation velocity data were then refined using a coherence mask created by LiCSBAS, resulting in a vector point layer. This layer includes the time series of deformation and velocity for each point, providing detailed insights into the geophysical changes of the area.

The MT-InSAR analysis in the study used the SBAS approach, considering the mixed urban and vegetated terrain. The precision of SBAS is about ~2 mm/year in velocity (Morishita et al. 2020). This methodological choice was based on its suitability for the characteristics of the terrain, balancing accuracy and applicability for the diverse land cover. This approach facilitates efficient analysis within JASMIN, the UK's data analysis environment, optimizing both time and disk-space usage. LiCSBAS's processing method includes the automatic identification and removal of interferograms with significant unwrapping errors, enhancing the reliability of the results. This step is crucial for ensuring the accuracy of the MT-InSAR time-series analysis. To further enhance data quality, atmospheric corrections are implemented using GACOS (Generic Atmospheric Correction Online Service for MT-InSAR). Results and discussion

3.1.3. Results and discussion

In this research, reliable time series and velocity data are obtained by using various noise indices for masking. The results indicated deformations in the Central Canton of San José in the range of -2 to 2 mm/year in the Line of Sight (LOS) direction, confirmed through both ascending and descending geometries (Figure 3.2). Validation of these results was conducted with data from the GNSS station located within the study area (AACR GPS; Lat: 9.939, Long: -84.118), as illustrated in the same figure as the LOS velocity maps. This station recorded a vertical displacement rate of -0.97 +/- 1.70 mm/year for the period 2012-2020, consistent with findings reported by Blewitt et al. (2018). Deformation at the GNSS station area is within the sensivity range of the technique of 0 to 2 mm/yr for both geometries, which indicate no detectable motion.

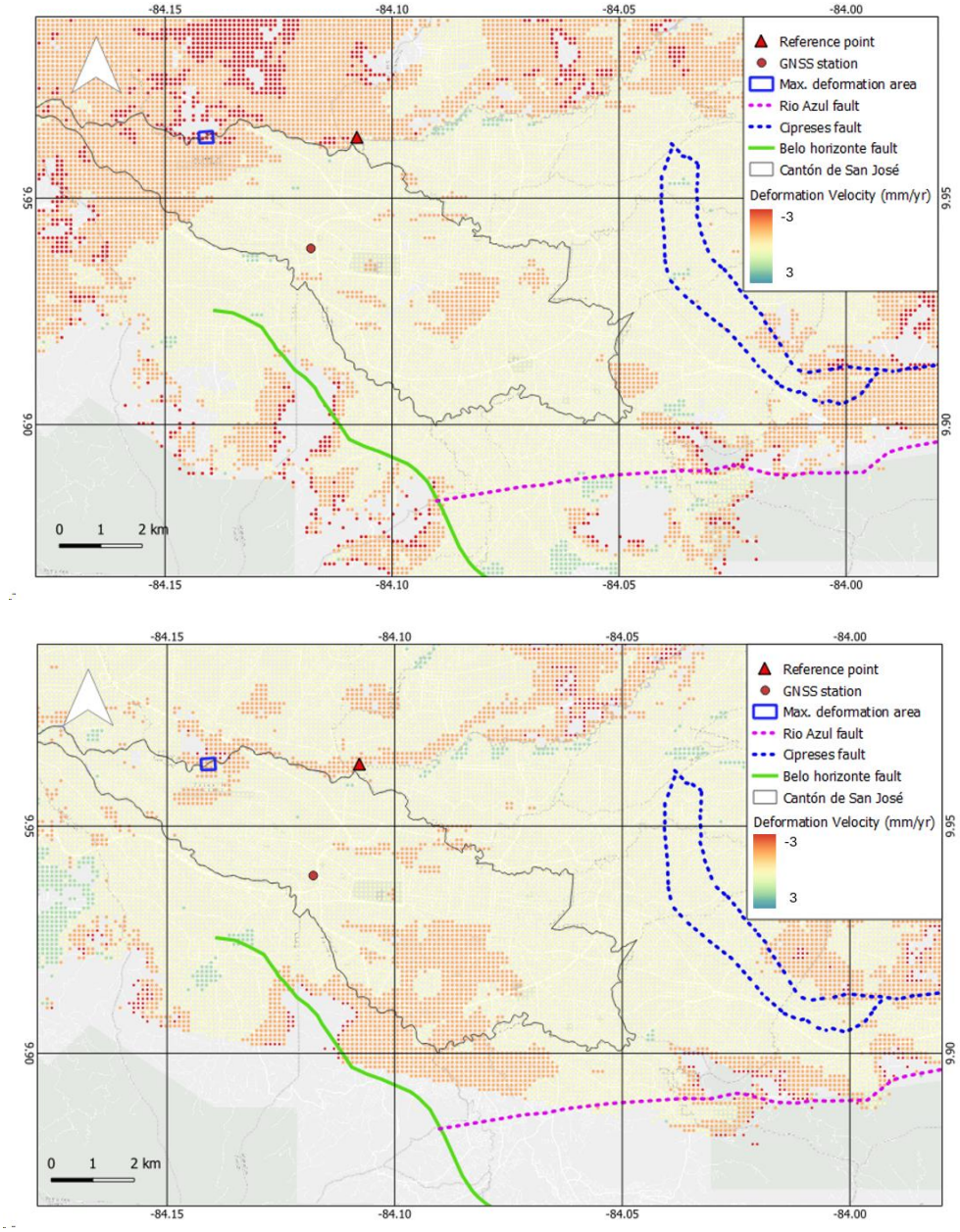

Figure 3.2:Deformation velocities for each geometry (a) ascending and (b) descending. Geographical Reference system WGS84

Figure 3.2 illustrates deformation the velocities using Sentinel-1 data in both ascending (a) and descending (b) geometries, measured in mm/year in the Line of Sight (LOS). The areas around the fault scenarios are depicted with shaded colors. Additionally, each subfigure includes a subset focused on the AACR time series, providing a detailed view of the deformation in these specific areas.

The deformation velocities around the three selected faults were analyzed, revealing estimated deformation rates for the past five years fluctuating between -3 mm/year (LOS) and 3 mm/year (LOS). These values align with the limits of the MT-InSAR's

accuracy, which is approximately 2 mm/year for LiCSBAS, as mentioned by Morishita, Y. et al. (2020). Figure 3.3 presents the frequency of velocity deformation rates (in mm/year) for the Central Canton of San José, considering both geometries.

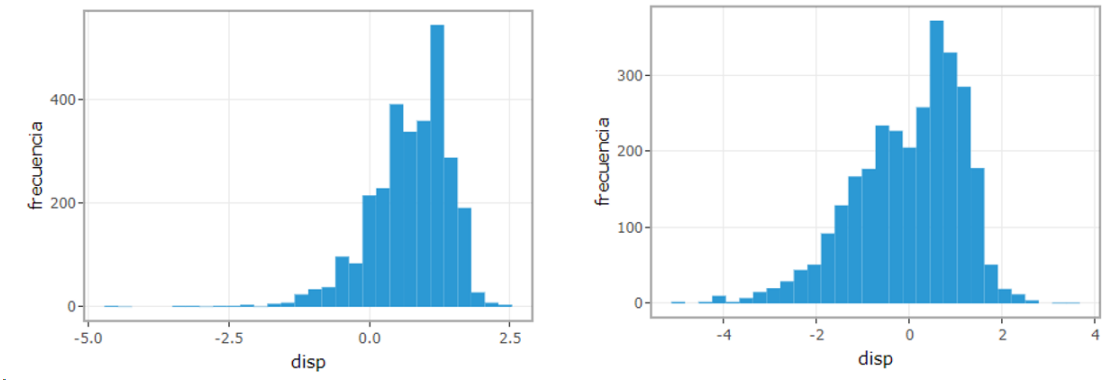

Figure 3.3: Data dispersion graph for Cantón Central, Ascending (left) descending (right)

Deformation pattern over faults area

In the analysis, measurements over the fault traces were primarily conducted focusing on the ascending geometry, as it covers a larger area across these structures. Some parts lacked data points due to coherence issues. Upon closer examination of the surfaces of the faults, it was observed that deformation was within similar ranges as those found in the Central Canton of San José area. The specifics of these observations and measurements are detailed in table 3.1.

Fault	Min	Max	P05	P95	Mean
Belo Horizonte	-3.4	2.4	-1.2	1.7	0.3
Cipreses	-3.5	2.5	-1.1	1.3	0.2
Río Azul	-3.1	2.8	-2	1.3	-0.1

Table 3.1: Metrics for the deformation information across the area of the faults (mm/yr) for ascending geometry

The analysis indicates a stable deformation range within -3 to 3 mm/year in the Central Canton of San José. These measurements align with the GNSS station data in the area, which records a subtle vertical movement. When examining the three faults identified as critical, the detected deformation is less than the prominent left-lateral faults in the Central Valley: the Aguacaliente-Navarro Fault System shows

a gradual deformation of about 1 cm/year (GNSS measurements). Low deformation levels at Bello Horizonte, Cipreses, and Rio Azul faults suggest aseismic energy release or slow strain accumulation, raising the possibility of potential seismic events (Portela Fernández et al., 2020).

Relationship of deformation and local events

The Central Canton of San José exhibits a general deformation pattern within +/-2 mm/yr, although it is noted that some movements might not be detectable within the accuracy range of the LiCSBAS technique (~2 mm/yr). Notably, active deformation patterns are identified around the periphery of the Central Canton, particularly near the steep margins of river courses. These areas of maximum deformation are highlighted in Figure 3.1. Additionally, Figure 3.4 presents the cumulative deformation observed at seven specific points along the margins of the main valley, providing a focused view of deformation in these key areas.

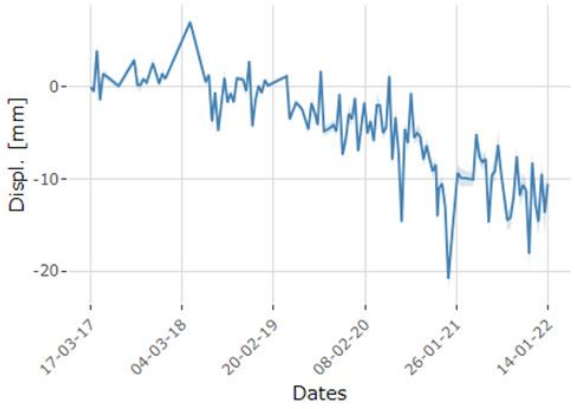

Figure 3.4: Shows the metrics for the deformation time series in an area within the Canton the San Jose, framed in figure 3.1 above

Comparison of identified deformation compared to other areas

The multi-temporal MT-InSAR analysis from March 2017 to January 2022 in the Central Canton of San José reveals low deformation rates, ranging from -3 mm/year to 3 mm/year (LOS). Previous MT-InSAR studies in Costa Rica, such as that undertaken in the Nicoya Peninsula, have shown larger deformations (around 10–15 mm/yr LOS in the Southern coast, as per Xue (2015). Additionally, Araya Rodriguez (2019)conducted MT-InSAR analysis for the period from April 2015 to July 2016, identifying significant deformations between the Caño Negro fault (CNF) and the Upala Fault (UF), with a notable uplift of 6 cm in 2016 and considerable SE horizontal displacement.

3.1.4. Conclusions

The MT-InSAR technique is instrumental in evaluating and understanding seismic risks in urban areas such as San José. The study has demonstrated the ability of MT-InSAR, through the SBAS approach and LiCSBAS software, to provide detailed and reliable data on ground deformation. This capability is crucial for the monitoring of seismic activities, especially in regions with complex fault systems like the Central Valley of Costa Rica.

The research reveals that San José experiences stable deformation rates, with findings from the GNSS station in alignment with MT-InSAR data, suggesting low seismic activity but a potential for future seismic events due to the identified aseismic energy release or slow strain accumulation. These results are particularly significant when compared to other areas of Costa Rica, which have shown larger deformations, underscoring the localized nature of seismic hazards.

Additionally, the analysis of deformation around key faults in the Central Canton of San José provides insights into the dynamics of these faults and their potential impact on the city's seismic resilience. The low deformation levels observed suggest that current seismic risk exists; however, the data is vital for city planners and emergency services to develop effective emergency plans and mitigation measures.

Overall, the application of MT-InSAR in this context underscores the value of this technique in supporting traditional seismic risk assessment methods and enhancing the understanding of urban resilience in the face of natural hazards. The findings from this study contribute to the broader field of geological hazard prevention and offer a template for similar analyses in other seismically active urban areas.

3.2. Volcanic risk in La Palma

3.2.1. Introduction

The 2021 eruption on La Palma is the most damaging and long-lasting eruption since historical records began in the Island of La Palma. According to the Copernicus (European satellite system) disaster monitoring programme (Copernicus Emergency Management Service, EMS), lava flows extended over an area of 1219 ha, affecting, or damaging 3216 buildings, destroying at least 1676 buildings registered in the Spanish basatada, forcing the evacuation of about 7500 residents

(2329 directly affected), while also severely affecting or destroying irrigation systems on several farms, 73.8 km of roads and a 370 ha. of cropland (mostly bananas but also some vineyards and avocado plantations). Initial estimates put losses at more than 1025 million US dollars. The government has assigned 70 million US dollars in direct aid for the local farming and fishing industries in the impacted area. The eruption of the Tajogaite volcano at La Palma attracted the attention of the world due to its wide media coverage and its effects on the population. At least 528 accredited scientists visited the volcano during the eruption to contribute their experience, learn lessons for future events and observe the successful functioning of the emergency management in order to report these observations to their countries. The eruptive event at Cumbre Vieja has been the subject of various research investigations using MT-InSAR techniques. The approaches have been highly diverse, ranging from characterizing the seismicity that preceded and accompanied the eruption (De Luca et al., 2022) , characterizing the underground dynamics (Fernández et al., 2022) or determining the volume and rate of efusion during the eruption to control lava flows (Plank et al., 2023).

The main novelty of this work lies in the analysis of deformation and identification of main patterns seen through MT-InSAR. Subsequently, these results are compared to geodetic and geophysical parameter data from a multidisciplinary perspective, leading to results with important implications for future disaster management planning. More specifically, seismological data and geothermal anomaly results were used to attain a greater understanding of the volcanic processes at the 2021 Tajogaite eruption (Benito et al., 2023).

3.2.2. Data and methods

Study area

La Palma is a salient example of a steep-sided composite volcano. Its volcanic edifice rests on the oceanic crust at a sea-floor depth of 3000 m, and the subaerial topographic elevations reach around 2426 m a.s.l. (meters above sea level). It is a triangular-shaped island measuring 45.5 km from north to south and 27.5 km from east to west at its widest part (figure 2.1). It has an area of 708.4 km^2 The geology of La Palma has been reviewed by (Carracedo et al., 2021).

The surface deformation was monitored during the pre-eruptive and eruptive phases identified in the seismic analysis, through MT-InSAR. Taking into account the nature of the terrain and the slope of the western side of La Palma, the SBAS

approach was selected. The degree of uncertainty using SBAS methods is similar to that of Persistent Scatterers Interferometry (PSI techniques), in the order of~1 mm/year (Lanari et al., 2004).

Data and analysis

LiCSBAS pre-processing allows users to save time and disk space while obtaining the results of MT-InSAR time-series analysis in the frame of JASMIN, the UK's collaborative data analysis environment (Lawrence et al., 2013). During the LiCSBAS processing, interferograms with many unwrapping errors are automatically identified by loop closure and removed. Reliable time series and velocities are derived with the aid of masking using several noise indices. The straightforward implementation of atmospheric corrections to reduce noise is achieved with the Generic Atmospheric Correction Online Service for MT-InSAR (GACOS). The reference points for the analysis were the GNSS stations located in the area, namely LP02, LP03 and LP04 and their displacements were published online (IGN 2021) (Table 3.2).

GNSS station	Latitude N	Longitude W	Displacements (Sep 1- Oct 1, 2021)		
	Degree (WGS84)	Degreee (WGS84)	East (mm)	North (mm)	Uplift (mm)
LP02	28º 40' 03.07"	17º 56' 28.90"	ND	ND	NDX
LP03	28º 34' 45.35"	17º 52' 13.21"	ND	-131	211
LP04	28º 32' 23.27"	17º 51' 59.35"	39	-125	76

Table 3.2: References GNSS stations for the MT-InSAR analysis (2021). ND stands for "not detected at +/- 5 mm resolution". Displacements were estimated from official plots published at IGN

For the analysis of deformation of La Palma Island, we worked with the frames provided by COMET (2021) using the available data from Sentinel-1 A/B. The

frames 060A_00001_030604 and 169D_00001_020800 include 1222 interferograms obtained between January 2019 and December 2021, 522 from Sentinel-1 images on the ascending track 60 and 700 from the descending track 169, respectively (COMET, 2021). A first processing (P1) was carried out "in the middle of the eruption," to check the feasibility of quick MT-InSAR processing during emergencies. This processing included available COMET interferograms from September 1, 2020 to October 14, 2021. They were processed using LICSBAS on a 100*100 m grid, taking the GNSS station LP02 (IGN, 2021) located in the northern block of the island as a reference point. The stability of LP02 allowed the velocities and deformations to be compared with the GNSS stations. Ascending and descending geometries were considered and processed, performing vectorial decomposition to determine net vertical movements as proposed by García et al. (2018) based on the developments by Fialko et al. (2001) and Diao et al. (2016). A second processing (P2) was carried out with the updated interferograms released by COMET in December 2021, providing a longer record on the ascending Sentinel-1 track 60 and descending Sentinel-1 track 169, up to the 1222 interferograms calculated from January 2019 to December 2021 (COMET ;2021). The area of maximum deformation was delineated by selecting the points with velocities over 20 mm/year for the monitored periods, resulting in 2838 points from the 100*100 m grid in P1 processing (September 1, 2020 to October 14, 2021). We calculated the main statistics of deformation (mm) for each date: average, maximum, minimum, standard deviation, 95% percentile and 5% percentile.

The deformation estimated with MT-InSAR was validated with the time series of displacements of available GNSS stations LP03 and LP04, taken from official plots published at the IGN website (2021) using WebPlotDigitizer 4.5. The average vertical deformation time series were calculated for all the deformation points included in the surrounding 500 m buffer of the GNSS stations and were compared with the recorded displacements at these stations.

This section relies on the multidisciplinary work developed by Kuk-Ahpan research group; different analyses were done under the common purpose of understanding the volcanic eruption at Tajogaite in 2021 (Benito et al., 2023), as a result from this work, nine phases were identified in the whole process of the eruption; this was helpful to understand the MT-InSAR results.

3.2.3. Results and discussion

Ground deformation was analyzed in an initial fast response processing (P1) for the period from September 1, 2020, to October 14, 2021. This processing highlighted an area of maximum deformation (ca. 31 km²) on the SW slope of the Cumbre Vieja complex delimited by coordinates 17.9196 W, 28.5213 N and 17.8576 W, 28.6123 N (WGS 84), with uplift velocities of over 20 mm/year. The area is framed by the former Todoque village (North) and the GNSS stations LP03 (East) and LP04 (South) (figure 3.4). The deformation pattern was analyzed during the pre-eruptive and eruptive phases, emphasizing the behavior of the area of maximum deformation with higher uplift velocities than the rest of the island during the monitored period (September 2020–October 2021) (figure 3.5a).

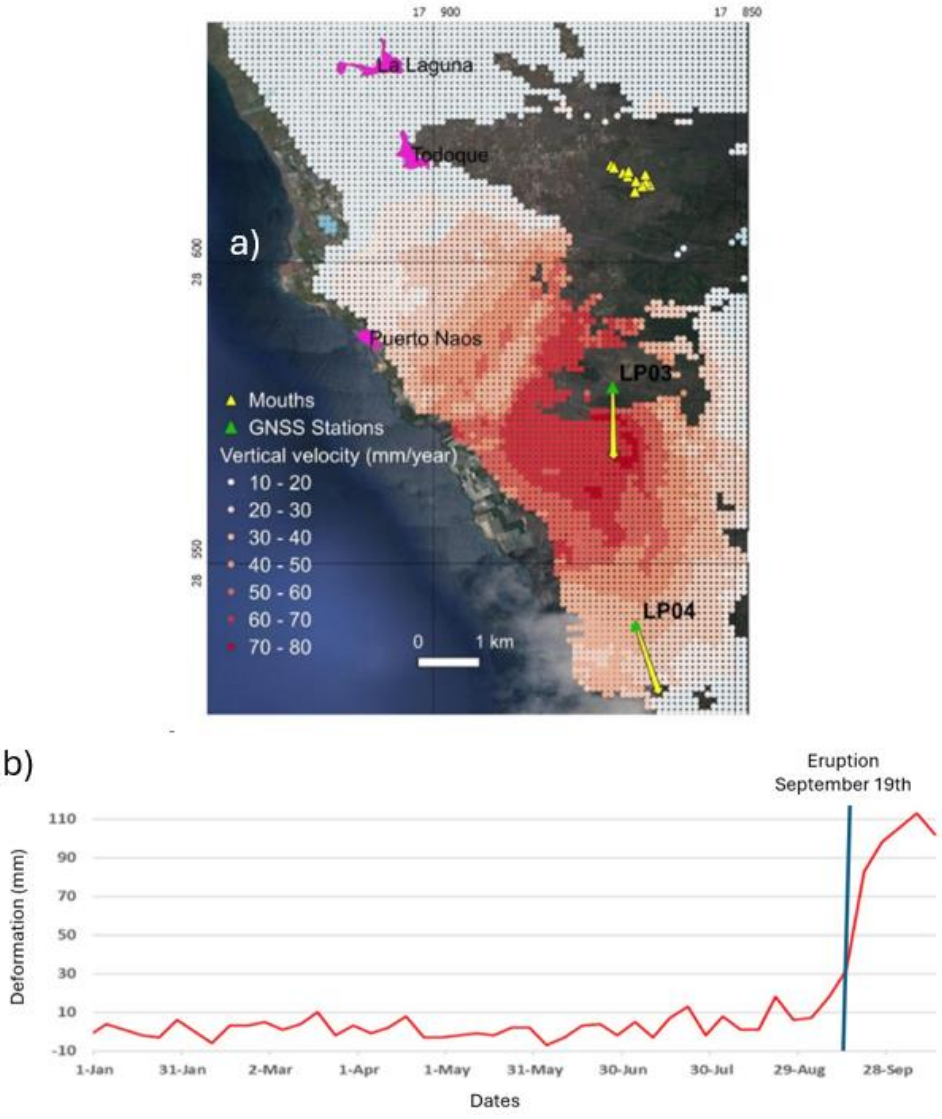

Figure 3.5:A Vertical deformation velocity (mm/year) decomposed from the line-of-sight displacements measured from the ascending and descending Sentinel-1

images (September 2020–October 2021). Yellow arrows show the scaled planimetric displacements of GNSS station (IGN 2021) B Vertical deformation time series of a point (zoomed) at −17.8896 (W) and 28.5943 (N) from the maximum deformation area.

The deformation trend in this area was an uplift that began to increase shortly before the eruption (mid-August) with a breaking point around September 11, after which, deformation accelerated sharply reaching a global maximum by the beginning of October (figure 3.4b). A vectorial decomposition of displacements was performed, integrating the results of Sentinel-1 ascending and descending tracks. The decomposition shows a net uplift movement of the points located at the identified deformation area (figure 3.4b). The vectors of planimetic displacement of GNSS stations were drawn in figure 3.4a based on data presented in Table 2 (IGN, 2021). LICSBAS processing provided few points with deformation time series around LP03 station due to decorrelations, with the nearest point at 427 m (ellipsoidal length). Figure 3.5 shows the comparison of the deformation series of LP03 and LP04 stations with the average vertical deformation of points located within the 500 m buffer (7 points for LP03 and 70 for LP04).

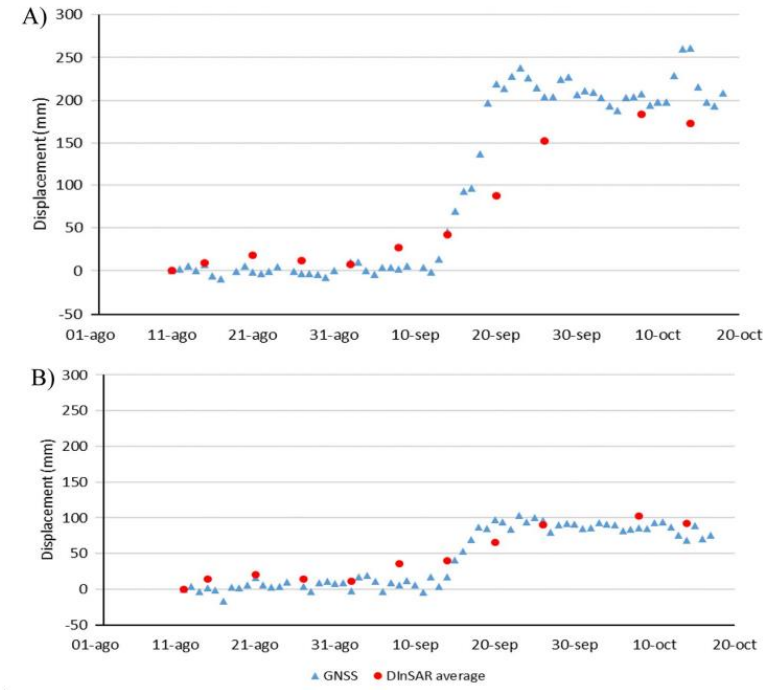

Figure 3.6:Vertical deformation (mm) in the period August 11 to October 18, 2021 measured at GNSS stations versus average vertical deformation of MT-InSAR points in the 500 m buffer of LP03 (A) and LP04 (B)

Benito et al. (2023) defined 9 phases (Figure 3.6) of the eruption which helped the evolution of the event to be analyzed. The differentiation of phases within this study allowed us to identify the way in which deformation data aligns with various volcanological indicators such as eruptive columns, sulfur dioxide emissions, and the emergence of new volcanic vents. This alignment also included geodetic and thermal data, with noticeable pre-eruptive anomalies being observed two months prior to the onset of the eruption. Building on the analysis of recent volcanic activity, the study proposes two potential scenarios for future volcanic hazards. The insights gained from this research could be instrumental in enhancing the current practices in emergency response, monitoring, and prediction of future volcanic events.

The second LICSBAS processing (P2) allowed the pattern of deformations during the identified seismic phases up until December 19, 2021 to be analyzed (Figure 3.6a).

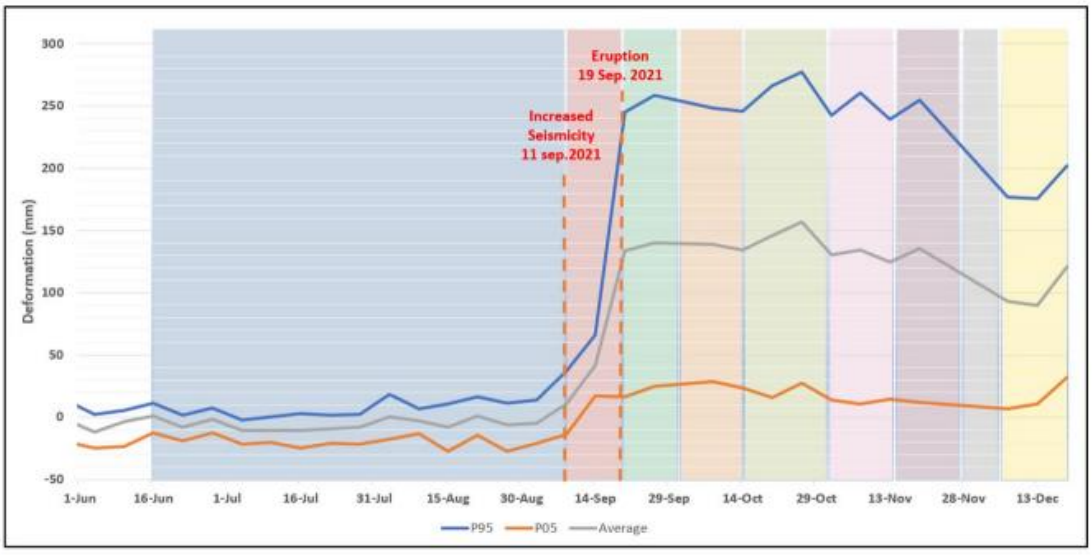

Figure 3.7: Temporal evolution of the pattern of deformation in LOS direction (mm): average, 95% and 5% percentiles for the deformation area processed using LICSBAS with automatic reference point

Note the sharp increase in deformation parallel to the peak of seismicity around September 11, 2021, (Phase 2), eight days before the eruption (September 19). The latter phases showed fluctuations up until the extinction of the volcanic activity. In order to better characterize the pattern of deformation, the velocities of deformation in LOS direction were calculated for each of the identified phases. This analysis allows the characterization of deformation during the pre-eruptive and eruptive periods (Figure 3.7). The results show a net increase in velocities in phase 2, with

relatively stable phases 3 and 4, followed by a reactivation in phase 5. Phases 7 and 8 showed fluctuations up until the end of the eruption.

When integrated with MT-InSAR data, the graph highlights the spatial extent of ground deformation, enriching the seismic activity profile (Figure 3.8). MT-InSAR's precise deformation measurements provide a spatial context to the seismicity, such as correlating ground deformation with the depth and magnitude of earthquakes. Moreover, it aids in cross verifying the rise in volcanic activity, indicated by parameters like the height of the eruptive column and SO2 emissions, with actual surface changes. This integrated approach, leveraging MT-InSAR data, offers a multi-dimensional view of the geophysical processes at play, underscoring the dynamics between subsurface movements and their surface manifestations.

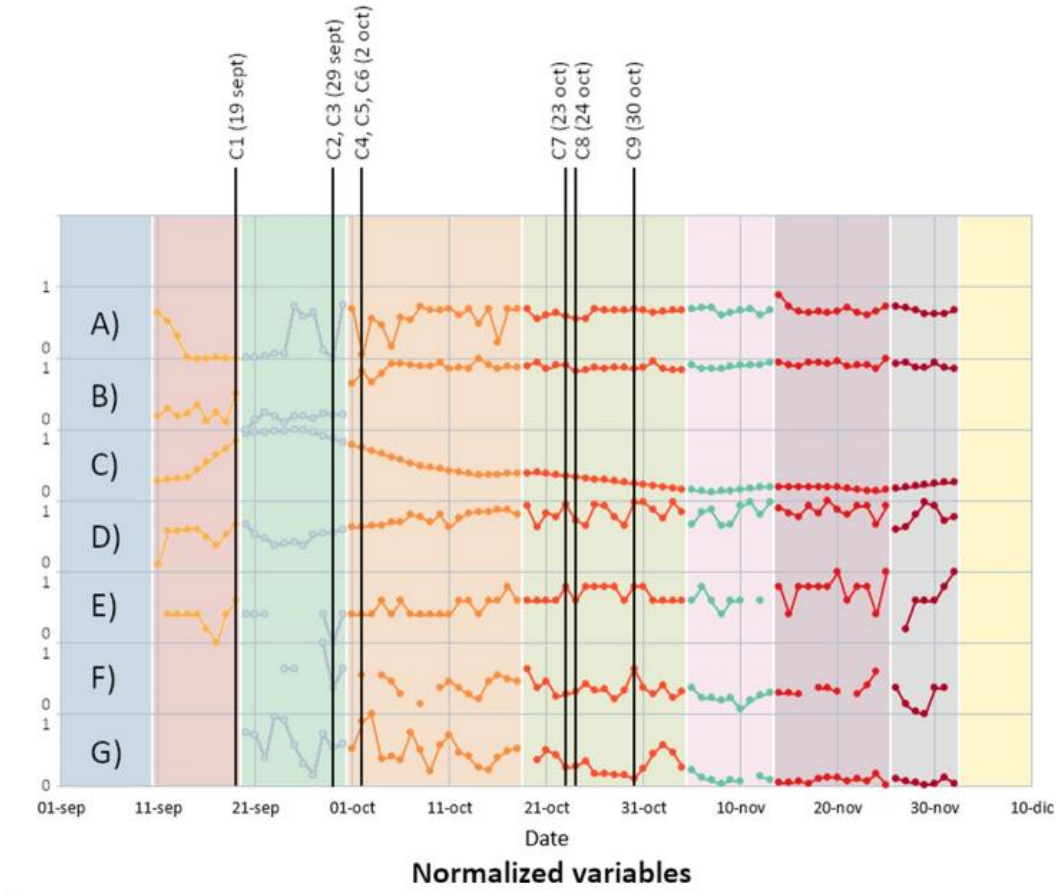

Figure 3.8: Summary of the evolution of different indicators in each of the seismic phases (starting in phase 2). Normalized scales between 0 and 1. The opening of eruptive mouths and their dates are indicated. A minimum depth of the earthquakes, B maximum depth, C deformation of the ground, D maximum magnitude of the earthquakes, E maximum intensity, F height of the eruptive column, G SO2 emissions

3.2.4. Conclusions

This research underscores the significance of pre-eruptive anomalies identified two months prior to the eruption, highlighting MT-InSAR's critical role in predicting volcanic events. Such early warnings are indispensable for implementing effective emergency preparedness and response mechanisms, potentially saving lives and reducing economic impacts.

Integrating MT-InSAR deformation data with additional volcanological, geodetic, and thermal information has revealed a comprehensive view of the underlying processes of the eruption. This multidisciplinary approach not only enhances the accuracy of monitoring volcanic activities but also contributes significantly to hazard assessment. By developing two potential hazard scenarios based on the recent eruptive history of La Palma, this study provides a valuable framework for disaster management and planning, emphasizing the importance of preparedness for future volcanic events.

The findings from this section highlight the potential for improving emergency measurement monitoring and forecasting of future eruptions. Such improvements are essential for enhancing the resilience of communities prone to volcanic hazards. The insights gained from analyzing the Tajogaite eruption through MT-InSAR offer a methodological template for future research in other volcanically active regions. This approach demonstrates the importance of continuous and integrated monitoring efforts in managing volcanic risks effectively.

In essence, this section of the thesis reinforces the value of MT-InSAR in supporting traditional seismic risk assessment methods and advancing the understanding of urban resilience against natural hazards. The comprehensive analysis presented here contributes to the broader field of geological hazard prevention, offering critical insights for the development of more robust emergency plans and mitigation measures in the face of volcanic threats.

3.3. Outcomes

It is evident that MT-InSAR is a robust tool for monitoring deformation related to seismic and volcanic activities. The case studies of San José in Costa Rica and La Palma in Spain offer valuable insights into the capabilities of MT-InSAR techniques. The deformation patterns of the Central Canton of San José suggest a relatively stable ground motion, with the peripheries indicating more activity,

particularly near river margins. In contrast, the 2021 eruption on La Palma provides a scenario where MT-InSAR played a critical role in mapping the deformation related to volcanic activity.

In conclusion, the successful application of MT-InSAR in these geographically and geologically distinct areas underscores its versatility and reliability. It proves that MT-InSAR can make significant contributions to hazard assessment and mitigation strategies. Future work should continue to refine these methods, considering the limitations and opportunities presented by different geological settings. The integration of MT-InSAR with other geodetic and geophysical data remains essential for comprehensive hazard monitoring and risk management

4. Analysis of ground deformation dynamics in Guatemala City with MT-InSAR

Chapter based on the following publication…

García-Lanchares, C., Marchamalo-Sacristán, M., Fernández-Landa, A., Sancho, C., Krishnakumar, V., & Benito, B. (2023). Analysis of Deformation Dynamics in Guatemala City Metropolitan Area Using Persistent Scatterer Interferometry. Remote Sensing, 15(17), 4207.

4.1. Introduction

Research has evidenced that water pumping for urban and agricultural use is one of the primary factors triggering land subsidence (Chaussard et al., 2014, 2017; Engi, 1985; Ezquerro et al., 2020; Koudogbo et al., 2012; Normand & Heggy, 2015; Zhu et al., 2015). MT-InSAR is an accurate tool that can be applied to groundwater management and used to monitor changes in urban areas and predict disasters to avoid economic, environmental, and human losses. The conservation and efficient use of water resources is of great concern to the RMG government. Factors such as climate change, environmental degradation and pollution have contributed to water scarcity in Guatemala (I. R. Herrera Ibáñez & Brown Manrique, 2011; I. Rodolfo Herrera Ibáñez, 2018). Due to population growth, there has been an increase in groundwater exploitation, resulting in lower water levels in some wellfields (I. R. Herrera Ibáñez & Brown Manrique, 2011; I. rodolfo Herrera Ibáñez, 2018; Morales, 2012). In addition, deforestation of hydrographic basins has led to an increase in surface runoff, hence decreasing infiltration into the soil. The sealing of land through construction and urbanization of areas, excessive use of aquifers by public and private entities, lack of regulations and control on the use of water resources along with other factors, threaten the availability of this vital resource (Recinos et al. 2019).

Guatemala City is located in an area that has been affected by highly destructive earthquakes throughout history. Specifically it has suffered 21 major earthquakes, with an intensity on the Mercalli scale greater than VIII (Lang et al., 2009). The study area contains important faults and volcanic elements, with the Mixco and Pinula fault structures being the main faults located within the study area, and Santiaguito, Fuego, and Pacaya being the main volcanoes (Pérez, 2009).

Several sinkholes and some other local events have been identified in the study area. A major sinkhole cited in the literature (Hermosilla, 2012) appeared in the year 2007, measuring 30 m in diameter and 60 m in depth. In the short period between June and October 2022, nine sinkhole events (Domínguez & Vega, 2022), with associated collapsed buildings, were recorded in the study. As mentioned above, this study focuses on diagnosing the patterns of deformation in the main urbanized zones of RMG and aims to locate and quantify the severity of the deformation phenomenon in the area.

The use of MT-InSAR technology is being contemplated as a potentially economically sustainable approach to detect areas of instability. Given the reported

cases in the literature of environmental characteristics and population growth in the area, addressing this case study is deemed important. Understanding the conditions of change is crucial in meeting the most affected areas and can aid in finding the causes and developing solutions to avoid future problems.

4.2. Data and Methods

4.2.1. Study area

The study area encompasses the municipalities of Guatemala City, Mixco, Villa Nueva, San Miguel de Petapa, and Santa Catarina de Pinula. They integrate the RMG (Región Metropolitana de Guatemala), spanning a total area of 47,218 hectares.

The Guatemala City valley lies at the intersection of three tectonic plates: North America, Caribbean, and Cocos. The Cocos plate subducts under the Caribbean plate in the Mesoamerican trench, giving rise to the Central American mountain range of volcanoes. This range has attained its maximum growth in Guatemala, and is characterized by calderic cones and depression outcrops, with acid volcanism represented by rhyolites, ignimbrites, and pyroclasts. The Guatemala City valley can be defined as a graben or trench bounded on the east by the Pinula and on the west by the Mixco faults (Pérez 2009; Guzmán Ramírez 2002). The geological formations in the area consist of granitic intrusive rocks, rhyolitic lava flows, sediments, and tuffs, which constitute the Tertiary volcanic group. Additionally, there are Quaternary volcanic deposits in the form of tephras (pyroclasts) that culminate in alluvial deposits. The geology was reclassified into four classes: alluvium, sedimentary rock, tephra, and other volcanic rocks (Figure 4.1) (Brown et al., 1980; Koch & McLean, 1981; Pérez, 2009; Vaides del Valle, 1973).

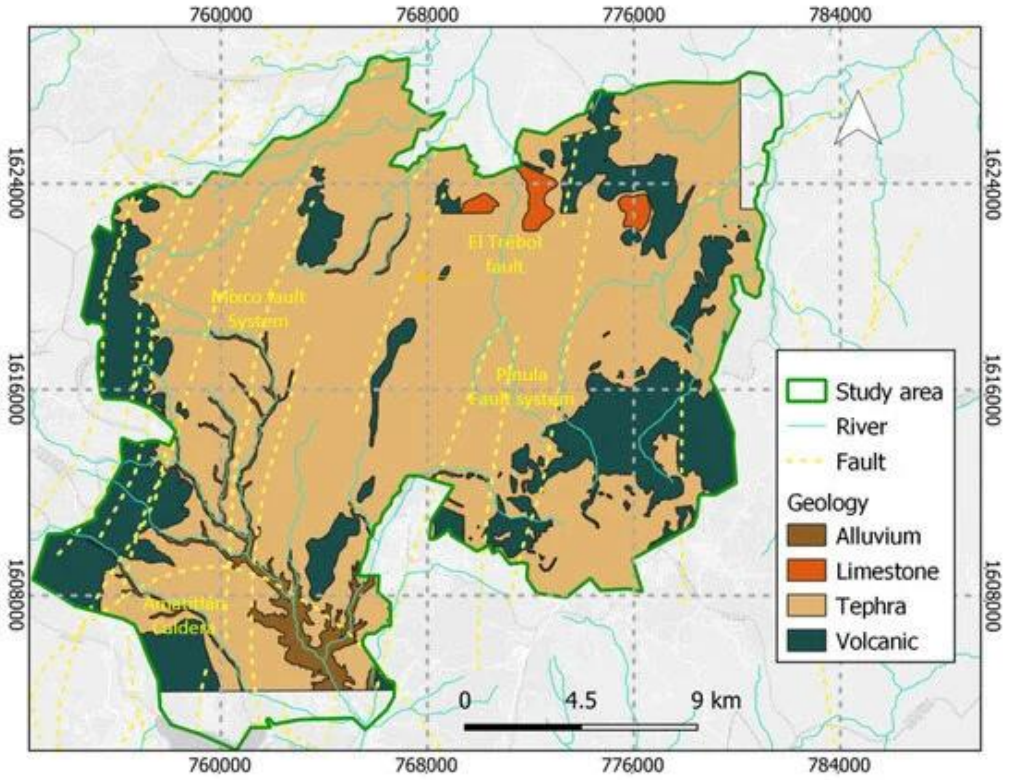

Figure 4.1:Geomorphology, hydrology, and geology of the Metropolitan Region of Guatemala. Projected coordinate system WGS84 UTM zone 15N

The formation process of the Guatemala City valley is intricately linked with the Motagua and Jalpatagua faults, and the zone of distension that arose at their intersection. During the Middle Miocene, the Motagua and Pinula faults became increasingly active (Weyl, 1980) , resulting in the creation of a weaker zone that facilitated the rise of magma to the volcanic structures of the Pinula and El Naranjo volcanoes. While this zone initially served as a channel for magma to rise, continuous movements of the faults in the distension zone eventually led to the formation of the Mixco fault. The shape of the Mixco fault closely follows the contour of the relict structure of the Pinula volcano, and its movements induced the subsidence of the valley and its volcanic structures. The boundary between the depression and the volcanic structure is delineated by the El Trébol fault within the Guatemala City valley (Pérez, 2009). Guatemala City was established as the capital of the country in 1773, after the former capital of Santiago de los Caballeros was devastated by the Santa Marta earthquake (Benito Oterino & Torres Fernández, 2009).

Analyzing isophreatic lines from 1978, 1995, and 2012 (I. Rodolfo Herrera Ibáñez, 2018) , a decline in the water table over the past three decades of exploitation was observed. In sedimentary rock deposits, the water table has decreased by −3 to −5.5 m/year, while volcanic aquifers have decreased by around −3.4 m/yr. Due to uncontrolled exploitation of aquifers without legal regulation, excessive groundwater extraction is taking place in the area, risking premature depletion of the reserves (I. Rodolfo Herrera Ibáñez 2018).

4.2.2. Data

A total of 226 SAR images were processed, including both ascending and descending geometries from Sentinel-1 constellation satellites A and B (Figure 4.2). All images are Single Look Complex (SLC) TOPSAR data acquired in Interferometric Wide (IW) swath mode with VV polarization, for the time frame of January 2017 to September 2021 (Table 3.3).

Satellite	First Image	Last Image	Geometry	Orbit	Images	Polarization	Mean Inc. angle (ª)	Heading Angle (º)
S1A	08/01/2017	08/09/2021	Asc	136	112	VV	39.2	349.3
S1B	12/01/2017	12/09/2021	Desc	26	114	VV	36.5	190.6

Table 4.1: Sentinel-1 image characteristics

The SeNtinel Application Platform (SNAP) version 9.0.0 developed by the European Space Agency (ESA), snap2stamps, and the Stanford Method for Persistent Scatterers (StaMPS) software were used following SNAP-StaMPs integrated processing for Sentinel-1 PSI (Foumelis et al., 2018).

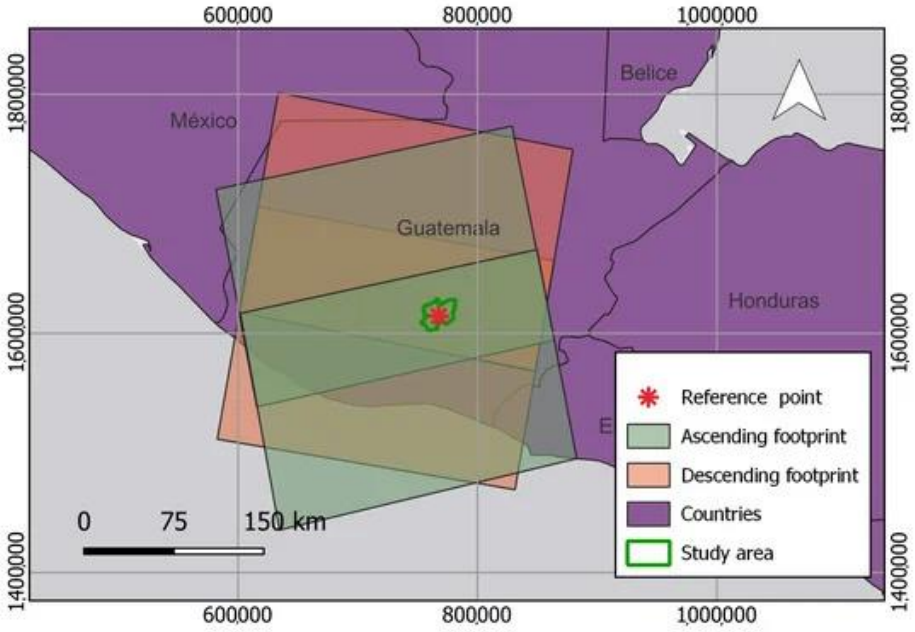

Figure 4.2: Study area and footprints of ascending and descending images. Projected coordinate system WGS84 UTM zone 15N

To achieve satisfactory outcomes, it is crucial to appropriately configure the input parameters for StaMPS processing to prevent the occurrence of non-natural artifacts. StaMPS parameters significantly influence the final results. The characteristics of the analyzed movements impact the processing results, emphasizing the importance of appropriate settings. In our case, default parameter values led to an irregular stepped trend in several PS time series. To address this, parameters related to atmospheric filtering, phase unwrapping, and estimation of the Spatially Correlated Look Angle (SCLA) error have been set to values explained by Balbi et al. (2021). Specifically, these modified parameters introduced in the final steps of StaMPS that allowed us to obtain a more natural trend are as follows: "unwrap_time_win" set to 24 days (default 730 days) to smooth the phase in time by estimating noise for each pair of neighbouring pixels; "unwrap_grid_size" set to 10 m (default 200 m) for spacing of the resampling grid; "unwrap_gold_n_win" set to 8 (default 32) for the size of the window used in the Goldstein filter; "scla_deramp" set to "yes" (default "no") to estimate the phase ramp for each interferogram; and "scn_time_win" set to 50 days (default 365) for the window size of the low-pass temporal filter.

MT-InSAR Processing and Vectorial Decomposition

Both geometries were referenced to a compact area with highly temporal coherence (>0.8) near the GNSS station GUAT (14.590, −90.520) (Blewitt et al., 2018). The reference point is in a flat area (slopes close to zero degrees) over the tephra geology class. Line-of-Sight (LOS) ascending and descending series were combined in a vectorial decomposition to obtain the vertical and east–west displacements. Each point in the ascending geometry is paired with the nearest neighbour point in the descending geometry, not further than a given predefined threshold. This distance threshold has been defined according to the accuracy of the position of the PS. Under the assumption that there is no movement in the north–south planimetry direction, it is possible to decompose LOS movements on the vertical and east–west planimetry directions. For each ascending/descending pair of points, we compute decomposed movements following Equations 4.1 and 4.2. This decomposition approach has been successfully applied in previous studies (Delgado Blasco et al., 2019; Ruiz-Armenteros et al., 2023):

$$d_{east} = \frac{cos\theta^{desc} d_{LOS}^{asc} - cos\theta^{asc} d_{LOS}^{desc}}{cos\theta^{asc} cos\phi^{desc} sin\theta^{desc} - cos\theta^{desc} cos\phi^{asc} sin\theta^{asc}} \quad (4.1)$$

$$d_{up} = \frac{sin\theta^{desc} cos\phi^{desc} d_{LOS}^{asc} - sin\theta^{asc} cos\phi^{asc} d_{LOS}^{desc}}{cos\theta^{asc} cos\phi^{desc} sin\theta^{desc} - cos\theta^{desc} cos\phi^{asc} sin\theta^{asc}} \quad (4.2)$$

Equation 4.1 and equation 4.2

where $dascLOS$ and $ddescLOS$ are the measured displacements in the Line-Of-Sight (LOS) direction for the ascending and descending datasets, θasc and $\theta desc$ are the looking angles for the ascending and descending LOS directions, ϕasc and $\phi desc$ are the horizontal angles of the LOS directions measured from the north in a clockwise direction, and d_{up} and d_{east} are the decomposed mean deformations in the vertical and east directions (Figure 4.3).

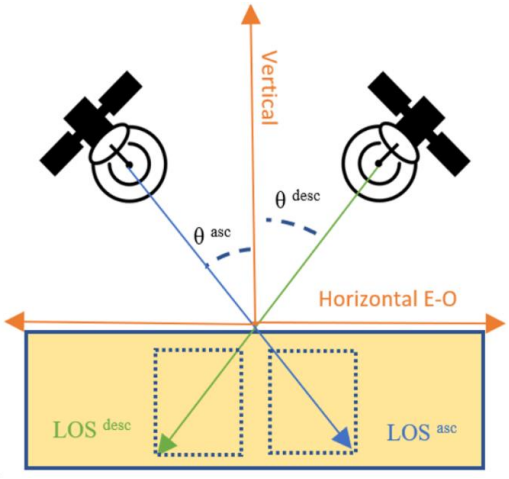

Figure 4.3: Decomposition of the vertical and horizontal (east–west) components of deformation

The combination of ascending and descending PS was performed in the vector domain (Delgado Blasco et al., 2019; Samieie-Esfahany et al., 2009), combining PSs based on spatial proximity. Any PS located in one geometry that lacked neighbouring PSs in the opposite geometry within a designated search radius of 10 m were omitted.

4.2.3. Deformation Analysis and Identification of Critical areas of Subsidence

With the aim of highlighting the existing patterns over the vertical velocity deformation maps, a Jenks classification with six classes was performed with QGIS software (Jenks, 1989; Jenks & Caspall, 1971). Class ranges were rounded to closer multiples of 10, considering the range and variability of vertical deformations in the area of study. Velocity profiles were drawn over the areas with the largest subsidences to perform a qualitative analysis of the trends and patterns of the vertical and east–west deformation average velocities. Kriging techniques (Oliver & Webster, 1990) were applied to delineate the critical areas of subsidence. In the generated rasters, regions displaying subsidence rates exceeding 10 mm/yr were carefully identified and outlined as areas with the most significant subsidence patterns. The administrative zones and the Global Human Settlement Built-up area product (Pesaresi & Politis, 2022) were employed to accurately quantify the extent and severity of the impact on each of these administrative zones.

In order to delve deeper into the analysis and identify consistent patterns of deformation, a comprehensive examination was conducted within the study area. Specifically, relevant Areas of Interest (AOIs) were delineated and characterized, aiming to pinpoint distinct zones exhibiting significant subsidence. These AOIs were defined as areas where vertical deformations exceeded 10 mm/yr and encompassed an area larger than 50 hectares.

The deformation patterns of each AOI were examined independently and in conjunction with other variables. Deformation maps were analyzed jointly with slope (%), elevation (m.a.s.l.), aspect, and geology class. For this purpose, we used a DTM from Alos Palsar-1 (Japanese Aerospace Exploration Agency, 2023) and the geology map classification developed by Intituto Geográfico Nacional in Guatemala (Brown et al., 1980; Koch & McLean, 1981; Ritchie, 1977; Vaides del Valle, 1973) . This map was reclassified according to the four main geology classes that can be found in the area: sedimentary rocks, alluvium, tephra, and other volcanic rocks.

In each of the AOIs, areas representing a subsidence trend were selected. Subsequently, the time series of deformation for these areas were analyzed to assess variations in subsidence trends and accelerations during the specified period.

4.3. Results and discussion

A total of 269,205 PSs were obtained after the decomposition into vertical and east–west directions. A point density of 189 PS/km2 was obtained for the urban surface inside the study area (Figure 4.4). According to the Global Human Settlement Built-up area product(Pesaresi & Politis, 2022), 48% of the analysis area is urbanized, while 51% is vegetated.

The obtained PS density coincides with other studies carried out in urban areas using PSI MT-InSAR (Sadeghi et al., 2021). As expected, information gaps or low-PS density areas correspond to regions with vegetation or complex topography. In situations where subsidence is the predominant process, it can be postulated that the horizontal displacement is directly proportional to the first spatial derivative of the vertical deformation (Kratzsch, 1983; Samieie-Esfahany et al., 2009). By applying this hypothesis, the horizontal displacement reaches zero in the maximum subsidence point and at the edges of the subsidence bowl-like patterns. Conversely, it attains maximum values where the first spatial derivative of vertical deformation is at its maximum, which aligns with observations made in other cases

worldwide (Cigna et al., 2021; Cigna & Tapete, 2022; Kim et al., 2019; Samieie-Esfahany et al., 2009; Zhu et al., 2015).

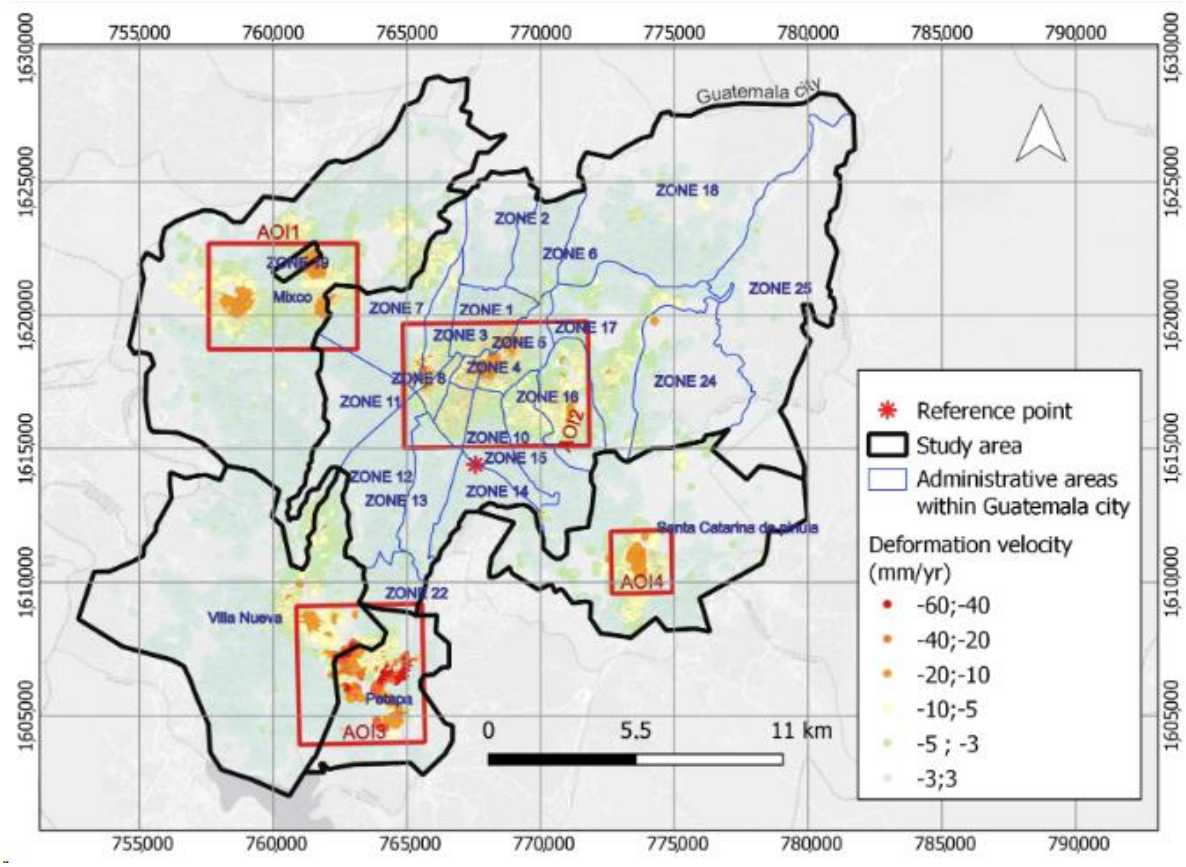

Figure 4.4: General map of the vertical deformation velocities for the study area. AOIs are located across five municipalities (Ciudad de Guatemala, Santa Catarina de Pinula, Villanueva, Mixco, and Petapa), demarcated by black lines, and Ciudad de Guatemala is further divided into 22 administrative zones, represented by blue lines. The projected coordinate system used for the map is WGS84 UTM zone 15N

Administrative Area	Vertical Deformation Velocity > 10 mm/yr (ha)	Total Urban Area (ha)	Ratio (%)
Zone 1	6	609	1
Zone 3	31	246	13
Zone 4	13	97	14
Zone 5	100	485	21
Zone 7	18	955	2
Zone 8	12	150	8
Zone 16	13	416	3
Zone 19	17	97	17
Mixco	185	4560	4
Petapa	355	1242	29
Santa Catarina de Pinula	57	1458	4
Villa Nueva	84	4019	2

Table 4.2: Total urban surface per administrative area affected by vertical deformations over 10 mm/yr

4.3.1. Description of the deformation areas

The areas most affected by deformation in terms of surface are Petapa and Mixco, located in the south and northwest of the study area, respectively, with urban surface areas accounting for 355ha in the case of the former and 185 ha the latter. Santa Catarina de Pinula, Villanueva, and Zone 5 (Guatemala City) also reach subsidences of over 10 mm/yr in areas larger than 50 ha (Table 4.1).

Figure 4.5 presents the distribution of the PS vertical velocities for the main geology classes. This distribution shows that the largest subsidence is located in the alluvium class. The presence of numerous and widely scattered outliers for sedimentary, tephra, and volcanic rock indicates a higher degree of variability and potentially complex deformation patterns in these geology classes.

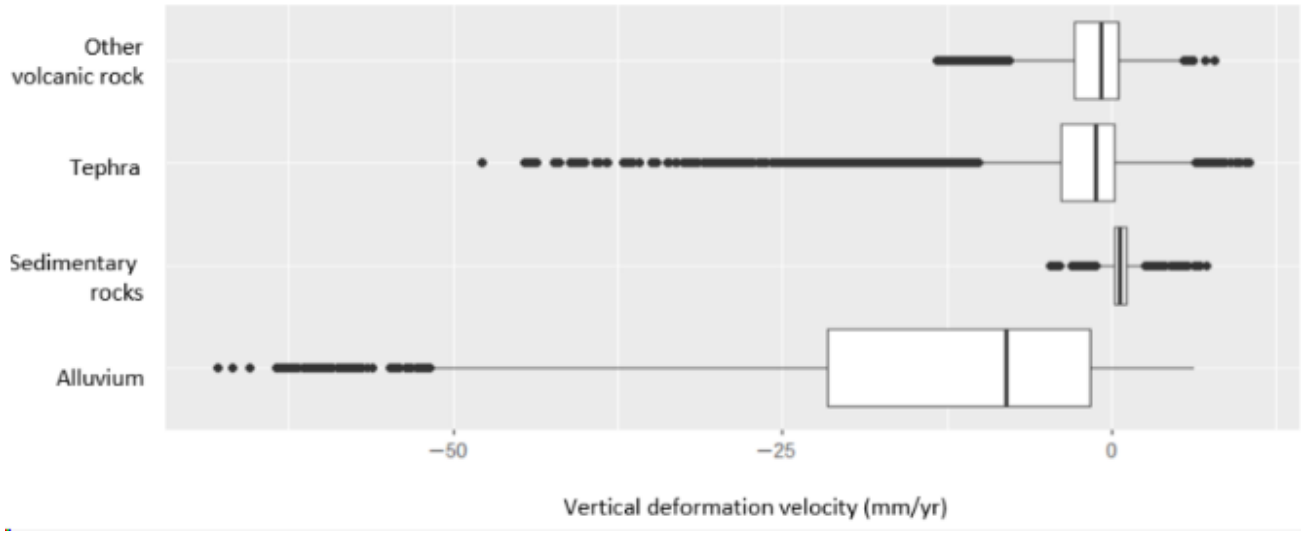

Figure 4.5:Boxplots for PS subsidence velocity and the geology class

Most of the alluvium class is situated in the municipality of Petapa, which coincides with the area where the highest deformation magnitudes have been observed. Non-meaningful results were obtained in the comparison of deformation patterns with the rest of the analyzed variables, such as slope, elevation, and aspect.

4.3.2. Areas of Interest: Critical Areas of Subsidence

Four different AOIs were identified and characterized, all of them presenting subsidence velocities greater than 10 mm/yr in areas exceeding 50 ha (Figure 4.6). These areas are located within the following zones: (i) Mixco and Zone 19 (AOI 1), (ii) historical area (AOI 2), (iii) Petapa and Villanueva (AOI 3), and (iv) Santa Catarina de Pinula (AOI 4). In all these areas subsidence velocities exceed 20 mm/yr, reaching up to 6 cm/yr in Petapa/Villanueva.

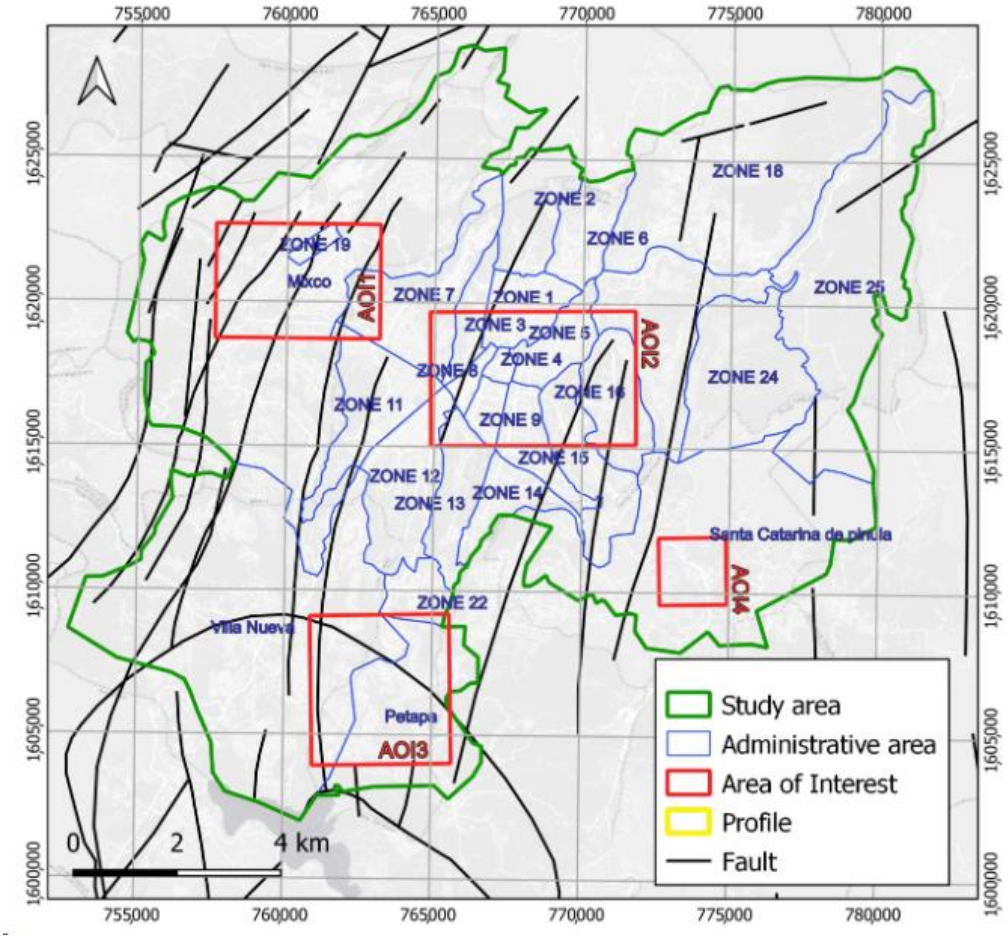

Figure 4.6: Administrative areas, geological structures, and critical areas of subsidence (AOIs) in the Metropolitan Region of Guatemala. Projected coordinate system WGS84 UTM zone 15N

The largest areas affected by subsidences of over 10 mm/yr are in AOIs 1 (Mixco/Zone 19) and 3 (Petapa/Villanueva), which reach 216 and 440 ha, respectively, representing 1% and 2%, respectively, of the total urbanized surface area in the RMG.

Figure 4.7 (AOI 1, 2, and 4) and Figure 4.8 (AOI 3) present the vertical and east–west planimetry deformation patterns in the AOIs. Figure 4.9 presents the corresponding profiles of vertical and horizontal deformation for the selected cross sections. Subsidence bowl-like patterns, or depression cones, with a radial displacement in planimetry towards the center of maximum subsidence, were detected in AOI 1 (Mixco and Zone 19), AOI 2 (historical area), and AOI 4 (Santa Catarina de Pínula). In AOI 1, three subsidence zones were identified. The subsidence in Zone 19 exhibits a subsidence bowl pattern, while in the Mixco subsidence area, western PSs were not obtained due to dense vegetation, hindering

the confirmation of a subsidence bowl pattern. However, we observed westward movements in the eastern part of that region. The third one, located south from Zone 19, shows net subsidence.

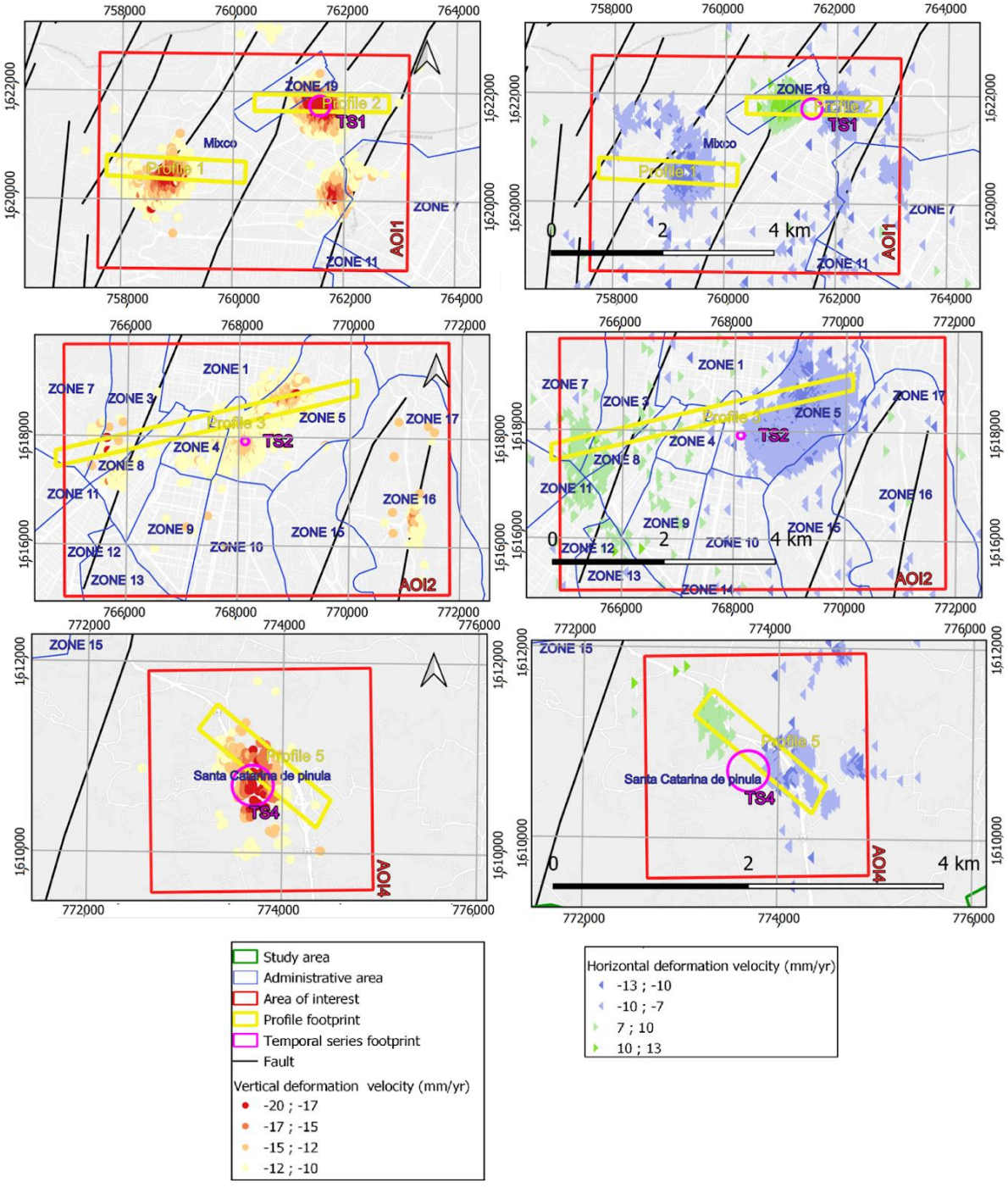

Figure 4.7: Deformation patterns for AOIs 1, 2, and 4 showing vertical (left, red–yellow) and horizontal (right, blue–green) deformations over 10 mm/yr and 7mm/yr, respectively. Yellow rectangles indicate the location of the velocity profiles and pink circles show the location of the selected PS time series for each Area of Interest. Black lines indicate geological features. Projected coordinate system WGS84 UTM zone 15N

In AOIs 1, 2, and 4, we identified a pattern coherent with these subsidence bowl deformation processes, or depression cones, associated with groundwater extraction. This pattern is characterized by convergent horizontal deformations (eastward movements in the western margin and westward movements in the eastern margin) towards the areas of maximum subsidence. North–south displacements cannot be estimated due to the geometry of the image acquisition and further decomposition; therefore, the movements along the north–south axis could present the same order of magnitude as the east–west movements, thus fitting the theoretical 3D cone shape. These conical strains have maximum deformation velocities in the centre of the areas that taper to the edges. This phenomenon was documented by (Hu et al., 2009) in the Yang-tze delta, revealing a discernible correlation between groundwater extraction and a temporal and spatial pattern of land subsidence. A previous study in Guatemala (Kim et al., 2019) confirms the patterns appreciated in the present study, compatible with depression cones caused by aquifer extraction.

Zhu et al. (2015) identified an area in northern Beijing with deformations of 55 mm/yr in the vertical component, partially matching the theoretical distribution of a groundwater subsidence cone. This study attributes the irregularities to the unequal thickness of the deposits. However, groundwater volume analysis using the MT-InSAR technique is not fully feasible without accurate knowledge of the lithology and stratigraphy of the study area (Ezquerro et al., 2020). Calibration data are also required for the validation of groundwater management models. The need for consistent information is one of the major challenges in hydrogeology (Castellazzi et al., 2016).

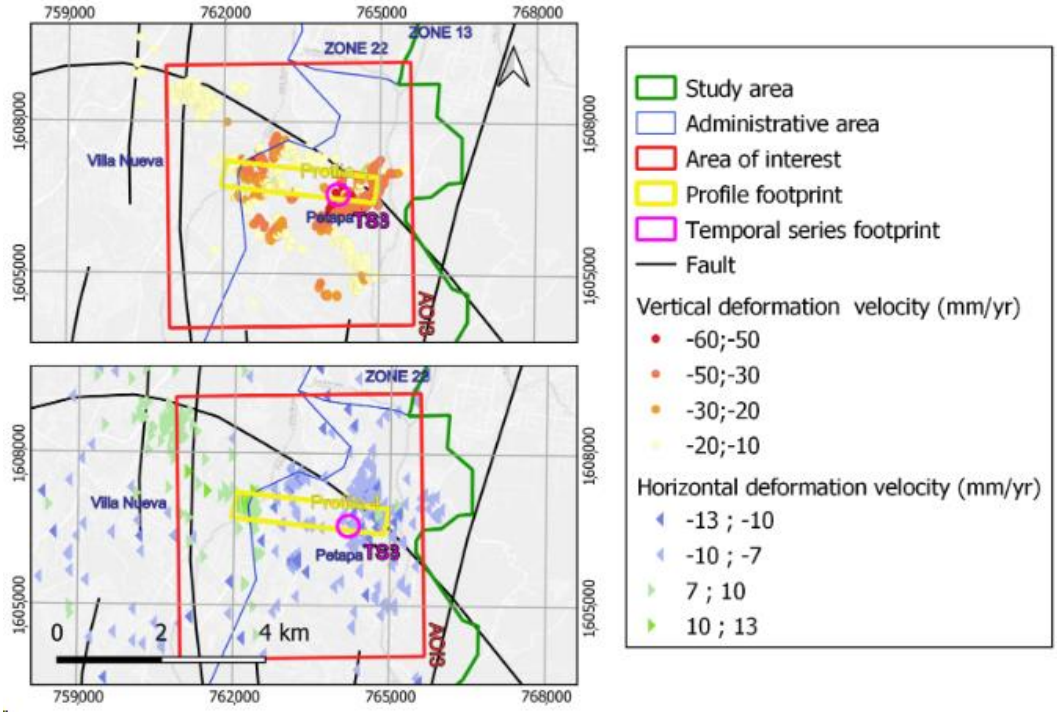

Figure 4.8:Deformation patterns for AOI 3 (top, red–yellow) and horizontal (bottom, blue–green) deformations over 10 mm/yr and 7mm/yr, respectively. Yellow rectangles indicate the location of the velocity profiles and pink circles show the location of the selected PS time series for each Area of Interest. Black lines indicate geological features. Projected coordinate system WGS84 UTM zone 15N

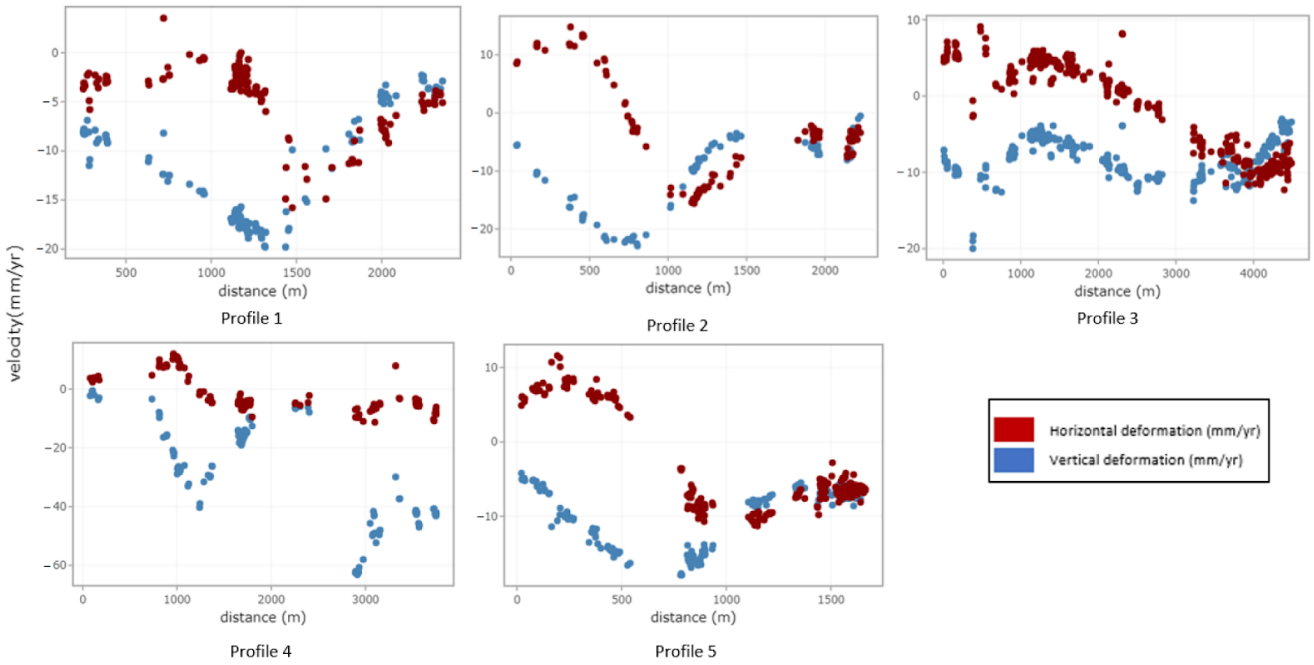

Figure 4.9:Longitudinal profiles of horizontal and vertical deformation velocities (mm/yr) for the sections displayed in Figure 4.7 and Figure 4.8

4.3.3. Deformation time series

Figure 4.10 shows representative deformation time series for each of the subsidence areas in the AOIs (footprints of selected areas located in Figure 4.7 and Figure 4.8. For AOI 1 (Zone 19), the time series integrates the deformation of 47 points situated at the center of the subsidence area, covering an area of 6.1 ha. The average subsidence velocity for this time series is 21.28 mm/yr. Notably, there is a sudden increase in subsidence velocity, commencing after October 2018. As for AOIs 2, 3, and 4, their respective time series exhibit average subsidence velocities of 13.4 mm/yr, 59 mm/yr, and 16.2 mm/yr. These values were calculated based on 48, 58, and 74 points located within the subsidence areas, spanning 1.4 hectares, 3.4 hectares, and 2.9 hectares, respectively.

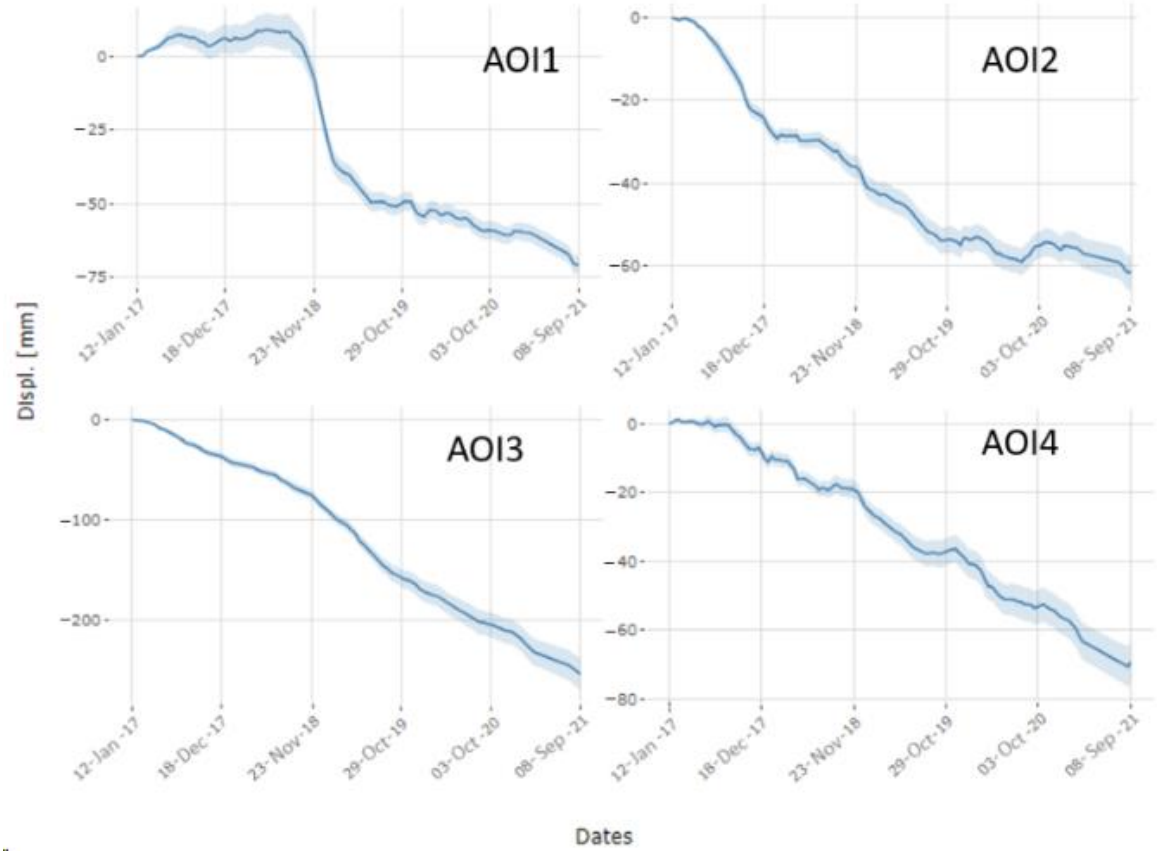

Figure 4.10: Representative deformation time series for the subsidence areas in the four identified AOIs, displayed as pink circles in Figure 4.7 and Figure 4.8. Time series show the pattern of several PSs (ranging from 47 to 74), where the bold continuous blue line shows the average time series of all selected PSs, and the light blue shadow represents the standard deviation of all these selected PSs

All these time series show different trends. The time series of AOI 1 shows a sudden increase in subsidence velocity starting from October 2018 to May 2019. The times series of AOI 3 show an increase in velocity from October 2018, while the time series of AOI 2 show a slight deceleration from October 2018 and a stronger deceleration from October 2019. Subsidence velocity remains constant for the time series of AOI 4 over the entire study period.

Kim et al. (2019) conducted a previous MT-InSAR study in a subset of the area of study in Guatemala City, for the period between late 2014 and March 2018 (Kim et al., 2019). Comparison of the observed patterns from this previous study with those of the present study reveals a general agreement, considering the limited overlap of only 15 months and the different areas of analysis. The behavior of the central historical area (AOI 2) shows similar results in both studies, with a maximum subsidence deformation of 27 mm/year, consistent with our findings for the overlapping period. Similarly, east–west deformation shows similar patterns. There are other areas in (Kim et al., 2019) that present no significant deformations in our study period (January 2017–September 2021). The first of these is located in the southeastern area of administrative Zone 6 (north of AOI 2), with a measured subsidence of up to 17.5 mm/year between 2014 and 2018. However, in our longer time series (2017–2021), this area showed mean subsidences of under 5 mm/year, explained by the double deceleration that the time series shows for October 2018 and October 2019 (Figure 4.10). There are also two subsidence areas located in administrative Zones 10 and 14 (south of AOI 2), consistent with Kim et al. (2019). However, our results show no meaningful subsidence in central administrative Zone 16 (eastern AOI 2) due to a lack of PSs.

Deformation time series for AOI 1 (Figure 4.10) shows a sudden increase in subsidence velocity starting from October 2018 to May 2019. This area is affected by the Mixco fault system (Guzmán Ramírez, 2002; Pérez, 2009). The change in the time series coincides in time with two registered earthquakes of over 5.4 Mw reported on October 12th and 18th 2018 (United Stated Geological Survey, 2018).

In AOI 2, the subsidence and east–west deformations expand over the entire AOI, indicating either a wide subsidence bowl or a combination of diverse subsidence processes, as shown in the profiles in Figure 4.9. AOI 4 also shows a pattern compatible with a subsidence bowl or depression cone pattern. In these AOIs (1, 2, and 4), the subsidence velocities reached 20 mm/yr, while the planimetry magnitudes remained below 13 mm/yr.

The results for AOI 3 show that the deformation points are mainly located within the boundaries of the Amatitlán caldera, with a significant concentration of PSs displaying an eastward movement within the Amatitlán caldera and along the southern part of the Mixco fault system (Bohnenberger, 1996). In this AOI, the planimetry magnitudes remained below 13 mm/yr, as in the other AOIs, but subsidence velocities reached up to 60 mm/yr.

The deformation time series of AOIs 2 and 3 show trend changes after October 2018: the time series of AOI 2 decelerate, while the time series in AOI 3 accelerate. Analyzing the possible effects of seismic events in triggering deformation dynamics would appear to be of considerable importance. The velocity profile of AOI 2 (Figure 9) shows a subsidence bowl pattern in the first part of the profile. The distribution of the vertical deformations in the profile shows different overlapping areas of subsidence, which suggests a combination of different driving processes (water extraction, geological activity, anthropogenic works, etc.).

In AOI 3, the alluvial sector in the south of the study area presents higher values of subsidence, coinciding with an area of water extraction. The deformation pattern is intense and more uniform than in the other classes of geology. This behavior can be related to three phenomena: first, water withdrawal in Ojo de Agua, which is the group of water wells from which around 72% of the groundwater from the aquifers of the central valley is extracted (Herrera & Orozco, 2010; I. Rodolfo Herrera Ibáñez, 2018); second, alluvium areas happen to be prone to seismic hazards (Blissenbach, 1952; Davis, 1925; Eckis, 1928; Sharp & Nobles, 1953); third, its location at the boundaries of the Amatitlán caldera and the presence of associated faults (Bohnenberger, 1996).

The characterization of the deformation patterns in the RMG opens up new avenues for investigating their origins and can lead to improved urban and infrastructure management practices. Further research in this area would enable the identification and anticipation of local events, such as landslides and sinkholes, as well as the monitoring of infrastructure during construction and operation. Developing a historical database of such incidents would facilitate the application of machine learning algorithms to predict future events and plan appropriate measures to mitigate potential harm and losses.

Moreover, the integration of data from other SAR sensors (such as L-band and X-band) and combination with other MT-InSAR algorithms (Berardino et al., 2002) based on distributed scatterers would prove advantageous, particularly in regions with challenging topography or dense vegetation. L-band SAR data could improve

the monitoring in vegetated areas, whereas distributed scatterer processing would provide results in the less coherent areas. Conducting small-scale investigations that incorporate physical and environmental data, along with detailed GNSS information, would further support future research efforts and enhance the validity of our findings.

As an illustrative example, we refer to a recent news report by García and Kestller in September 2022 (García & Kestller, 2022) , highlighting how several buildings in the municipality of Petapa have been affected. Petapa municipality reached maximum subsidence velocities exceeding 6 cm/yr in our study. This demonstrates the real-world implications and significance of studying deformation patterns for the betterment of local communities and infrastructure management.

4.4. Conclusions

The results of this study indicate that the application of MT-InSAR in the Central American region can provide valuable insights into surface deformation dynamics and associated risks. MT-InSAR also provides valuable information for urban planning and management, allowing authorities to identify areas of potential disaster and take appropriate action and/or planning measures.

This research confirms that MT-InSAR PSI processing is a competent method for characterizing deformation patterns in the Metropolitan Region of Guatemala (RMG). However, the intricate topography and dense vegetation in the area posed challenges with regard to accurately characterizing the deformation patterns. Further research is necessary to combine data from different SAR bands, such as using the vegetation penetration capabilities of L-band and combining PSI and distributed scatterer algorithms to complete the characterization of the identified deformation patterns. Critical areas in the RMG were identified for the monitored period. The delineation was based on qualitative analysis and Jenks classifications. Future studies will focus on clustering and machine learning methods considering time series of relevant variables and time-precise variations based on registered events (such as earthquake records).

Additional research is needed to characterize some of the observed deformations, such as the subsidence bowl patterns, which are currently depicted in the literature as depression cones induced by water withdrawal processes. Furthermore, these patterns should be verified alongside the water extraction and precipitation data records.

It is also recommended that we analyze the influence of tectonics and geological factors in the observed deformation patterns, excluding other driving forces, such as anthropogenic activities. The study area is traversed by dense geological structures (faults, calderas, etc.) and complex river networks, making it difficult to characterize the relationships between deformation dynamics and causative factors. In the case of tectonics, a reliable database of events and affected areas and structures is required to conduct a thorough analysis. The collection and consolidation of these data pose a challenge due to the lack of resources or governance structure in some countries.

5. Study of the relationships between hydrogeological dynamics and land deformation in Guatemala City

Chapter based on the following publication…

García-Lanchares, C., Marchamalo-Sacristán, M., Fernández-Landa, A., (2024). Using MT-In SAR to analyze the influence of groundwater management on land subsidence in the Metropolitan area of Guatamala City (Publication ready to send)

5.1. Introduction

This section addresses the relations between observed deformations and groundwater management in Guatemala Metropolitan Region, an area characterized by multiple deformation processes. This study focuses on understanding and characterizing these phenomena through various methodologies and data collected from multiple sources. García-Lanchares et al.(2023) identify and characterize the main deformation processes in Guatemala City, reporting multiple causes and proposing a more in-depth analysis of this issue. The Metropolitan Region of Guatemala, characterized by a diverse and active geological framework (Andretti, 1978; Denyer, n.d.), has historically recorded recurrent earthquakes, landslides, and local subsidence phenomena (Domínguez & Vega, 2022; García-Lanchares et al., 2023; Kim et al., 2019). The localized vertical deformations typically reach -20 mm/year, reaching values below -60 mm/year in the area between Villanueva and Petapa municipalities. García-Lanchares et al. (2023) applied the MT-InSAR SNAP StaMPS algorithm to detect and characterize these processes in 22 zones of the main city and 4 municipalities. (see figure 4.5)

Several precedents suggest that one of the causes of these phenomena in Guatemala City may be the intense extraction of water to supply the increasing population. The identification of subsidence bowl patterns in basins identified through the MT-InSAR technique suggests a direct relationship with the extraction of groundwater, a phenomenon globally recognized and evidenced in metropolises like Jakarta (Abidin et al., 2011) and Semarang; Mexico (Cigna & Tapete, 2022; Figueroa-Miranda et al., 2018; Zhu et al., 2015). In Guatemala City, the monitoring of management and hydrological characterization has been relevant as evidenced in hydrogeological and geological studies (Herrera & Orozco, 2010; I. Rodolfo Herrera Ibáñez, 2018; JICA, 1986; Morales, 2012). These studies emphasize the need for continuous monitoring in response to the strong demand and the need for sustainable urban development

Context of Guatemala City: Population and water resources

The demographic growth in Guatemala, particularly in its metropolitan areas, has led to a considerable increase in the demand for natural resources. According to Tzampoglou et al. (2023) technological advancements have contributed to an exponential increase in industrial and agricultural production, as well as extensive urbanization, predominantly in large cities. This phenomenon is directly linked to increased use of water resources, as described by Bahri (2012). Bahri notes that

migration to urban areas and their expansion generates a growing demand for water for various uses, leading not only to its intensive extraction but also to its contamination.

The XII Population Census and VII Housing Census indicate that Guatemala's population stands at 14,901,286 individuals (Instituto Nacional de Estadística Guatemala, 2019), with an annual growth rate of 1.8% between 2002 and 2018. The Department of Guatemala, encompassing Guatemala City and 16 additional municipalities, hosts the most significant percentage of the country's population, accounting for 20.2% of the total. This growth has led to increased infrastructure development and the exploitation of resources such as groundwater. Between 2017 and 2019, the construction of 2 to 3 million square meters was authorized, with 45% of these new construction areas corresponding to the municipality of Guatemala. Construction and urban growth must be carried out within a framework that considers risk assessments and disaster risk reduction (UNISDR, 2010). The use of land sensitive techniques to disaster risks, urban planning, safe construction, and robust infrastructure will not only contribute to improve water management but will also protect lives and properties, thereby benefiting cities.

In terms of water resources, the sources for domestic use in and around Guatemala City are diverse, encompassing rivers, groundwater, lakes, and springs. These are vital for supplying potable water and fulfilling other domestic and industrial requirements of the population. The dependence on these resources emphasizes the crucial need for integrated and sustainable management of urban water to tackle the challenges arising from urban sprawl and population increase. Persistent groundwater depletion or overexploitation can result when groundwater extraction surpasses its recharge across large areas and over extended durations, as indicated by Gleeson et al. (2010) and Wada et al. (2010).

Hydrologic background

Documented investigations into the hydrogeological framework and utilization of wells in Guatemala City started with the INSIVUMEH, IGN, UN in the study Andretti (1978), also by the Japan International Cooperation Agency JICA (1986). This research, centered on tracking aquifer levels, prompted the drilling of many wells that would eventually see widespread use. Additional studies in this field have been carried out by Jacqueline Imelda Morales (2012), and Herrera and his team (2010, 2011, 2018).

In the context of the metropolitan aquifer, the research by Morales (2012) provides crucial data to enhance water extraction systems and to develop management and prevention strategies. This study focused on determining the water table level of 32 wells, evaluating their spatial and temporal variation, and the annual extraction rate, identifying critical wells in various sectors. The temporal piezometry series of this work, covering the period from 2000 to 2011, has been instrumental in understanding the evolution of water resources in relation to the current situation.

Herrera underscores the significance of managing aquifers sustainably, alerting to the ramifications of overexploiting them. Despite efforts to monitor the situation, Guatemala lacks comprehensive hydrogeological maps essential for the effective utilization of groundwater. Moreover, Herrera (2018) study underlines the diverse geological and climatic conditions in Guatemala, noting a lack of in-depth hydrogeological research. The upcoming decade is expected to see a heightened demand for groundwater in the nation, driven by over-extraction and the contamination of surface water, highlighting the need for more efficient water resource use and identifying aquifers nationwide for the exploitation and conservation of groundwater (Herrera Ibáñez, 2018). Therefore, it was necessary to define and characterize the volcanic aquifers that not only supply potable water but also meet the industrial and irrigation needs of the communities above them, hence aiding the sustainable development of the nation (Herrera Ibáñez, 2018). The key reference is a manual by Alvarado et al. (2013) which addresses the management of water resources in Guatemala City, providing a basis for their utilization.

Additionally, within the context of piezometric analysis, there are two more recent references. Recinos et al. (2019) conducted a general analysis of flow networks in the municipalities that formed the 2012 Mancomunidad Gran Ciudad Sur, comprising Mixco, Villanueva, Amatitlán, Petapa, and Villa Canales. This group aims to coordinate legislative actions within the context of the water situation. One of the most significant outcomes of this study is the provision of spatial information on the variation in equipotential piezometric surfaces of the groundwater level and the directions of the main groundwater flows. In figure 5.1, a simplification of the main emission and reception zones of water flows for the year 2018 can be observed.

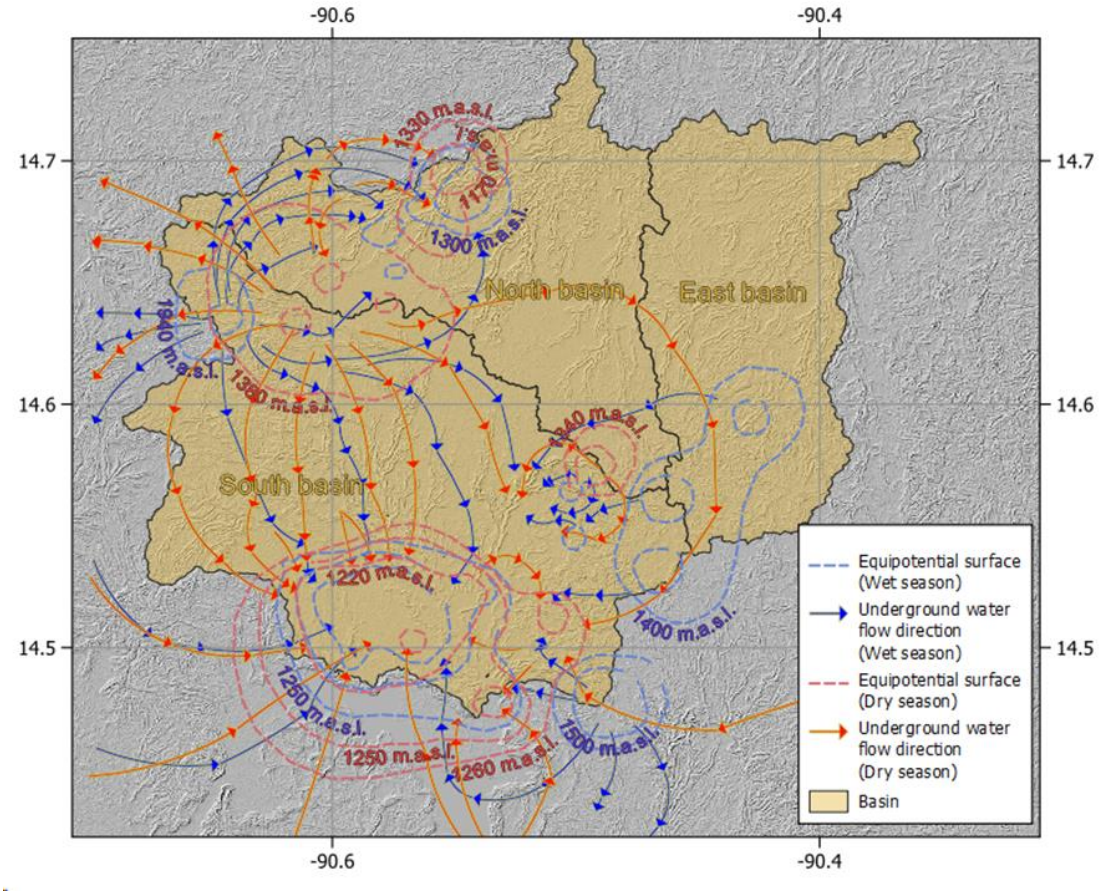

Figure 5.1: Study area showing the three main basins, underground flow directions and equipotencial surfaces for each season (wet and dry). Geographical Reference system WGS84 (Elaborated from Funcagua, 2019)

The evolution of the groundwater level can be observed for a representative well within each basin in Figure 5.2. All three of them show constant depletion on the water level. Historical series records for the east basin are only available from the year 2000, since this was the last area to be settled and therefore the area where natural resource consumption is most recent.

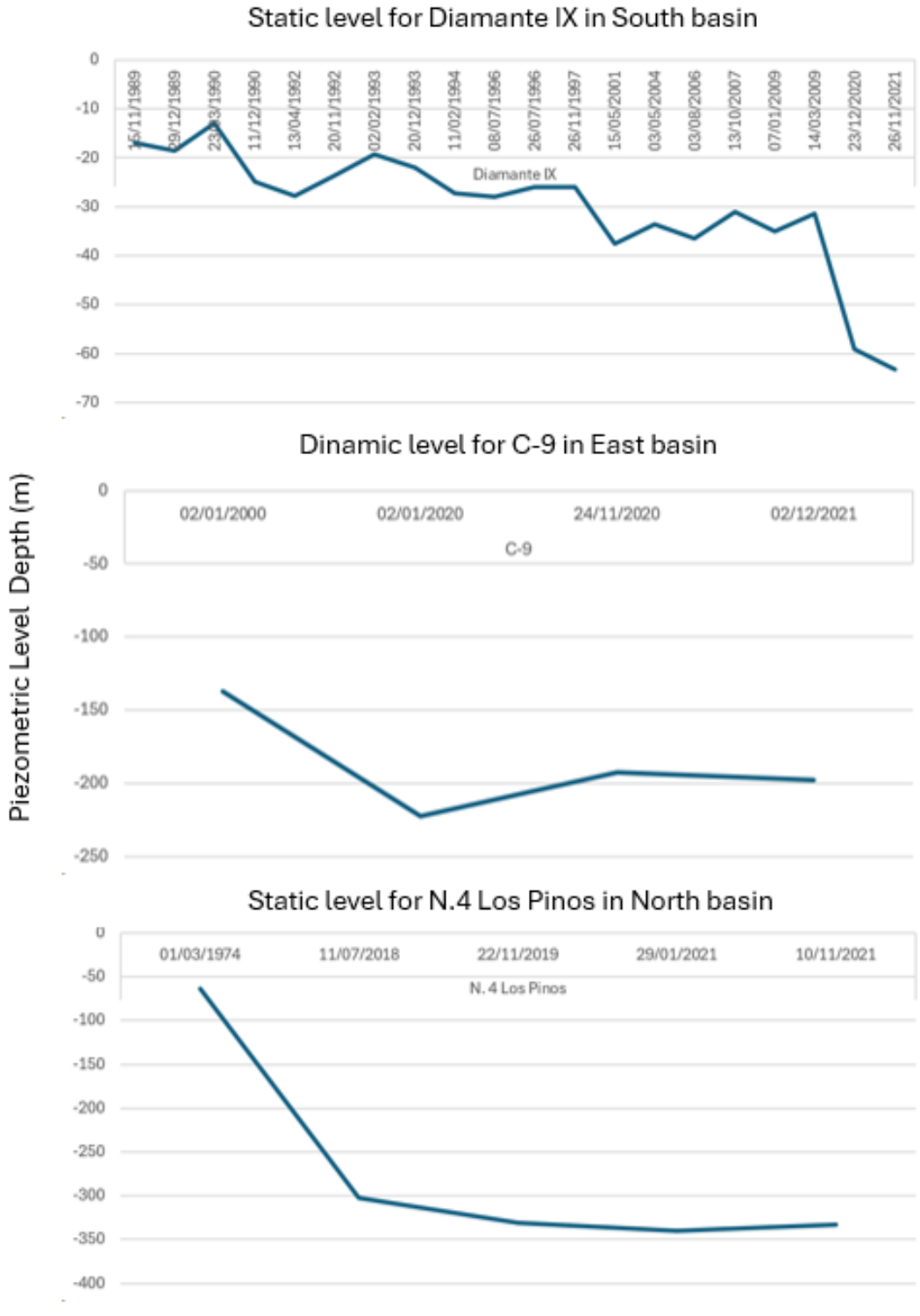

Figure 5.2:Historical series for reference wells piezometric level for each of the basins (Morales, 2012; Recinos et al., 2019)

Finally, the most recent historical piezometric information is of vital importance since it also provides a more detailed geological and hydrogeological characterization of Guatemala City. Empagua et al. (2023). This research was carried out by Empagua, the AECID, and the IGME (2023). The data obtained from this study, through various techniques over the period 2020-2023, have been crucial for this research.

MT-InSAR as a tool for water management

Various spatial remote sensing techniques can be utilized to study the overexploitation of groundwater and its consequences for human settlements without the need to rely on extensive field data campaigns. These techniques include multispectral imaging, radar, and gravimetry. Among these,MT-InSAR (Massonnet & Feigl, 1998) has proven effective in studying the response of aquifers to over-pumping (Galloway & Hoffmann, 2007) and its impact on urban infrastructures (Bru et al., 2013), as well as in several other cases presented in table 5.1.

Reference	Study area	Max vertical sub (mm/yr)	Time range	Method	Geology	SAR Sensor
Castañeda et al., 2009	Zaragoza (Spain)	17	1995-2000	SBAS	Alluvial	ERS-1/2
Cigna et al., 2021	Aguascalientes valley (Mexico)	140	1996-2002	SBAS	Alluvial/Fluvial	ERS-1/2
		100	2003-2010			Envisat
		120	2014-2020			Sentinel-1
Navarro-Hernández et al., 2023	Geediz Rivere Basin (Turkiye)	90	2016-2021	SBAS	Alluvial and lacustrine sedimentary rocks	Sentinel-1
Foroughnia et al., 2019	Tehran (Iran)	130	2004-2010	PSI	Colluvial	Envisat
		150	2014-2017			Sentinel-1
Tamayo Duque et al., 2023	Bogota (Colombia)	60	2014-2021	PSI	lacustrine, fluvial, and fluvioglacial clay	Sentinel-1
Coda et al., 2019	Campania (Italy)	15	1992-2000	PSI	Pyroclastic-alluvial-lacustrine complex	ERS-1/2
		16	2002-2010			ENVISAT
Putri et al., 2013	Jakarta (Indonesia)	1750	2010-2013	DINSAR	Alluvial	TerraSAR-X
Osmanoğlu et al., 2011	Ciudad de Mexico	300	2004-2006	PSI	Alluvial	Envisat

Table 5.1:References on MT-InSAR study cases of subsidence due to water withdrawal

In this complex scenario, the use of Synthetic Aperture Radar Interferometry (MT-InSAR) has proved to be as a valuable tool. According to research by Castellazzi et al. (2016), Galloway et al. (2007), and Bru et al. (2013), MT-InSAR has proven effective in studying the response of aquifers to overexploitation and its consequences on urban infrastructures. For example, in Ezquerro et al. (2014) the correlation analysis conducted between displacement and piezometric time series provides a correlation coefficient of over 85% for all wells, demonstrating its efficacy in such applications. Despite its usefulness, it has been observed that MT-InSAR does not detect deformation dynamics equally in all soil structures or for every depth (Radutu et al., 2017). For example, F. Chen et al. (2012) shows that Quaternary sediments are highly related to significant displacements (primarily at a rate of −15 to 15 mm/yr), although other significant structures such as faults should be considered to establish a characterization of an area. The same authors suggest that different sediments with different porosities can induce uneven displacement trends, which should be considered in city planning. Furthermore, Ezquerro et al. (2014) showed that in the case of the detritic aquifer of the city of Madrid, the correlation between displacement and piezometric measurements is four times higher for linear behavior than for non-linear. However, the specific impact of soil types on the capabilities of MT-InSAR requires further investigation.

In the case of Guatemala city, periodic general measurements have been conducted at same wells along with other hydrological factors, as corroborated by various studies (Alvarado et al., 2013; Andretti, 1978; Ezquerro et al., 2014; Herrera & Orozco, 2010; I. R. Herrera Ibáñez & Brown Manrique, 2011; I. rodolfo Herrera Ibáñez, 2018; JICA (Agencia de Cooperación Internacional del Japón), 1986; Morales, 2012; Velásquez, 2018).

This study focuses on assessing the extent to which water extraction can be monitored via remote sensing tools, a method that is increasingly necessary given the urgent need for cost-effective and globally applicable techniques to study groundwater depletion and its impacts, as highlighted by Famiglietti (2014) and Castellazzi et al. (2016). This endeavor is supported by literature highlighting the role of hydrogeology in explaining the correlation between hydrogeology and MT-InSAR analyses, as seen in studies by Castellazzi et al. (2016), Chaussard et al. (2017), Cigna et al. (2021), Ezquerro Martín (2021) and Galloway & Hoffmann (2007).

Research Questions and Objectives

The growing interaction between urban development and hydrogeological dynamics in Guatemala City raises significant challenges and critical research questions. Given the intensification of water resource usage and the subsidence of certain areas due to water extraction, it is crucial to explore how subterranean characteristics impact and are impacted by such extraction. In this context, the question arises of whether there is a correlation between the velocities detected by MT-InSAR and specific soil characteristics. Moreover, the study aims to understand whether there are any particular qualities that make the soil more prone to collapse and whether it is possible to identify areas which are less vulnerable to subsidence due to water extraction.

The primary goal of this study is to analyze and explain the piezometric evolution in the metropolitan area of Guatemala City and its adjacent municipalities, using data provided by the MT-InSAR SNAP-StaMPS technique. This research will focus on hydrogeological characterization and soil variational behavior. Despite limitations due to the sample size and the scale of cartographic and hydrogeological data, the aim is to shed light on underground dynamics. The relationship between piezometric differences and deformation rates observed by MT-InSAR will be examined, with a particular focus on characterizing water wells based on their location, depth, and lithological features. Additionally, potential areas for intensive monitoring will be identified, where further piezometric measurements could more accurately reflect the actual state of the aquifer. This comprehensive approach seeks to provide a deeper understanding of how water resource management and urban design can adapt to the complex geological and hydrological conditions of the region, thereby contributing to the long-term sustainability of Guatemala City and its surroundings. Hence, the main questions addressed in this study are as follows:

- Is there a relationship between deformation rate detected by MT-InSAR and the piezometric measurements?
- What is the relevance of the specific soil characteristics in Guatemala City and its adjacent municipalities?
- Which are the geological types where deformations are more related to aquifer variation?

5.2. Material and methods

To address the above stated questions and goals, an overview of the analyses conducted is provided. This includes a statistical analysis aimed at examining the direct correlations between MT-InSAR data and piezometric information. As highlighted in the introduction, the hydrogeological characterization was given significant attention. Therefore, data were categorized based on this characterization. Owing to the constraints of the available data, this environmental characterization was estimated by drawing on prior studies undertaken in the same study area.

5.2.1. Study area

The primary area covered by the data encompasses three basins that comprise the urban area, consisting of Guatemala City and adjacent municipalities. These basins are typically referred to as east, north, and south basins (Figure 5.1).

The hydrogeological framework of the area under study is determined by both regional and local tectonic events, as described by (F. Hu y Wu 2018). This is marked by a system of blocks that undergo subsidence and uplift, interconnected throw hydrogeological process primarily through open fractures perpendicular to fault planes and horizontal joints. Active zones for water storage and circulation are present in the subsided blocks, which exhibit regional continuity. These subsided blocks are recharged by water coming from the uplifted blocks, with this recharge being transmitted via a network of lateral cracks and fractures. This network facilitates the direct connection of porous materials with the fracture system, thus aiding the movement and distribution of groundwater in the studied area.

The composition of blocks includes various types of strata or aquifers, which may be interconnected. These aquifers can be categorized based on origin, behavior, or, most commonly, location. There are two main types of aquifers distinguished by their vertical location and differentiation: the lower and upper aquifers. The thickness and composition of these aquifers vary depending on their specific location.

- **Upper alluvial aquifer:** The study area is extensively overlain with volcanic ash, pyroclastic materials, and alluvial deposits, with the latter being nearer to the

surface. According to JICA (1986), these volcanic sediments have been shaped by river erosion, creating deep, branched gullies with depths varying from 150 to 250 meters. Superficial aquifers are located within these sediment layers. The alluvium constitutes a notably shallow aquifer, generally under 50 meters deep, with the extracted water primarily designated for non-potable uses. These aquifers are situated in valley beds and colluvial deposits formed from Quaternary erosion on the slopes. Given the significant reduction in flow during droughts and hydraulic connection to rivers, these aquifers are not regarded as viable for hydrogeological exploitation, owing to their depletion risk. Additionally, they lack both vertical and horizontal continuity. The alluvial sediments consist of rounded pebbles, gravels, sands, silts, and clays, presenting average permeabilities between 3.8 and 14 m/d.

- **Upper Pyroclastic Aquifer:** The aquifer composed of pyroclasts or volcanic fillings can extend to depths ranging from 200 to 400 meters. Its transmissivity depends on the material's porosity. Rainfall infiltration recharges this aquifer type, but at some levels, such compactness occurs that it restricts permeability. In terms of watershed divides, it is conceivable that two pyroclastic bodies, each in a separate basin, might form distinct aquifers. Pumice pyroclasts exhibit primary permeability, typically in the medium range of 1.3 to 20 m/d, attributed to the abundance of fine materials and the compaction of these materials.

The zone of hydrogeological significance is defined in a vertical extent, beginning at an elevation of 1,100 meters above sea level, encompassing a layer about 400 meters in thickness. The stratigraphy of this zone varies depending on geographic location and is primarily made up of volcanic tuffs, tertiary-era lava flows, and ignimbrites from the base upwards. The presence of these materials plays a crucial role in shaping the hydrogeological properties of the region, affecting both the availability and the dynamics of the groundwater movement in the area (Recinos et al., 2019).

- **Andesitic and basaltic lava formations,** due to their nature, exhibit depositional structures, consolidation processes, and a notable tendency to develop open fractures. These features, along with their hardness, render them effective aquifer materials. On the other hand, the local sedimentary rocks, comprising limestone and dolomitic limestone, are equally recognized as suitable aquifer materials because of their high degree of tectonization. This aspect is conducive to aquifer system development, with their efficiency reliant on connections to broad recharge

zones that support the renewal and preservation of subterranean water resources (JICA, 1986).

- **Lower Andesitic Lava Aquifer:** Found at deeper levels, this aquifer is composed of hard and impermeable material derived from old volcanic flows. Its water storage is confined to areas that are fractured or have significant structural discontinuities, such as faults. Water recharge occurs not only from infiltration from the overlying strata but also from surface outcrops. The aquifer, formed by a combination of dacitic and andesitic lavas and some layers of welded vitric tuffs, has average permeabilities between 1.7 and 32 m/d. (JICA, 1986)

- **Lower Limestone Aquifer:** Comprising ancient, isolated limestone, this aquifer system operates distinctly due to its reliance on conduits rather than pore spaces. (JICA, 1986) The intrinsic porosity of the limestone varies, and its secondary permeability in carbonate aquifers results from the dissolution of bedding planes, fractures, and faults, rendering them highly anisotropic and heterogeneous. The permeability values range from 0.1 to 18 m/d. Consequently, there are highly variable transmissivity rates: from 10 to 80 m2/day in less fractured rocks, 250 to 500 m2/day in moderately fractured limestone, and 1,000 to 5,000 m2/day in extensively fractured limestone (I. Rodolfo Herrera Ibáñez, 2018).

Characterization of Each Hydrological Basin

Finally, a detailed examination of the various types of aquifers present in each basin will be conducted. Along with the explanation of each of the basins, figures 5.3 and 5.4 provide insights into hydrogeologic structure.

- **Northern basin**: corresponding to the Las Vacas River basin, which is fed by the Chinautla and El Zapote rivers. Geologically, this area is marked by the uplift of the Cretaceous carbonate basement. Here, Tertiary volcanic rocks to the south with thicknesses of 500 m and Quaternary pumice pyroclasts with thicknesses of 40 to 120 meters can be observed. The limestones outcrop in the middle part of the basin and reach thicknesses of 600 m. Water circulation is limited, with values of 3 liters/second, and the environment is highly fractured. In the northern basin of Guatemala City, two aquifers are identified: one of limestones in the central and northern parts, and another volcanic aquifer formed by tuffs and volcanic lavas, both exhibiting secondary permeability due to fracturing (Herrera Ibáñez, 2018).

Moreover, while there used to be approximately 150 drilled wells (Andretti, 1978); it is now estimated that there are around 1,000 drilled wells, both municipal and private.

- **Southern basin**: As detailed by (Hererra Ibáñez & Barrientos, 2016), the hydrogeological units in this area are illustrated in Figure 5.4. This area encompasses fractured volcanic formations, pumice pyroclastic deposits, and the alluvial materials of the Villalobos River. The volcanic components, made up of dacites, andesites, and Tertiary welded tuffs with thicknesses exceeding 500 meters, form the saturated zone and a fissured environment or a rock formation with fractures. In contrast, the unsaturated zone primarily consists of Quaternary pumice pyroclasts. In the southern section near the Villalobos River, the river's fluvio-lacustrine sediments and alluvium are saturated and make up a phreatic upper aquifer. It is estimated that there are currently more than 500 wells in the basin, according to data from the Institute of Agriculture, Natural Resources and Environment of Rafael Landívar University and The Nature Conservancy (IARNA-URL and TNC) in 2012.
- **Eastern basin:** The hydrogeological structure of this basin is characterized by fractured volcanic rocks from the Tertiary period. These include vitric welded tuffs and basaltic andesitic lavas, which are over 500 meters thick, creating a saturated zone that extends beyond 200 meters deep. Additionally, the unsaturated zone is primarily made up of Quaternary pyroclastic deposits, with thicknesses between 80 and 120 meters observed in the northern and southern regions of the basin. While 60 wells have been documented in this area, the estimated total number of wells is believed to be around 100 (Hererra Ibáñez & Barrientos, 2016).

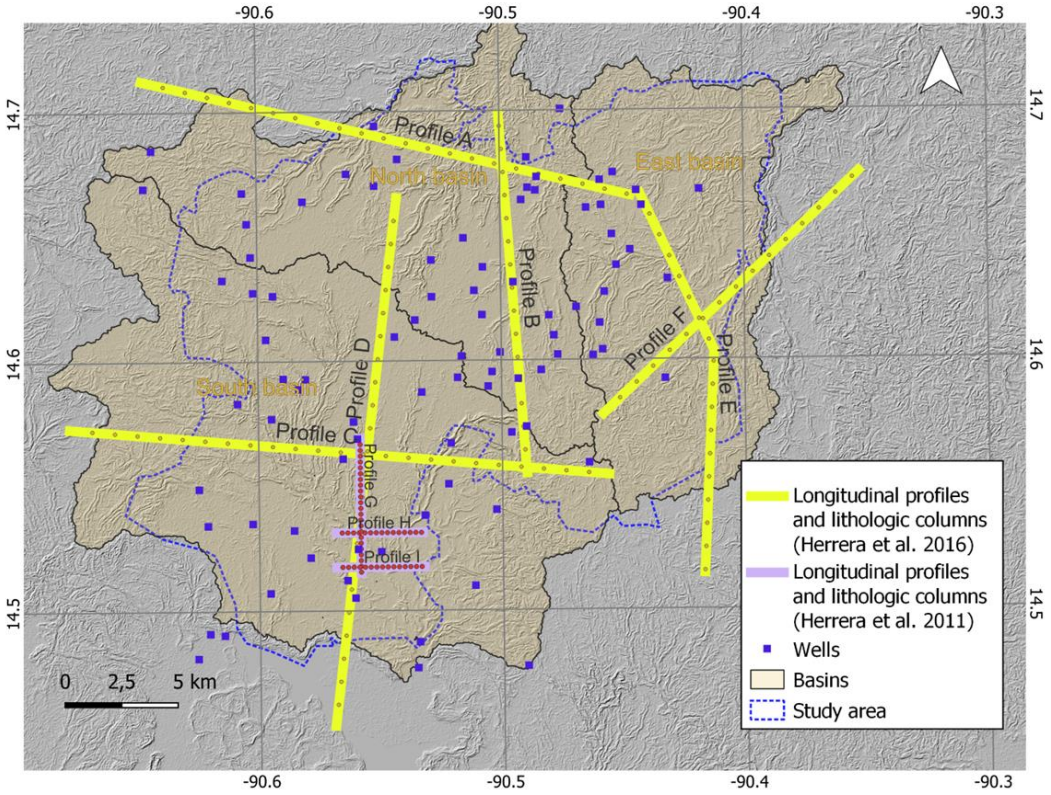

Figure 5.3: Lithologic profiles used for acquiring the data (Herrera Ibáñez & Barrientos, 2016, 2018)

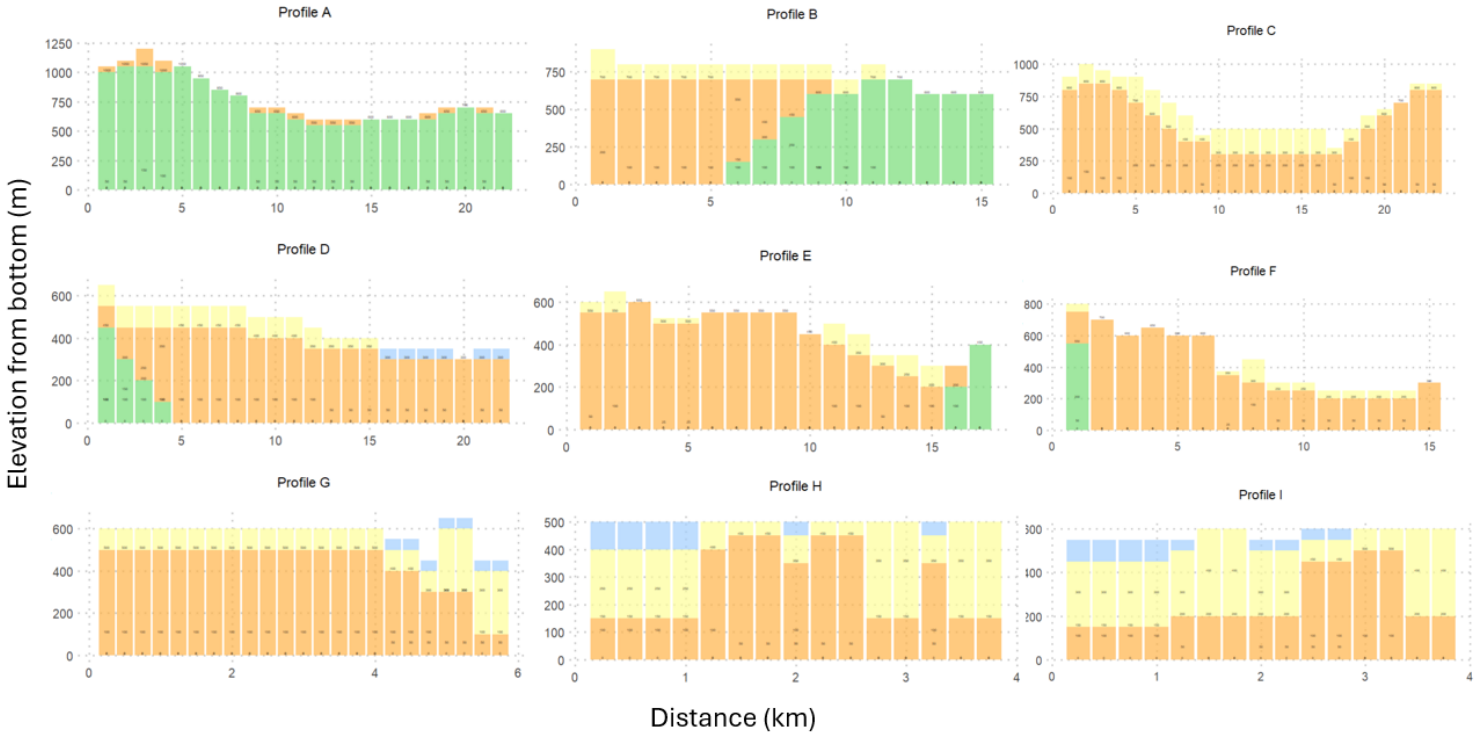

Figure 5.4: Longitudinal profiles information referred to figure 5.3 (Herrera Ibáñez & Barrientos, 2016, 2018)

5.2.2. Data

The primary variables studied were deformation rate (mm/year) and piezometric difference across two distinct dates: January 2021 and November 2021, measurements were planned considering the end of wet and dry seasons (April for wet and November for dry) but these had to be delayed due to covid pandemic.. All analyses were executed using R statistical software.

MT-InSAR Processing: A total of 218 SAR images, encompassing both ascending and descending geometries from the Sentinel-1 A and B satellites, were processed. These images, TOPSAR data in Single Look Complex (SLC) format, were acquired in Interferometric Wide (IW) mode with VV polarization, spanning from January 2020 to November 2021 (refer to Table 5.2). The integrated SNAP-StaMPs processing for Sentinel-1 PSI employed version 9.0.0 of the Sentinel Application Platform (SNAP), developed by the European Space Agency (ESA), in conjunction with snap2stamps and the Stanford Method for Persistent Scatterers (StaMPS) software (Foumelis, 2018). The MT-InSAR processing to obtain the vertical deformation information, was performed following the same process as in chapter 4.

Satellite	First Image	Last image	Geometry	Orbit	Images	Polarization	Mean inc angle	Heading angle
S1A	02/01/2020	09/01/2020	Asc	136	107	39.2	39.2	349.3
S1A	19/12/2021	11/12/2021	Desc	26	111	36.5	36.5	190.6

Table 5.2: Sentinel 1 images detail

Hydrogeological characterization

Piezometric data were measured for 89 wells within the study region (refer to figure 5.3), utilizing a piezometric probe (Empagua et al., 2023). Data were gathered for two moments in time: the initial campaign in January 2021 and a later period in November 2021. For computational purposes, January 30th and November 15th were chosen as median dates within each data collection range. The location and altitude relative to sea level the piezometry of each well were documented. This information was translated into well depth relative to the surface by considering the discrepancy with the Alos Palsar-1 digital terrain model (JAXA, 2023), which has a resolution of 12.5 meters.

The final data utilized for the analysis represents the variation in the depth of each well, calculated by subtracting the first measurement (Δf1) from the second (Δf2), thus determining the change over the two periods (Δf2-f1)

Definition of deformation area of influence per well

Previous studies highlight a strong link between hydrogeology and ground deformation, and potentially with MT-InSAR data, depending on the soil's conditions and properties. For this reason, we undertake a characterization of the wells using the available geological and hydrogeological data. This data is leveraged to group wells to elucidate similar patterns between the two variables constituting the statistical analysis.

There is a lack of reference information regarding the size of the area that mirrors the extraction behavior of a given well', or whether this area is even consistent or circular. To examine this, we plan to repeat the statistical analyses with varying radius. The minimum radius is determined as 50 m, with the goal of obtaining a statistically representative sample of wells with Persistent Scatterers (PS) in the defined buffer.

Assigning a Lithologic Information Column to Each Well

The geological information used to characterize the wells was obtained from the publications in figure 5.4, which compiles information from various drilling companies, and from Herrera Ibáñez y Barrientos (2016) . These surveys indicate that in the study area, where the wells are located, there are four types of geologies both horizontally and in depth, which can independently form aquifers: Alluvial, Pyroclastic, Andesitic Lavas, and Limestone Rocks.

We applied a method for assigning a lithologic column to each well, based on two criteria: a) selection of the lithologic column of the nearest prospected well that, b) is in the same physiographic unit (Soil Survey Staff, 1993, p. 8, Miller et al. 2016). To characterize the physiography of each well and lithologic column, a GIS analysis is conducted using a spatial join tool between the wells layer and the geological information provided by Herrera & Orozco (2010, 2018), as well as slopes derived from JAXA's 12-meter resolution MDT layer, classified according to (FAO, 2009) standards. Finally, the well allocations were reviewed to ensure that the physiographic units had been appropriately classified: slope, summit, or valley.

Slope (º)		
Type	Range	Group
Flat-swiftly sloped	[0-3)	1
Sloped	[3-6)	2
Moderately sloped	[7-8)	3
Steep	[8-17)	4
Strongly steeped	[17-30)	5

Table 5.3:slopes factor and qualitative ranges (FAO, 2009)

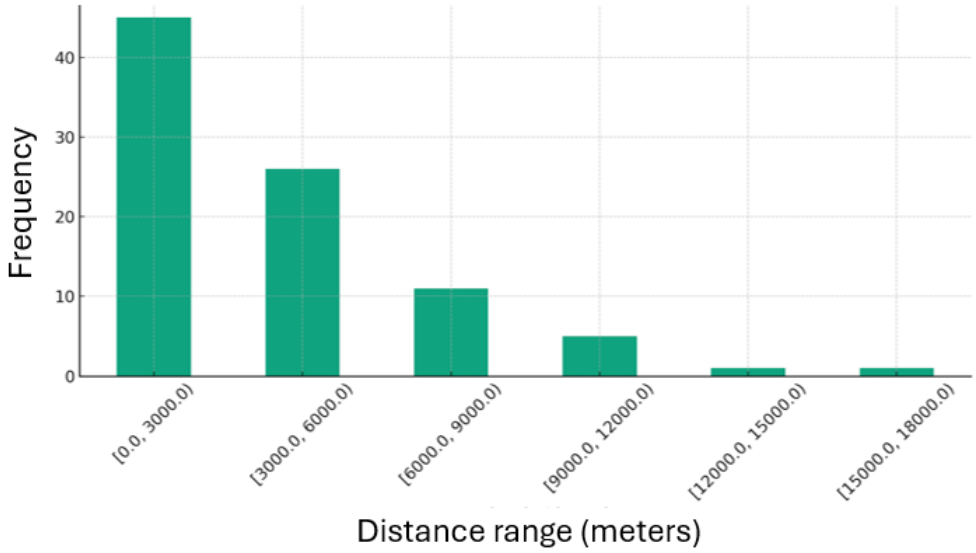

Figure 5.5:General distribution of the distance between the wells and the applied lithological column

5.2.3. Analysis

Statistical analysis

Pearson correlation (Pearson, 1896) was utilized to evaluate the linear correlation between the deformation rate throughout the entire study period (mm/year) and the piezometric difference within each categorized group, with the aim of

understanding the relationship of these variables in distinct hydrogeological and geographical settings.

A comprehensive statistical analysis was executed to explore the connections among different geological and geophysical variables. Key variables of the study encompassed the rate of deformation (mm/year) and the piezometric difference between the two monitored dates. The R statistical software was employed for all analyses.

Two types of well groupings were made for the described statistical analyses. Firstly, wells were grouped based on lithological characteristics identified in the previous step:

- Surface Geology according to Applied Lithologic Column: Geology associated with each well at the surface layer.
- Geology coinciding with the Mean Water Table Level of Measurements: Geology associated with each well that matches the average of the two piezometric measurements.
- Lithologic Column Models: Considering the types of aquifers in each column and their spatial arrangement, typical column models were established.

Additionally, three more classifications were considered based on spatial analyses derived from other relevant products:

- Surface Geology according to the map proposed by Gamboa et al. (2023). This map categorizes the surface considering the soil surface hardness for the calculation of seismic hazard (*NEHRP* , 2020). In the study area, four types are identified: "BC", "C", "CD", and "D", based on hardness of classified soil.
- Hydrological Basin: Using hydrological basin cartography. The basins described in the introduction were delimited based on the 12.5 m resolution Digital Terrestrial Model (DTM) (JAXA, 2023).
- Areas of Deformation in the RMG >5mm/year and >10mm/year (García-Lanchares et al., 2023) we compared our results with the areas of vertical deformation identified in the previous chapter. These were considered if the well sample was representative.

For each defined group, the relationship between deformation rate and piezometric difference was explored by calculating the Pearson correlation coefficient (Pearson,

1896). This approach replaced fitting a linear model, focusing instead on measuring the linear association between variables.

Scatter plots were used to visualize the relationship between deformation rate and piezometric difference in each group. These plots helped illustrate the data distribution and provided a clear representation of variability in the measurements.

5.3. Results and discussion

This section presents significant findings on the hydrogeological dynamics in relation to the urban growth of Guatemala City, based on MT-InSAR SNAP-StaMPS data. The results from our study are compared with those of previous studies, followed by an analysis of the congruencies between aquifer descriptions and geological composition. Finally, we explore the relationship between piezometric difference, deformation rates, and the historical evolution of the water table. These results are essential for understanding the interactions between water usage and the geological stability of the region.

This summary highlights the multi-faceted approach taken in the study, combining advanced satellite data analysis with geological and hydrogeological insights. By correlating these diverse data sets, the research provides a comprehensive view of how urban expansion impacts the underlying hydrological and geological frameworks, which is crucial for informed urban planning and resource management in Guatemala City.

5.3.1. Relation of ground deformation and hydrogeological data

In the analysis of groundwater dynamics and ground deformations in the metropolitan region of Guatemala City, three studies stand out for their significant contributions. Recinos et al. (2019)provides a detailed municipal analysis of piezometric levels, including profiles and flow lines for each climatic season, and presents equipotential curves crucial for understanding underground flow networks. Kim et al. (2019) contribute to the analysis of land deformation between 2014 and 2017, utilizing the SNAP-StaMPS algorithm and Sentinel 1 data. García-Lanchares extends this research to 2021, maintaining the methodology to provide an updated and comprehensive perspective of the phenomenon.

The related maps seen in figures 5.1 for the dry and wet seasons reflect the observations from these studies, showing a notable consistency in the location of equipotential surfaces and areas of deformation. The zones of depression cones, primarily identified in Mixco and the extensive areas of Villanueva and Petapa, are consistent with the underground flow directions reported by FUNCAGUA.

A total of 495,791 Persistent Scatterers (PSs) were identified following their decomposition into the vertical component. This resulted in a point density of 986.1 PSs per square kilometer for the urban surface within the study area (Figure 5.6). Based on the Global Human Settlement Built-up area product (Pesaresi & Politis, 2022). Most of the PSs are found in constructed zones, as dense vegetation impedes the acquisition of PSs derived from C band data.

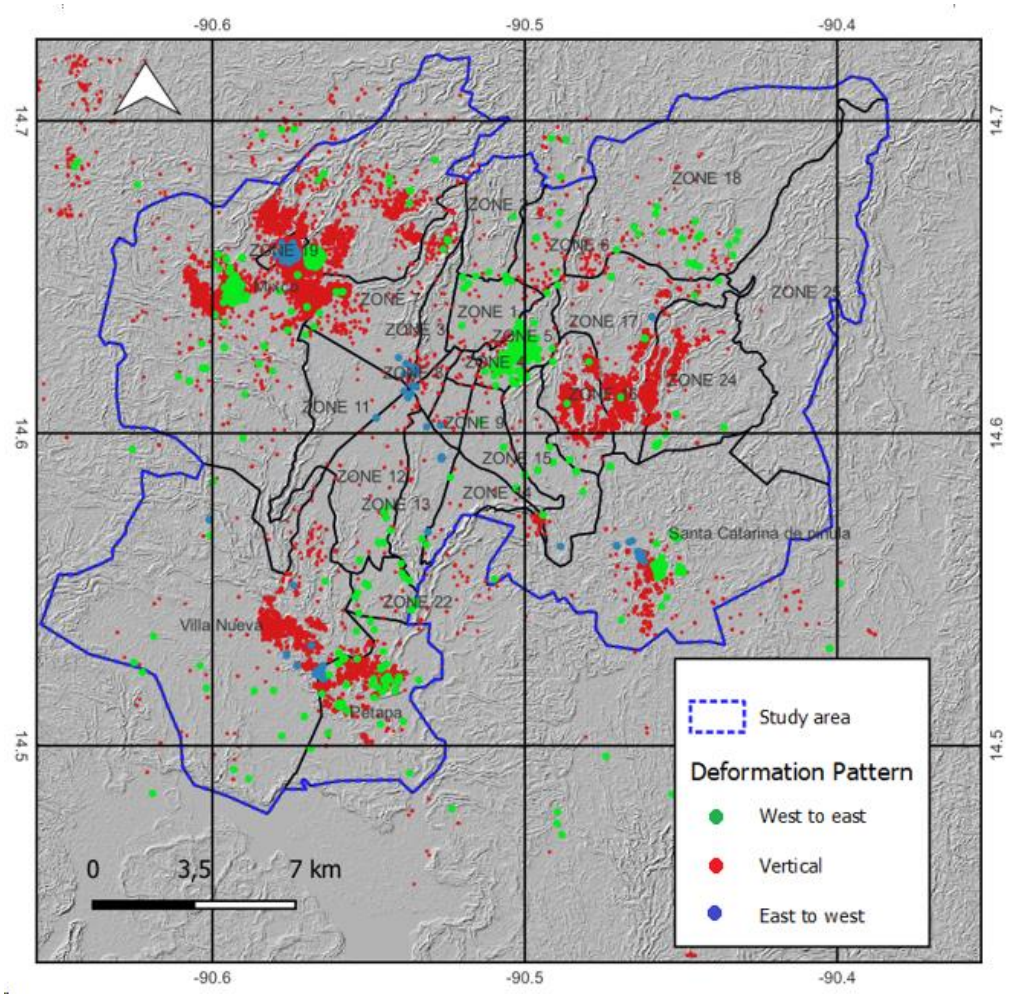

Figure 5.6: Subsidence and planimetric deformations in the study area for MT-InSAR process within the years 2020-2021. Geographical Reference system WGS84

Recinos et al. (2019) delivers an in-depth analysis of piezometric levels by municipality, including seasonal profiles and flow lines, including equipotential curves for interpreting subsurface flow patterns. Kim et al. (2019) reported the main zones of ground deformation from 2014 to 2017 through SNAP-StaMPS algorithm and Sentinel 1 data analysis. García-Lanchares et al. (2023) updated this work identifying main deformation areas up to 2021, using the same methodology to present a current comprehensive perspective on the ongoing changes.

The comparative maps shown in figures 5.7 - 5.9 for both the dry and wet seasons corroborate the observations from these studies, revealing a notable consistency in the positioning of equipotential surfaces and deformation zones. The identified depression cones, especially those in Mixco and across the expansive areas of Villanueva and Petapa, are in accordance with the subsurface flow directions documented by FUNCAGUA (see figure 5.1). The fractures are open and have good intercommunication, as was proven by the drilling of wells 312/I and 318/I. Within the lower aquifer, there are different levels with varying degrees of fracturing. At the place known as Ojo de Agua (Figure 5.9), there is a spring with a flow rate that varies between 516 and 244 liters per second, which occurs in fractured andesitic lavas, covered at the top by pyroclastic materials (Andretti, 1978).

An overarching pattern identified in our study is the water flow direction, originating from the western edge of the northern basin (refer to figures 5.7 and 5.8), with altitudes ranging from 1300 to 1500 meters above sea level (m.a.s.l.) during the dry season, and from 1900 to 1300 m.a.s.l. in the wet season. This flow demonstrates a tendency to spread in all four cardinal directions. However, within our specific area of study, the water predominantly tends to head southward (see figures 5.8 and 5.9), moving towards or down to 1200 m.a.s.l.. This is of particular significance in understanding the subsurface dynamics within pivotal regions like Mixco, which overlaps with deformation zones detected by MT-InSAR as indicated by García-Lanchares 2,3, and 5; and Villanueva and Petapa, corresponding to deformation zone 6 as reported by García-Lanchares (2023).

Additionally, zones 4 and 10, as detailed by García-Lanchares et al. (2023), and deformation zone D, as identified by Kim et al. (2019), correspond to certain well depths that have increased since the year 2000 Morales (2012) to the present measurements. For example, the depth of well H-2 has increased by 142 meters.

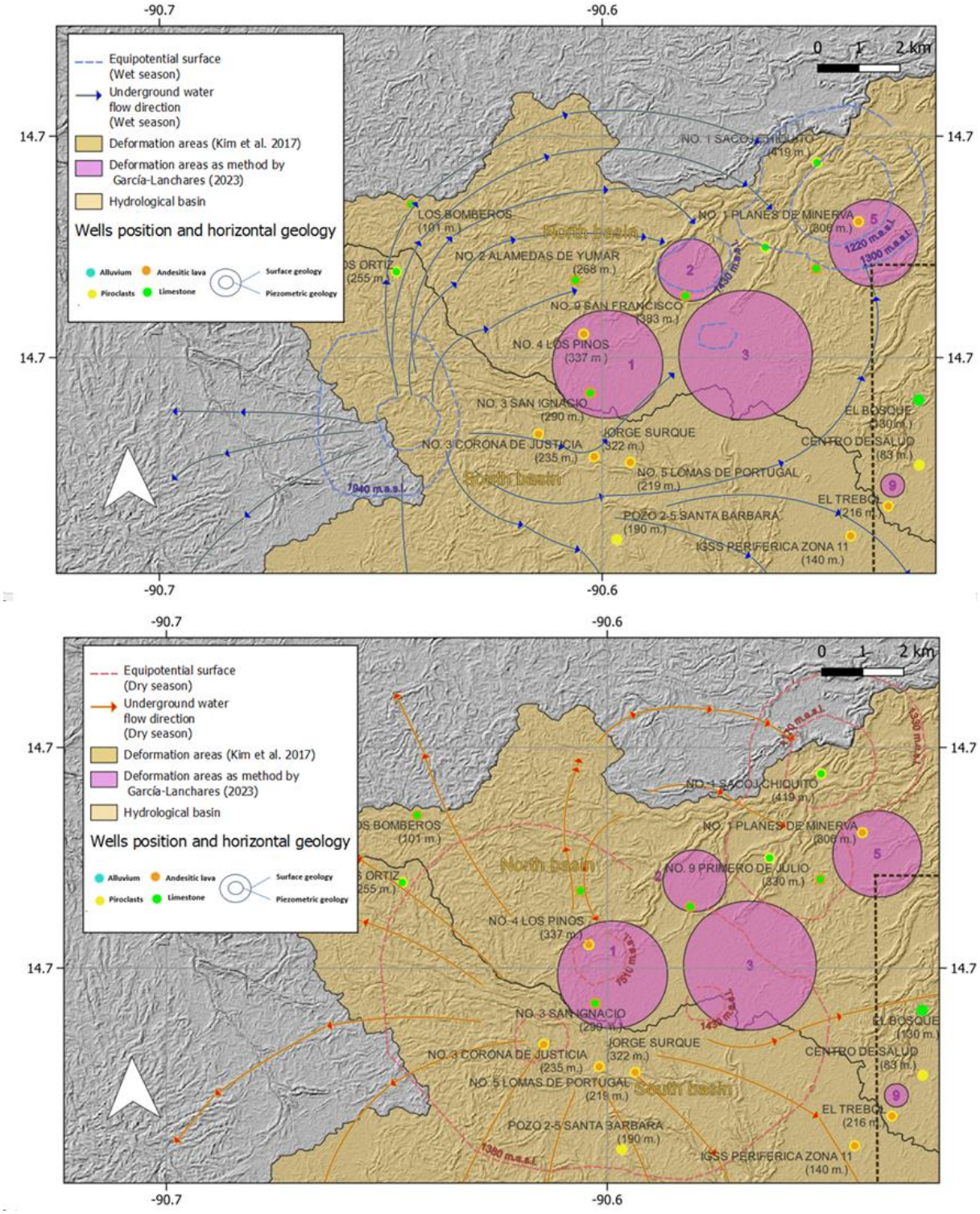

Figure 5.7: Main subsidence areas and wells located in North basin with equipotential areas for both seasons (wet above and dry below). Geographical Reference system WGS84

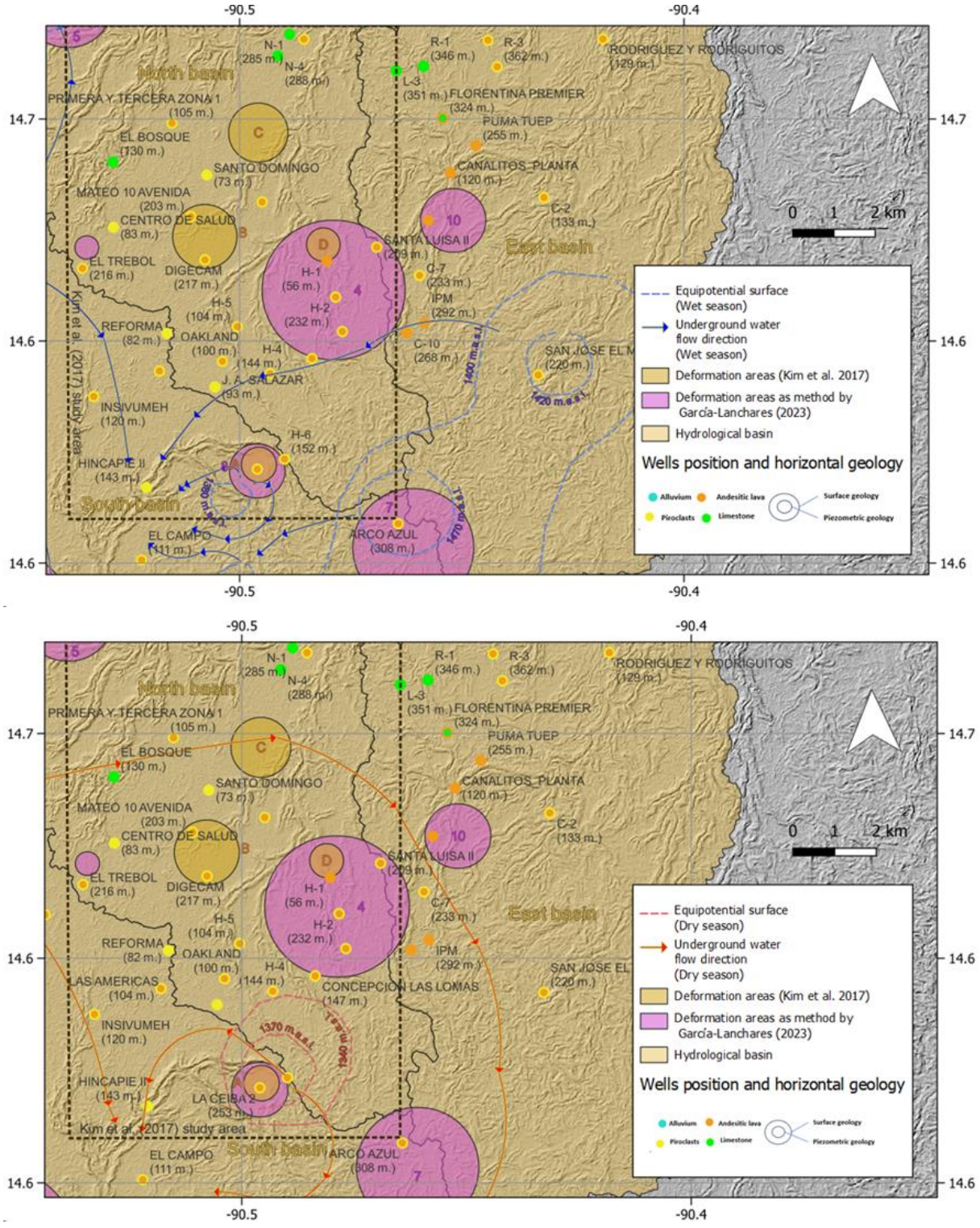

Figure 5.8: Main subsidence areas and wells located in East basin with equipotential areas for both seasons (wet above and dry below). Geographical Reference system WGS84

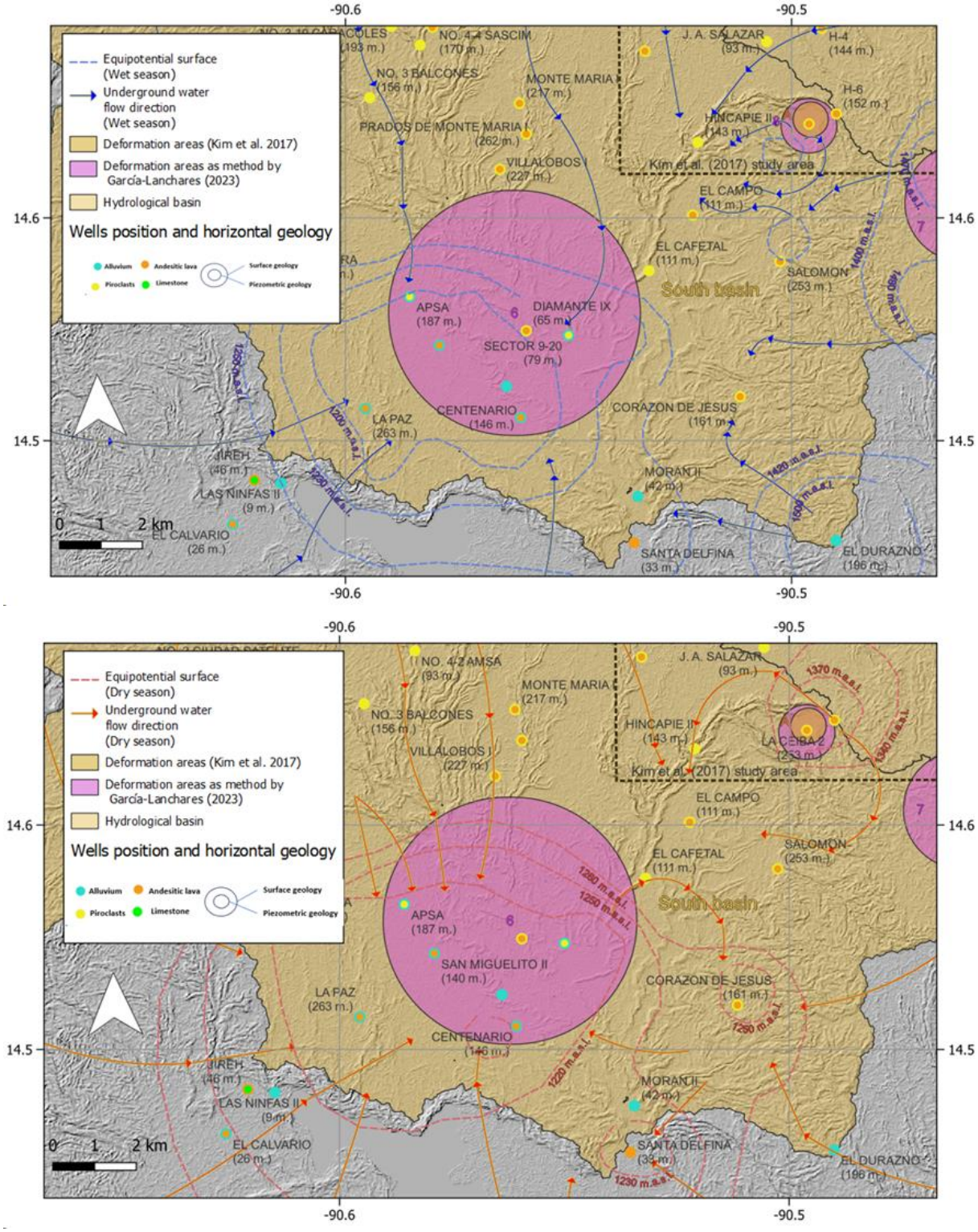

Figure 5.9: Main subsidence areas and wells located in South basin with equipotential areas for both seasons (wet above and dry below). Geographical Reference system WGS84

5.3.2. Analysis of the lithological columns of the wells

As we further explore the subterranean characteristics of the Guatemala City metropolitan area, the methodology employed has facilitated the application of a lithological column to the 89 wells provided by Empagua et al., (2023). These longitudinal profiles, detailed in figure 5.3, are essential for understanding the subsurface stratification and its impact on groundwater dynamics. Data from this sample are crucial to illustrate the general distribution of typical lithological columns. Results will subsequently be presented which give a clear view of these data, providing a solid foundation for geological interpretation and water resource management. As the lithological column applied to its corresponding well depends firstly on them having similar physiography, the distances will vary as shown in figure 5.4, with most of the wells being between 0 and 6,000 meters.

The study delineated seven different lithological column configurations (refer to figure X-D and distribution in figure 5.10d), encompassing four types of aquifer strata. Each well was characterized with one of these configurations based on approximate data on the depths of the aquifers. The diagram schematically displays these classifications, and although it does not show the exact dimensions of the underground layers, it highlights a noticeable predominance of the column type that features pyroclastics in the upper stratum and andesitic lavas in the lower stratum, indicative of the upper and lower aquifers. There is also most wells located between depths of 100 and 300 meters, which extract from a volcanic aquifer.

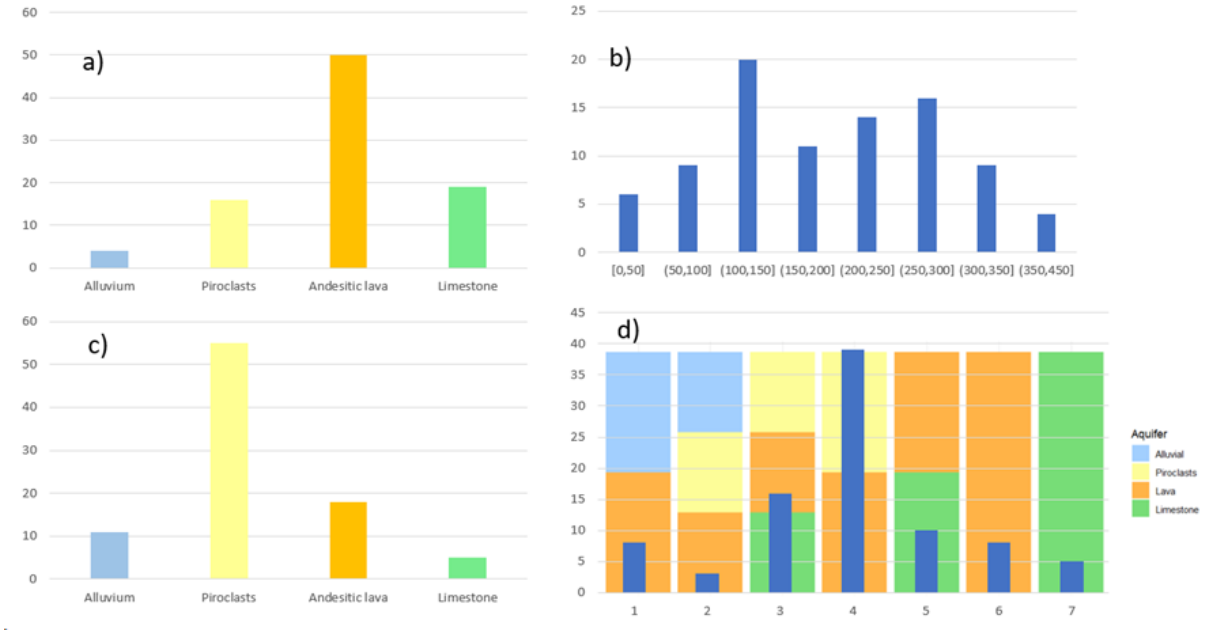

Figure 5.10: Distribution of wells by (a) piezometric geology, (b) depth ranges of piezometric level, (c) surface geology, (d) lithologic column model. The distribution of well depths, as shown in Figure 5.3, highlights a higher frequency of wells with depths rang

As regards the wells of the South basin, there are references matching the Ojo de Agua area, which is the main destination point for groundwater flows according to Recinos et al. (2019) in both dry and wet periods. This description aligns with that of (JICA,1986), which mentions a water level at about 100 meters, and the existence of wells in both the upper aquifer (alluvial or pyroclastic stratum) and the lower aquifer. The groundwater level in the southern sector has a depth of less than 100 meters and depths between 150 and 180 meters. Therefore, it can be concluded that in this sector there are both upper and lower aquifers; there are also shallow wells, less than 100 meters deep, that extract from the alluvial or pyroclastic aquifer" (JICA 1986). Only one of the wells, Diamante IX (In the southern basin, Figure 5.9), is shallow (65 m) and extracts from a volcanic aquifer.

There are also wells that extract from the upper aquifer in the alluvial or pyroclastic stratum (Figure 5.9).

5.3.3. Statistical analysis of the relation between deformation and piezometric change

Statistical analyses showed that each of the aquifer presents different behaviors; it also presented variations depending on the basin.

- **Alluvial aquifer:** The Figure 5.10a shows a strong correlation with a Pearson coefficient of 0.988, despite being based on a small sample of only three measurement points, all within a 150-meter buffer. This strong relationship indicates a significant connection between piezometric difference and deformation rate in areas identified by Recinos et al. (2019) as concentrations of groundwater flows. Furthermore, these points correspond to areas with the highest rates of deformation, reaching up to -60 mm/year according to García-Lanchares et al. 2023, and are also the zones where the highest water extraction is recorded, according to JICA (1986).

  This phenomenon is observed in more alluvial basins; studies around the world have suggested that there is a direct relationship between significant subsidence and groundwater extraction. For example, Castellazzi et al. (2016) observed high rates of subsidence in Aguascalientes and Toluca (up to 10 cm/year), while Celaya and Morelia presented lower rates (from 2 to 5 cm/year). Furthermore, the thesis by Ezquerro Martín (2021) suggests that a combination of common factors such as flat, densely populated areas, along with strong accumulations of sedimentary materials in river basins and coastal plains, seem to favor the emergence of this type of problems. Moreover, Brunori et al. (2015) and Coda et al. (2019) explain that the reduction in the pressure of pore water causes an increase in the overburden stress, leading to an immediate compaction of the soil which, if it exceeds the preconsolidation stress of the sediments, results in irreversible deformation caused by the non-reversible reorganization of the sediment grains.

  Navarro-Hernández et al. (2023) investigated land subsidence in the Alas¸ehir-Sarıgol graben in Türkiye, an area known for its graben structure and intensive water extraction for agriculture and industry. Utilizing Sentinel-1 images for an MT-InSAR analysis, they found that areas with the thickest, soft soil layers (ranging from 50 to 100 meters) experienced the most significant subsidence, with rates reaching up to -4 cm/year. These findings underscore the critical influence of graben fill sediment thickness on land subsidence rates, a phenomenon that aligns closely with the characteristics observed in the study case due to the presence of a graben, substantial subsidence over thick alluvial deposits, and extensive water extraction practices.

- **Piroclasts aquifer:** Figure 5.10b shows a significant positive correlation, with a Pearson coefficient of 0.869, between the piezometric difference and the deformation rate for wells with a water table in pyroclastic geology. This reflects the fact that an increase in the piezometric difference, measured within a 50-meter buffer from the center of the wells, is associated with an increase in the rate of ground deformation. These wells are distributed throughout the North and South basin areas.

  Referring to figure 5.11, the data, represented by scattered points, align around a blue trend line with a slope of 2.3, and the gray shadow indicates the confidence interval for this linear estimation. This correlation implies that variations in groundwater level, possibly due to hydrological factors, are closely linked to changes in ground deformation rates.

- **Andesitic aquifer:** It can be observed that the geology of the piezometric level consists of andesitic lavas or limestone. As regards the correlation found for the wells of the East basin, for an optimal buffer of 150 meters is 0.796 (Figure 5.11c an d).

  The fact that tests suggest a direct relationship between the rate of deformation and piezometry between the two dates suggests that there is some type of variability among the wells with piezometric geology in the rest of the basins: firstly, it may be due to a difference in fracturing and therefore in transmissivity in the rest of the basins. At least in the southern area, Andretti (1978) suggests that within the lower aquifer, different levels or degrees of fracturing exists. It could also be because the layer of andesitic lavas is more superficial or does not appear in combination with alluvial or pyroclastic strata: The range of 50 meters or less corresponds to pyroclastic materials or tuffs where there is the possibility that it is saturated with groundwater. In the rest of the basins, however, it is deeper and therefore more compact. The lower aquifer is also under free and semi-confined conditions, mainly because compact pumice pyroclasts and, to a lesser extent, alluvial sediments, which have a lower permeability than the fractured lavas of the aquifer, lie above this aquifer (Andretti, 1978). As for the range of 100 meters or more, this corresponds to welded tuff or andesite-basaltic lava, where the range greater than 100 meters is associated with limestone or basalt from the Cretaceous period (JICA, 1986).

The correlation for the andesitic lava wells within the previous sample, optimal for a 150-meter buffer, has a value of 0.723 (Figure 5.11).

- **Limestone Aquifer:** The scarce data from the limestone aquifer reveal no strong direct relationship, which could be attributed to a lack of understanding of the internal structures resulting in a wide diversity of transmissivity. Given the limited sample size of only n=5, the data from the limestone aquifer show no correlation with the observed piezometric dynamics. The highly anisotropic and heterogeneous nature of carbonate aquifers, as reported by Herrera et al. (2018), results from secondary permeability created by dissolution processes in stratification planes, fractures, and faults. This leads to variable primary porosity in limestone and significant differences in transmissivity measurements, ranging from 10 to 80 m²/day in poorly fractured rocks, from 250 to 500 m²/day in moderately fractured limestones, to 1,000 to 5,000 m²/day in highly fractured limestones. This great variability in transmissivity reflects the difficulty in establishing solid statistics for these aquifers.

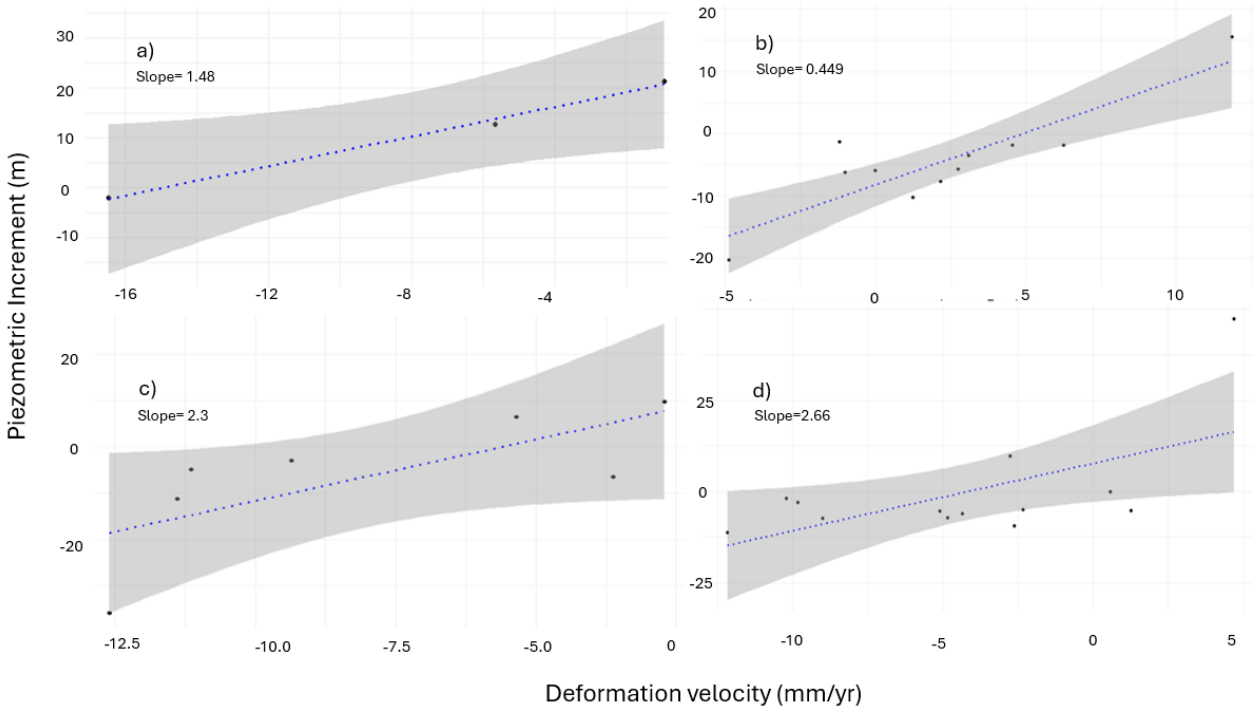

Figure 5.11:Correlation analysis between deformation rates and piezometric levels difference (January 2023- November 2023) for (a) alluvial piezometric level, (b) pyroclasts piezometric level, (c) column 6 wells, and (d) Basin east wells

5.4. Conclusions

The research on hydrogeological dynamics and land deformation in the metropolitan region of Guatemala City, utilizing the MT-InSAR SNAP-StaMPS technique, has provided significant insights into how groundwater management influences the observed subsidence. Through comparative analysis with previous studies and a detailed evaluation of the relationship between aquifer descriptions and geological composition, this work has identified key patterns and correlations impacting the region's geological stability.

The adopted methodology allowed for the characterization of 89 wells, provided by AECID, with a classification based on lithological columns integrating different aquifer strata. The identification of seven distinct lithological column configurations was crucial to understanding subsurface stratification and its impact on groundwater dynamics.

The correlation between piezometric difference and ground deformation rate, especially in alluvial and pyroclastic aquifers, reveals a significant connection with groundwater flow concentrations identified by (Recinos et al., 2019). Moreover, the observed relationship in the East basin, showing a positive correlation between these variables for wells with piezometric geology of andesitic lavas or limestone, suggests variability in transmissivity and fracturing conditions of these aquifers.

The study also highlights the influence of groundwater extraction on land subsidence, a globally recognized phenomenon observed in other metropolises. The research underscores the need for sustainable water resource management and continuous monitoring to mitigate negative impacts on urban infrastructure and ground stability.

In conclusion, this work significantly contributes to understanding the complex interactions between groundwater usage and geological stability in Guatemala City. The findings emphasize the importance of integrating hydrogeological characterization and land deformation monitoring into urban planning and water resource management to promote sustainable development in metropolitan areas.

6. Discussion

6.1. General considerations

The discussion and conclusion sections of this thesis synthesize the comprehensive findings from the application of MT-InSAR technology to monitor geological hazards. Through detailed analysis across diverse landscapes such as Guatemala City, San José, and La Palma, the effectiveness of MT-InSAR in predicting, understanding, and mitigating risks associated with ground deformation is highlighted. There are several reasons that endow this research with great importance. Firstly, its innovative nature: in San José, Costa Rica, and Guatemala City, there are no similar applications with the same spatial and temporal resolutions. Not only that, but they have also been validated with classical monitoring information in a multidisciplinary approach, and analyzed under the influence of groundwater management in the latter case study.

Specifically for La Palma, the social interest in the consequences and origins of this case has made it the study area for numerous investigations, which emerged simultaneously with the present work. However, as in the previous cases, it is important to highlight the innovative nature of the subsequent comparison of the MT-InSAR data with multi-source measurements in a multidisciplinary exercise.

6.1.1. Inherent sources of error in InSAR

A range of studies have explored the use of InSAR for surface deformation monitoring. In the context of InSAR technology, Hanssen (2012) delineates various error sources that can lead to the misinterpretation of "observed" deformation time-seires. The first type of error stems from atmospheric delays, which can introduce phase changes unrelated to ground movement. The troposphere and ionosphere, in particular, affect the radar signal as it travels from the satellite to the ground and back, leading to delays that may mimic or obscure true surface deformation. The second type pertains to orbital errors, which arise due to inaccuracies in the known satellite orbit. These inaccuracies can cause apparent shifts in the ground position, falsely suggesting movement where none has occurred.

6.1.2. Defining the added value for the InSAR processing

The classification of the research outputs presented in chapters 4, 5, and 6, according to the taxonomy of InSAR products proposed by Hansen (2023), provides an insightful perspective on how these investigations align with specific

application needs and data quality used. Below, the details of each chapter are discussed, along with their corresponding classification.

- **La Palma Island**: This section utilizes InSAR, coupled to a wide range of seismic variables, to analyze deformation during the 2021 Tajogaite eruption event, contributing to the characterization of the phases of the event (magnitudes, periods, and locations). Given the specific nature of this study, aimed at understanding a particular volcanic phenomenon, it could be classified as an AA-product. This is because the study is clearly directed at solving a defined problem, with identifiable end-users (such as disaster management authorities and the scientific community).
- **San José, Costa Rica:** Here, InSAR is used to locate deformations in three faults within an urban area, selected by a group of local and international experts. This approach, given its goal of mitigating risks in populated areas, also fits within the AA-product category, as it pursues clear objectives of urban risk prevention and management, with direct applications in urban planning and emergency response.

The use of InSAR in Guatemala City to describe deformations focuses on an urban context with significant implications for planning and risk management. This study, as in that of San José, is oriented towards solving specific problems related to safety and urban infrastructure, thus being classified as AAA-product. The research is in response to concrete needs for geological monitoring in an area which is highly vulnerable to adverse geological phenomena.

6.1.3. Knowledge transference

In the context of the research on ground deformation dynamics in Guatemala City using MT-InSAR technology, a significant knowledge and findings transfer has been conducted towards Empagua, the entity responsible for urban water management in the region (Figure 6.1). This collaboration, materialized in an agreements, has facilitated the sharing of crucial insights into areas susceptible to significant deformations, potentially impacted by alterations in the water distribution system. The information provided has been essential for Empagua to evaluate and monitor these critical zones, aiming to identify and address any issues that might compromise urban water infrastructure. Furthermore, a joint follow-up process has been established to examine the correlation between ground deformation data obtained through MT-InSAR and the piezometric data provided

by Empagua. This synergy between geological research and urban water management underscores the value of applying advanced technologies like MT-InSAR in strategic decision-making and in the implementation of preventive measures to safeguard water distribution systems in urban areas.

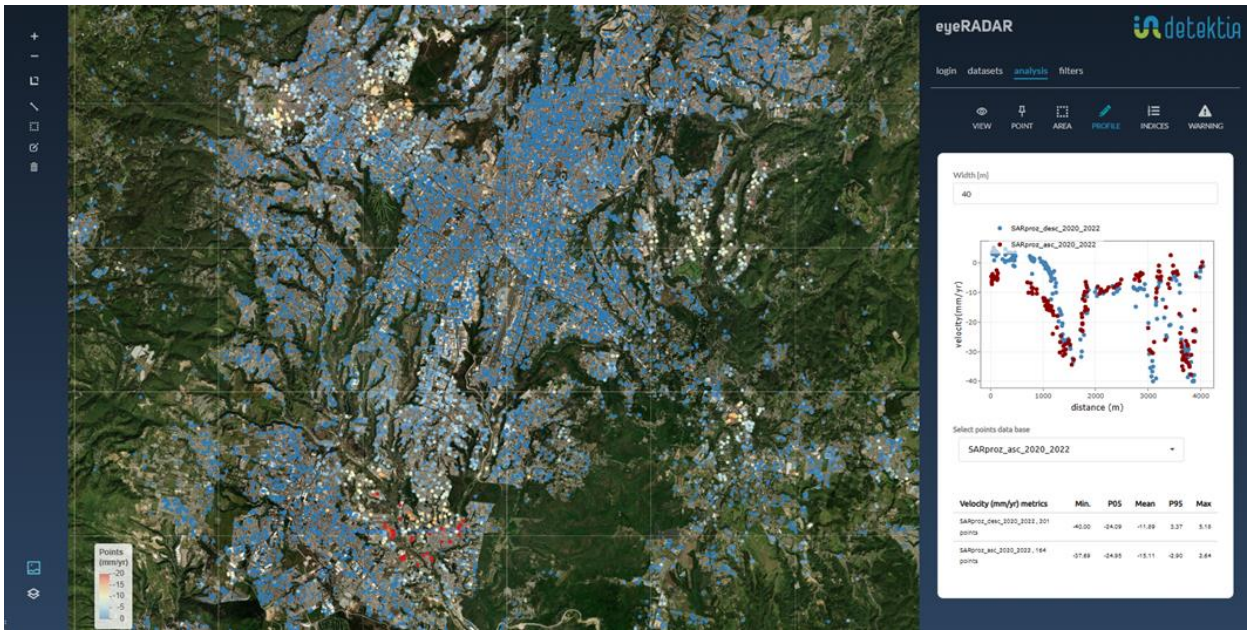

Figure 6.1:Screenshot of Guatemala City data viewed on the Detektia developed tool: Eyeradar

6.2. New Challenges

This section delves into the main challenges found in these Thesis, which are, the enhancement of locational accuracy of InSAR data and the development of predictive models for geological hazards. Through comprehensive case studies and integration of diverse data types—from piezometric and geological details to water dynamics and climate variations—we aim to refine risk assessment and mitigation strategies.

- **General Challenges: Enhancing Locational Accuracy:** A pivotal challenge is the enhancement of X-Y position accuracy in MT-InSAR analyses. This improvement is essential for the precise monitoring and assessment of geological hazards, facilitating the targeted implementation of risk reduction strategies. Enhancing locational accuracy will enable more detailed and location-specific predictions of ground deformation and hazard impact, thereby improving the efficacy of mitigation efforts.

- **Prediction of Geological Hazard Events:** The foundation of this research lies in the ability to anticipate geological events, which, while inevitable, can be

managed through well-designed actions to minimize loss and damage. The synthesis of various case studies, each with its unique geological and environmental parameters, is crucial for developing predictive models. By integrating detailed characterizations of different regions, this approach aims to tailor predictions and interventions to the specificities of each case, thereby enhancing the preparedness and resilience of vulnerable areas.

- **Comprehensive Characterization for the Case Study:** By enhancing the depth and breadth of data analysis, this research aims to uncover the intricate interactions between hydrogeological processes and geological hazards, informing more effective risk management strategies.

- **Expansion of Piezometric Information**: Enhancing the temporal series of piezometric data is vital for a deeper understanding of groundwater dynamics and its impact on land subsidence. Continuous monitoring and the integration of long-term data series will provide insights into the trends and triggers of groundwater level changes.

- **Acquisition of Precise Geological Information**: Detailed geological mapping and characterization are imperative for correlating subsurface conditions with observed surface deformations. This information will refine the analysis of deformation patterns and contribute to more accurate risk assessments.

- **Mapping Water Withdrawal Stations and Flows:** Identifying and monitoring the locations of water extraction and the paths of water movement are essential for understanding the human impact on hydrogeological dynamics. This knowledge will aid in the development of sustainable water management practices.

- **Integration of Climate Data**: Incorporating detailed climate information will enhance the understanding of how climatic variations influence groundwater levels and, consequently, land deformation.

7. Conclusions

The doctoral research presented herein has significantly advanced the understanding and monitoring of deformation processes within regions of high geological risk, exemplified by areas in Central America and volcanic islands such as La Palma. Through a series of innovative, collaborative case studies, this work has demonstrated the efficacy of Multi-Temporal Synthetic Aperture Radar (MT-InSAR) in deciphering and managing both natural and induced geological threats at various scales.

The partnership between the technological startup Detektia and Universidad Politécnica de Madrid has been instrumental in propelling forward the capabilities of MT-InSAR technology. The integration into the KUK-APHÁN project, targeting seismic risk reduction, has proven successful, establishing the foundations for a globally marketable technology tailored to public administrations, construction companies, and risk management consultants. The following conclusions can be established:

Conclusion 1: MT-InSAR technology has been successfully validated for the evaluation of geological risks in urban areas of Central America and La Palma. The creation of risk scenarios allows future damages caused by adverse events to be minimized.

Conclusion 2: The deformation results obtained through MT-InSAR were successfully contrasted in different case studies with information from other disciplines such as geology, geotechnics, and hydrogeology. The integration and comparison of these data significantly validated and enriched the results, providing a more comprehensive and accurate view of geological risks.

Conclusion 3: The association between contemporary piezometric time-series and MT-InSAR results in the case study of Guatemala City were successfully determined for specific aquifer geologies. The analysis and correlation of the available piezometric data with the deformation results detected by MT-InSAR allowed for a better understanding of the causes and patterns of ground deformation in this specific area.

Conclusion 4: It was effectively established how MT-InSAR provides a solid basis for integration into an infrastructure monitoring system. The evaluation and proposal for integrating MT-InSAR data and methodologies into urban and interurban infrastructure monitoring systems have proven to be fundamental

for the management and prevention of geological risks, providing a robust platform for decision-making and the implementation of preventive measures. Although this objective has been partially achieved, knowledge transfer to the relevant administrations has been carried out, and further work will continue to fully accomplish this objective.

References

Ab Latip, A. S., Matori, A., Aobpaet, A., & Din, A. H. M. (2015). Monitoring of offshore platform deformation with stanford method of Persistent Scatterer (StaMPS). *2015 International Conference on Space Science and Communication (IconSpace)*, 79-83. https://doi.org/10.1109/IconSpace.2015.7283785

Abidin, H. Z., Andreas, H., Gumilar, I., Fukuda, Y., Pohan, Y. E., & Deguchi, T. (2011). Land subsidence of Jakarta (Indonesia) and its relation with urban development. *Natural Hazards*, *59*(3), 1753-1771. https://doi.org/10.1007/s11069-011-9866-9

Allen, S., Owens, I., & Sirguey, P. (2008). Satellite remote sensing procedures for glacial terrain analyses and hazard assessment in the Aoraki Mount Cook region, New Zealand. *New Zealand Journal of Geology and Geophysics*, *51*(1), 73-87. https://doi.org/10.1080/00288300809509851

Alvarado, R., Méndez de Penedo, L., Cabarrús, C., Rivera, A., Padilla, F., Gálvez, J., Saubes, N., & Monterosso, O. (2013). *Bases técnicas para la gestión del agua con visión de largo plazo en la zona metropolitana de Guatemala* (Instituto de Agricultura ,Recursos Naturales y Ambiente de La Universidad Rafael Landívar (IARNA-URL) y the Nature Conservacy). https://www.plazapublica.com.gt/sites/default/files/Bases_tecnicas_gestion_del_agua.pdf

Andretti, A. (1978). *Informe Final del estudio de Aguas subterráneas en el valla de la Ciudad de Guatemala* (p. 164) [Proyecto estudio de aguas subterráneas en Guatemala]. Insivumeh-IGN-ONU.

Araya Rodriguez, M. C. A. (2019). *Identifying active volcanic, tectonic and geothermal deformation at the Northern Costa Rican Volcanic Arc using InSAR.* [PhD Thesis, University of Bristol]. Bristol University. https://research-information.bris.ac.uk/en/studentTheses/identifying-active-volcanic-tectonic-and-geothermal-deformation-a

Bakon, M., Papco, J., Perissin, D., Sousa, J. J., & Lazecky, M. (2016). Multi-sensor InSAR Deformation Monitoring over Urban Area of Bratislava (Slovakia). *Procedia Computer Science*, *100*, 1127-1134. https://doi.org/10.1016/j.procs.2016.09.265

Balbi, E., Terrone, M., Faccini, F., Scafidi, D., Barani, S., Tosi, S., Crispini, L., Cianfarra, P., Poggi, F., & Ferretti, G. (2021). Persistent Scatterer Interferometry and Statistical Analysis of Time-Series for Landslide Monitoring: Application to Santo Stefano d'Aveto (Liguria, NW Italy). *Remote Sensing*, *13*(17), 3348. https://doi.org/10.3390/rs13173348

Bamler, R., Geudtner, D., Schattler, B., Vachon, P. W., Steinbrecher, U., Holzner, J., Mittermayer, J., Breit, H., & Moreira, A. (1999). RADARSAT ScanSAR interferometry. *IEEE 1999 International Geoscience and Remote Sensing Symposium. IGARSS'99 (Cat. No.99CH36293)*, *3*, 1517-1521. https://doi.org/10.1109/IGARSS.1999.772005

Bamler, R., & Hartl, P. (1998). *Synthetic aperture radar interferometry*.

Barquero, R., & Rojas, W. (2010). RESUMEN de la ACTIVIDAD SÍSMICA Y VOLCÁNICA EN COSTA RICA DURANTE EL año 2009. *REVISTA GEOLÓGICA DE AMÉRICA CENTRAL*, 9.

Benito, M. B., Alvarado, G. E., Marchamalo, M., Rejas, J. G., Murphy, P., Franco, R., Castro, D., Garcia-Lanchares, C., & Sanchez, J. (2023). Temporal and spatial evolution of the 2021 eruption in the Tajogaite volcano (Cumbre Vieja rift zone, La Palma, Canary Islands) from geophysical and geodetic parameter analyses. *Natural Hazards*, *118*(3), 2245-2284. https://doi.org/10.1007/s11069-023-06090-y

Benito Oterino, B., & Torres Fernández, Y. (2009). *Amenaza sísmica en América Central*.

Berardino, P., Fornaro, G., Lanari, R., & Sansosti, E. (2002). A new algorithm for surface deformation monitoring based on small baseline differential SAR interferograms. *IEEE Transactions on Geoscience and Remote Sensing*, *40*(11), 2375-2383. https://doi.org/10.1109/TGRS.2002.803792

Blewitt, G., Hammond, W., & Kreemer, C. (2018). Harnessing the GPS Data Explosion for Interdisciplinary Science. *Eos*, *99*. https://doi.org/10.1029/2018EO104623

Blissenbach, E. (1952). Relation of Surface Angle Distribution to Particle Size Distribution on Alluvial Fans. *Journal of Sedimentary Petrology*, *22*(1), 25.

Bohnenberger, O. (1996). *Revisión del sistema de fallas en la región metropolitana de Guatemala*. Sociedad Geológica de Guatemala.

Bommer, J., & Rodríguez, C. (2002). Earthquake induced landslides in Central America. *Engineering Geology*, *63*(3-4), 189-220. https://doi.org/10.1016/S0013-7952(01)00081-3

Bouraoui, S. (2014). *Time series analysis of SAR images using persistent scatterer (PS), small baseline (SB) and merged approaches in regions with small surface deformation*.

Brown, R., Lamarre, A., Lamarre, T., & Loucks, T. (1980). *Mapa geológico Hoja 2159 III* (1ra ed.) [Map]. Instituto Geográfico Nacional.

Bru, G., Herrera, G., Tomás, R., Duro, J., De La Vega, R., & Mulas, J. (2013). Control of deformation of buildings affected by subsidence using persistent scatterer interferometry. *Structure and Infrastructure Engineering*, 1-13. https://doi.org/10.1080/15732479.2010.519710

Brunori, C., Bignami, C., Albano, M., Zucca, F., Samsonov, S., Groppelli, G., Norini, G., Saroli, M., & Stramondo, S. (2015). Land subsidence, Ground Fissures and Buried Faults: InSAR Monitoring of Ciudad Guzmán (Jalisco, Mexico). *Remote Sensing*, *7*(7), 8610-8630. https://doi.org/10.3390/rs70708610

Carracedo, J. C., Badiola, E. R., & Guillou, H. (2021). *Geology and volcanology of la Palma and El Hierro, Western Canaries*.

Castañeda, C., Gutiérrez, F., Manunta, M., & Galve, J. P. (2009). DInSAR measurements of ground deformation by sinkholes, mining subsidence, and landslides, Ebro River, Spain. *Earth Surface Processes and Landforms*, *34*(11), 1562-1574. https://doi.org/10.1002/esp.1848

Castellazzi, P., Arroyo-Domínguez, N., Martel, R., Calderhead, A. I., Normand, J. C. L., Gárfias, J., & Rivera, A. (2016). Land subsidence in major cities of Central Mexico: Interpreting InSAR-derived land subsidence mapping with hydrogeological data. *International Journal of Applied Earth Observation and Geoinformation*, *47*, 102-111. https://doi.org/10.1016/j.jag.2015.12.002

Castellazzi, P., Garfias, J., Martel, R., Brouard, C., & Rivera, A. (2017). InSAR to support sustainable urbanization over compacting aquifers: The case of Toluca Valley, Mexico. *International Journal of Applied Earth Observation and Geoinformation*, *63*, 33-44. https://doi.org/10.1016/j.jag.2017.06.011

Chakraborty, M., Panigrahy, S., Rajawat, A. S., Kumar, R., Murthy, T. V. R., Haldar, D., Chakraborty, A., Kumar, T., Rode, S., Kumar, H., Mahapatra,

M., & Kundu, S. (2013). Initial results using RISAT-1 C-band SAR data. *CURRENT SCIENCE*, *104*(4).

Chaussard, E., Bürgmann, R., Shirzaei, M., Fielding, E. J., & Baker, B. (2014). *Predictability of hydraulic head changes and characterization of aquifer-system and.pdf*. https://doi.org/10.1002/2014JB011266

Chaussard, E., Milillo, P., Bürgmann, R., Perissin, D., Fielding, E. J., & Baker, B. (2017). Remote Sensing of Ground Deformation for Monitoring Groundwater Management Practices: Application to the Santa Clara Valley During the 2012–2015 California Drought. *Journal of Geophysical Research: Solid Earth*, *122*(10), 8566-8582. https://doi.org/10.1002/2017JB014676

Chen, C.-T., Hu, J.-C., Lu, C.-Y., Lee, J.-C., & Chan, Y.-C. (2007). Thirty-year land elevation change from subsidence to uplift following the termination of groundwater pumping and its geological implications in the Metropolitan Taipei Basin, Northern Taiwan. *Engineering Geology*, *95*(1-2), 30-47. https://doi.org/10.1016/j.enggeo.2007.09.001

Chen, F., Lin, H., Zhang, Y., & Lu, Z. (2012). Ground subsidence geo-hazards induced by rapid urbanization: Implications from InSAR observation and geological analysis. *Natural Hazards and Earth System Sciences*, *12*(4), 935-942. https://doi.org/10.5194/nhess-12-935-2012

Cigna, F., Esquivel Ramírez, R., & Tapete, D. (2021). Accuracy of Sentinel-1 PSI and SBAS InSAR Displacement Velocities against GNSS and Geodetic Leveling Monitoring Data. *Remote Sensing*, *13*(23), 4800. https://doi.org/10.3390/rs13234800

Cigna, F., & Tapete, D. (2022). Urban growth and land subsidence: Multi-decadal investigation using human settlement data and satellite InSAR in Morelia, Mexico. *Science of The Total Environment*, *811*, 152211. https://doi.org/10.1016/j.scitotenv.2021.152211

Coda, S., Confuorto, P., De Vita, P., Di Martire, D., & Allocca, V. (2019). Uplift Evidences Related to the Recession of Groundwater Abstraction in a Pyroclastic-Alluvial Aquifer of Southern Italy. *Geosciences*, *9*(5), 215. https://doi.org/10.3390/geosciences9050215

Colesanti, C., Ferretti, A., Novali, F., Prati, C., & Rocca, F. (2003). Sar monitoring of progressive and seasonal ground deformation using the permanent

scatterers technique. *IEEE Transactions on Geoscience and Remote Sensing*, *41*(7), 1685-1701. https://doi.org/10.1109/TGRS.2003.813278

Costantini, M., Minati, F., Trillo, F., Ferretti, A., Novali, F., Passera, E., Dehls, J., Larsen, Y., Marinkovic, P., Eineder, M., Brcic, R., Siegmund, R., Kotzerke, P., Probeck, M., Kenyeres, A., Proietti, S., Solari, L., & Andersen, H. S. (2021). European Ground Motion Service (EGMS). *2021 IEEE International Geoscience and Remote Sensing Symposium IGARSS*, 3293-3296. https://doi.org/10.1109/IGARSS47720.2021.9553562

Crosetto, M., Biescas, E., Duro, J., Closa, J., & Arnaud, A. (2008). Generation of Advanced ERS and Envisat Interferometric SAR Products Using the Stable Point Network Technique. *Photogrammetric Engineering & Remote Sensing*, *74*(4), 443-450. https://doi.org/10.14358/PERS.74.4.443

Davis, W. M. (1925). The Basin Range Problem. *Proceedings of the National Academy of Sciences*, *11*(7), 387-392. https://doi.org/10.1073/pnas.11.7.387

De Luca, C., Valerio, E., Giudicepietro, F., Macedonio, G., Casu, F., & Lanari, R. (2022). *Pre- and Co-Eruptive Analysis of the September 2021 Eruption at Cumbre Viejo Volcano (La Palma, Canary isalnds) Through DInSAR Measurements and Analytical Modeling*. https://doi.org/10.1029/2021GL097293

Delgado Blasco, J., Foumelis, M., Stewart, C., & Hooper, A. (2019). Measuring Urban Subsidence in the Rome Metropolitan Area (Italy) with Sentinel-1 SNAP-StaMPS Persistent Scatterer Interferometry. *Remote Sensing*, *11*(2), 129. https://doi.org/10.3390/rs11020129

Deng, Y., Yu, W., & Wang, R. (2014). On spaceborne synthetic aperture radar (SAR) systems in China. *2014 XXXIth URSI General Assembly and Scientific Symposium (URSI GASS)*, 1-4. https://doi.org/10.1109/URSIGASS.2014.6929613

Denyer, P. (s. f.). *GEOLOGÍA Y GEOTECTÓNICA DE AMERICA CENTRAL Y EL CARIBE*.

DEOS. (2008). *Delft Object-oriented Radar Interferometric Software User's manual and technical documentation Version: V4.02*. Delft University of Technology. http://enterprise.lr.tudelft.nl/doris/.

Domínguez, A., & Vega, J. M. (2022, octubre 18). Hundimientos en Guatemala: Dónde están y cómo son los que han aparecido en los úlitmos meses. *Prensa Libre*, 1338-1343.

Eckis, R. (1928). Alluvial Fans of the Cucamonga District, Southern California. *The Journal of Geology*, *36*(3), 224-247. https://doi.org/10.1086/623509

Empagua, Mancomunidad Gran Ciudad del Sur, UICN, & Aecid. (2023). *Estrategia de seguridad hídrica para los municipios de la mancomunidad Gran Ciudad del Sur, compatible con una explotación sostenible del acuífero del valle de la Ciudad de Guatemala*.

Engi, D. (1985). *Subsidence Due to Fluis Withdrawal: A Survey of Analytical Capabilities* (p. 114). Sandia National Laboratories.

Even, M., & Schulz, K. (2018). InSAR Deformation Analysis with Distributed Scatterers: A Review Complemented by New Advances. *Remote Sensing*, *10*(5), 744. https://doi.org/10.3390/rs10050744

Ezquerro Martín, P. (2021). *Estudio de la subsidencia del terreno producida por la explotación de acuíferos mediante datos de Interferometría Radar Satélite* [PhD Thesis, Universidad Politécnica de Madrid]. https://doi.org/10.20868/UPM.thesis.67786

Ezquerro, P., Del Soldato, M., Solari, L., Tomás, R., Raspini, F., Ceccatelli, M., Fernández-Merodo, J., Casagli, N., & Herrera, G. (2020). Vulnerability Assessment of Buildings due to Land Subsidence Using InSAR Data in the Ancient Historical City of Pistoia (Italy). *Sensors*, *20*(10), 2749. https://doi.org/10.3390/s20102749

Ezquerro, P., Herrera, G., Marchamalo, M., Tomás, R., Béjar-Pizarro, M., & Martínez, R. (2014). A quasi-elastic aquifer deformational behavior: Madrid aquifer case study. *Journal of Hydrology*, *519*, 1192-1204. https://doi.org/10.1016/j.jhydrol.2014.08.040

Famiglietti, J. S. (2014). The global groundwater crisis. *Nature Climate Change*, *4*(11), 945-948. https://doi.org/10.1038/nclimate2425

FAO. (2009). *Guía para la descripción de suelos Capítulo 3: Descripción de los factores formadores del suelo- Guías para la Descripción del suelo* (SOTER). https://www.fao.org/3/a0541s/a0541s.pdf

Fernández, J., Escayo, J., Camacho, A. G., Palano, M., Prieto, J. F., Hu, Z., Samsonov, S. V., Tiampo, K. F., & Ancochea, E. (2022). Shallow magmatic intrusion evolution below La Palma before and during the 2021 eruption. *Scientific Reports*, *12*(1), 20257. https://doi.org/10.1038/s41598-022-23998-w

Ferretti, A., Fumagalli, A., Novali, F., Prati, C., Rocca, F., & Rucci, A. (2011). A New Algorithm for Processing Interferometric Data-Stacks: SqueeSAR. *IEEE Transactions on Geoscience and Remote Sensing*, *49*(9), 3460-3470. https://doi.org/10.1109/TGRS.2011.2124465

Ferretti, A., Monti-Guarnieri, Prati, C., & Rocca, F. (2007). *InSAR Principles: Guidelines for SAR Interferometry Processing and Interpretation*. Karen Fletcher.

Figueroa-Miranda, S., Tuxpan-Vargas, J., Ramos-Leal, J. A., Hernández-Madrigal, V. M., & Villaseñor-Reyes, C. I. (2018). Land subsidence by groundwater over-exploitation from aquifers in tectonic valleys of Central Mexico: A review. *Engineering Geology*, *246*, 91-106. https://doi.org/10.1016/j.enggeo.2018.09.023

Foroughnia, F., Nemati, S., Maghsoudi, Y., & Perissin, D. (2019). An iterative PS-InSAR method for the analysis of large spatio-temporal baseline data stacks for land subsidence estimation. *International Journal of Applied Earth Observation and Geoinformation*, *74*, 248-258. https://doi.org/10.1016/j.jag.2018.09.018

Foumelis, M., Delgado Blasco, J. M., Yves-Louis, D., Engdahl, M., Fernández, D., Veci, L., Lu, J., & Wong, C. (2018). *ESA SNAP-STAMPS Integrated processing for sentinel-1 Persistent Scaterrer Interferometry*. IGARSS. https://doi.org/978-1-5386-7150-4

Galloway, D. L., & Hoffmann, J. (2007). The application of satellite differential SAR interferometry-derived ground displacements in hydrogeology. *Hydrogeology Journal*, *15*(1), 133-154. https://doi.org/10.1007/s10040-006-0121-5

Gamboa, C. J. G., Benito, M. B., & Flores, O. (2023). *Characterization of probable seismic scenarios and analysis of the structural response of the University of San Carlos of Guatemala, Guatemala*. https://doi.org/10.21203/rs.3.rs-2574589/v1

García, Ó., & Kestller, C. (2022, septiembre 18). Vecinos de la zona 7 de San Miguel Petapa alertan sobre formación de grietas en casas y calles. *Noticias Nacionales en Guatevisión*. https://www.guatevision.com/nacionales/vecinos-de-la-zona-7-de-san-miguel-petapa-alertan-sobre-formacion-de-grietas-en-casas-y-calles-breaking

García-Lanchares, C., Marchamalo-Sacristán, M., Fernández-Landa, A., Sancho, C., Krishnakumar, V., & Benito, B. (2023). Analysis of Deformation Dynamics in Guatemala City Metropolitan Area Using Persistent Scatterer Interferometry. *Remote Sensing*, *15*(17), 4207. https://doi.org/10.3390/rs15174207

Gleeson, T., VanderSteen, J., Sophocleous, M. A., Taniguchi, M., Alley, W. M., Allen, D. M., & Zhou, Y. (2010). Groundwater sustainability strategies. *Nature Geoscience*, *3*(6), 378-379. https://doi.org/10.1038/ngeo881

Goel, K. (2014). *Advanced Stacking Techniques and Applications in High Resolution SAR Interferometry*.

Grenerczy, G., & Wegmüller, U. (2011). Persistent scatterer interferometry analysis of the embankment failure of a red mud reservoir using ENVISAT ASAR data. *Natural Hazards*, *59*(2), 1047-1053. https://doi.org/10.1007/s11069-011-9816-6

Guarnieri, A. M., & Prati, C. (1996). ScanSAR focusing and interferometry. *IEEE Transactions on Geoscience and Remote Sensing*, *34*(4), 1029-1038. https://doi.org/10.1109/36.508420

Guzmán Ramírez, E. (2002). *Estudio geológico-geotécnico de la susceptibilidad de deslizamientos en la colonia El Carmen zona 12 de la ciudad de Guatemala* [Tesis de Grado]. San Carlos de Gautemala.

Hanssen, R. (1996, septiembre 30). A first quantitative evaluation of atmospheric effects on SAR interferometry. *03/1997*. Fringe 96, Zurich.

Hanssen, R. (2023, noviembre 10). *A new perspective on InSAR Quality Assurance and Quality Control: Double-A and triple-A products*. SARWatch Symposium, Porto.

Hermosilla, R. G. (2012). The Guatemala City sinkhole collapses. *Carbonates and Evaporites*, *27*(2), 103-107. https://doi.org/10.1007/s13146-011-0074-1

Herrera, I. R., & Orozco, E. O. (2010). *Hidrogeología de Ojo de Agua, cuenca sur de la ciudad de Guatemala*. *42*, 85-98.

Herrera Ibáñez, I. R., & Barrientos, D. (2016). *Estudio hidrogeológico de los acuíferos volcánicos de la República de Guatemala*. 121.

Herrera Ibáñez, I. R., & Brown Manrique, Ó. (2011). *Propuesta de una metodología para la estimación de áreas de recarga hídrica en Guatemala*. *20*(4), 48-52. Universidad Agraria de la habana Fructuoso Rodríguez Pérez.

Herrera Ibáñez, I. rodolfo. (2018). Sobreextracción de las aguas subterráneas en la cuenca norte de la ciudad de Guatemala. *Revista Científica de la Facultad de Agronomía Universidad de San Carlos de Guatemala*, *XXXVI*(2). http://cete.fausac.gt/wp-content/uploads/2018/10/TIKALIA-2-2018.pdf

Hooper, A., Zebker, H., Segall, P., & Kampes, B. (2004). A new method for measuring deformation on volcanoes and other natural terrains using InSAR persistent scatterers. *Geophysical Research Letters*, *31*(23). https://doi.org/10.1029/2004GL021737

Hu, J., Shi, B., Inyang, H. I., Chen, J., & Sui, Z. (2009). Patterns of subsidence in the lower Yangtze Delta of China: The case of the Suzhou-Wuxi-Changzhou Region. *Environmental Monitoring and Assessment*, *153*(1-4), 61-72. https://doi.org/10.1007/s10661-008-0336-0

Instituto Nacional de Estadística Guatemala. (2019). *XII Censo Nacional de población y VII de vivienda*. INE.

Japanase Aerospace Exploration Agency. (2023). *JAXA7 METI ALOS PALSAR L1.0* (L1.0 2007) [Map]. JAXA; ASF DAAC. https://asf.alaska.edu/data-sets/

Jenks, G. F. (1989). Geographic Logic In Line Generalization. *Cartographica: The International Journal for Geographic Information and Geovisualization*, *26*(1), 27-42. https://doi.org/10.3138/L426-1756-7052-536K

Jenks, G. F., & Caspall, F. C. (1971). Error on choroplethic maps: Definition, measurement, reduction. *Annals of the Association of American Geographers*, *61*(2), 217-244. https://doi.org/10.1111/j.1467-8306.1971.tb00779.x

JICA (Agencia de Cooperación Internacional del Japón). (1986). *Informe Final del estudio de Factibilidad Para el Desarrollo del Proyecto de Agua Subterránea*

(Para emergencia I) (8; p. 259). EMPAGUA (Empresa municipal de agua de la ciudad de Guatemala).

Joyce, K. E., Belliss, S. E., Samsonov, S. V., McNeill, S. J., & Glassey, P. J. (2009). A review of the status of satellite remote sensing and image processing techniques for mapping natural hazards and disasters. *Progress in Physical Geography: Earth and Environment*, *33*(2), 183-207. https://doi.org/10.1177/0309133309339563

Kääb, A., Huggel, C., Fischer, L., Guex, S., Paul, F., Roer, I., Salzmann, N., Schlaefli, S., Schmutz, K., Schneider, D., Strozzi, T., & Weidmann, Y. (2005). Remote sensing of glacier- and permafrost-related hazards in high mountains: An overview. *Natural Hazards and Earth System Sciences*, *5*(4), 527-554. https://doi.org/10.5194/nhess-5-527-2005

Kim, Y. C., Kim, D. jin, & Jung, J. (2019). Monitoring Land Subsidence in Guatemala City Using Time-Series Interferometry. *IGARSS 2019 - 2019 IEEE International Geoscience and Remote Sensing Symposium*, 2099-2102. https://doi.org/10.1109/IGARSS.2019.8899774

Koch, A. J., & McLean, H. G. (1981). *Mapa geológico Hoja 2060 II* (1ra ed.) [Map]. Instituto Geográfico Nacional.

Koudogbo, F. N., Duro, J., Arnaud, A., Bally, P., Abidin, H. Z., & Andreas, H. (2012). *Combined X- and L-band PSI analyses for assessment of land subsidence in Jakarta* (C. M. U. Neale & A. Maltese, Eds.). SPIE. https://doi.org/10.1117/12.974821

Kratzsch, H. (1983). *Mining Subsidence Engineering*. Springer Berlin Heidelberg. https://doi.org/10.1007/978-3-642-81923-0

Kwag, Y. K. (2013). *Spaceborne synthetic aperture radar in Korea*.

Lanari, R., Mora, O., Manunta, M., Mallorqui, J. J., Berardino, P., & Sansosti, E. (2004). A small-baseline approach for investigating deformations on full-resolution differential SAR interferograms. *IEEE Transactions on Geoscience and Remote Sensing*, *42*(7), 1377-1386. https://doi.org/10.1109/TGRS.2004.828196

Lang, D. H., Sergio, M., Crempien, J., & Erduran, E. (2009). *Reducción de Resgo Sísmico en Guatemala, El Salvador y Nicaragua con Cooperación regional a Honduras, Cota Rica y Panamá*.

Lawrence, B. N., Bennett, V. L., Churchill, J., Juckes, M., Kershaw, P., Pascoe, S., Pepler, S., Pritchard, M., & Stephens, A. (2013). Storing and manipulating environmental big data with JASMIN. *2013 IEEE International Conference on Big Data*, 68-75. https://doi.org/10.1109/BigData.2013.6691556

Lazecky, M., Bakon, M., Sousa, J. J., Perissin, D., Hlavacova, I., Patricio, G., Papco, J., Rapant, P., & Real, N. (2015, mayo 1). Potential of Multi-temporal InSAR Techniques for Structural Health Monitoring. *Proceedings of Fringe 2015: Advances in the Science and Applications of SAR Interferometry and Sentinel-1 InSAR Workshop*. Fringe2015: Advances in the Science and Applications of SAR Interferometry and Sentinel-1 InSAR Workshop. https://doi.org/10.5270/Fringe2015.pp324

Mancini, F., Grassi, F., & Cenni, N. (2021). A Workflow Based on SNAP–StaMPS Open-Source Tools and GNSS Data for PSI-Based Ground Deformation Using Dual-Orbit Sentinel-1 Data: Accuracy Assessment with Error Propagation Analysis. *Remote Sensing*, *13*(4), 753. https://doi.org/10.3390/rs13040753

Mårtensson, U. (2024). *Introduction to Remote Sensing and Geographical Information Systems*. Department of Physical Geography and Ecosystems Sciences Lund University. https://www.nateko.lu.se/sites/nateko.lu.se.sv/files/remote_sensing_and_gis_20111212.pdf

Massonnet, D., & Feigl, K. L. (1998). Radar interferometry and its application to changes in the Earth's surface. *Reviews of Geophysics*, *36*(4), 441-500. https://doi.org/10.1029/97RG03139

Mora, O., Mallorqui, J. J., & Broquetas, A. (2003). Linear and nonlinear terrain deformation maps from a reduced set of interferometric sar images. *IEEE Transactions on Geoscience and Remote Sensing*, *41*(10), 2243-2253. https://doi.org/10.1109/TGRS.2003.814657

Morales, J. I. (2012). *Evaluación del descenso del nivel freático en la parte norte del acuífero motropolitano en el valle de Guatemala* [San Carlos de Guatemala]. https://revistas.usac.edu.gt/index.php/asa/article/view/1487

Moreira, A. (2014). A golden age for spaceborne SAR systems. *2014 20th International Conference on Microwaves, Radar and Wireless*

Communications (MIKON), 1-4. https://doi.org/10.1109/MIKON.2014.6899903

Morishita, Y., Lazecky, M., Wright, T., Weiss, J., Elliott, J., & Hooper, A. (2020). LiCSBAS: An Open-Source InSAR Time Series Analysis Package Integrated with the LiCSAR Automated Sentinel-1 InSAR Processor. *Remote Sensing*, *12*(3), 424. https://doi.org/10.3390/rs12030424

Navarro-Hernández, M. I., Tomás, R., Valdes-Abellan, J., Bru, G., Ezquerro, P., Guardiola-Albert, C., Elçi, A., Batkan, E. A., Caylak, B., Ören, A. H., Meisina, C., Pedretti, L., & Rygus, M. (2023). Monitoring land subsidence induced by tectonic activity and groundwater extraction in the eastern Gediz River Basin (Türkiye) using Sentinel-1 observations. *Engineering Geology*, *327*, 107343. https://doi.org/10.1016/j.enggeo.2023.107343

NEHRP (National earthquacquake Hazards Reduction Program) Recommended Seismic Provisions for New Building and Other Structures (FEMA P-2082-1), volume I: Part 1 Provisions and Part 2 Commentary. (2020). Building Seismic Safety Council.

Normand, J. C. L., & Heggy, E. (2015). InSAR Assessment of Surface Deformations in Urban Coastal Terrains Associated With Groundwater Dynamics. *IEEE Transactions on Geoscience and Remote Sensing*, *53*(12), 6356-6371. https://doi.org/10.1109/TGRS.2015.2437368

Oliver, M. A., & Webster, R. (1990). Kriging: A method of interpolation for geographical information systems. *International Journal of Geographical Information Systems*, *4*(3), 313-332. https://doi.org/10.1080/02693799008941549

Osmanoğlu, B., Dixon, T. H., Wdowinski, S., Cabral-Cano, E., & Jiang, Y. (2011). Mexico City subsidence observed with persistent scatterer InSAR. *International Journal of Applied Earth Observation and Geoinformation*, *13*(1), 1-12. https://doi.org/10.1016/j.jag.2010.05.009

Oštir, K., Veljanovski, T., Podobnikar, T., & Stančič, Z. (2003). Application of satellite remote sensing in natural hazard management: The Mount Mangart landslide case study. *International Journal of Remote Sensing*, *24*(20), 3983-4002. https://doi.org/10.1080/0143116031000103826

Patruno, J. (2024). *Polarimetric RADARSAT-2 and ALOS PALSAR multi-frequency analysis over the archaeological site of Gebel Barkal (Sudan)*.

https://www.researchgate.net/publication/280792916_Polarimetric_RADARSAT-2_and_ALOS_PALSAR_multi-frequency_analysis_over_the_archaeological_site_of_Gebel_Barkal_Sudan

Pearson, K. (1896). *Mathematical Contribution to the Theory of Evolution.-III regression, Heredity, and Panmixia*.

Pérez, C. L. (2009). Estructura geológica del Valle de la Ciudad de Guatemala interpretada mediante un modelo de cuenca por distensión. *Revista Geológica de América Central*, *41*. https://doi.org/10.15517/rgac.v0i41.4179

Pesaresi, P., & Politis, P. (2022). GHS-BUILT-C R2022A - GHS Settlement Characteristics. *European Commission, Joint Research Centre (JRC) [Dataset]*. https://doi.org/10.2905/DDE11594-2A66-4C1B-9A19-821382AED36E

Plank, S., Shevchenko, A. V., d'Angelo, P., Gstaiger, V., González, P. J., Cesca, S., Martinis, S., & Walter, T. R. (2023). Combining thermal, tri-stereo optical and bi-static InSAR satellite imagery for lava volume estimates: The 2021 Cumbre Vieja eruption, La Palma. *Scientific Reports*, *13*(1), 2057. https://doi.org/10.1038/s41598-023-29061-6

Portela Fernández, J. J., Staller Vázquez, A., & Béjar Pizarro, M. (2020). *Cortical deformation in the Aguacaliente-Navarro fault system (Central Valley, Costa Rica) from Geodetic data (GNSS and InSAR)* [Other]. oral. https://doi.org/10.5194/egusphere-egu2020-12015

Putri, R. F., Bayuaji, L., Sri Sumantyo, J. T., & Kuze, H. (2013). Terrasar-X DInSAR for land deformation detection in Jakarta urban area, Indonesia. *Journal of Urban and Environmental Engineering*, 195-205. https://doi.org/10.4090/juee.2013.v7n2.195205

Radutu, A., Nedelcu, I., & Gogu, C. R. (2017). An overview of ground surface displacements generated by groundwater dynamics, revealed by InSAR techniques. *Procedia Engineering*, *209*, 119-126. https://doi.org/10.1016/j.proeng.2017.11.137

Recinos, I. N., Paiz, L. V., Fallas, W., & Barales Cabrera, L. E. (2019). *Análisis piezométricos de pozos de agua para los municipios de la mancomunidad Gran Ciudad del Sur:Amatitlán, Mixco, San Miguel Petapa, Santa Catarina Pinula, Villa canales y Villa Nueva, Guatemala*. Fundación para la

Conservación del Agua en la Región Metropolitana de Guatemala (FUCAGUA), Guatemala.

Ritchie, A. W. (1977). *Mapa geológico Hoja 2160 III* (1ra ed.) [Map]. Instituto Geográfico Nacional.

Römer, H., Willroth, P., Kaiser, G., Vafeidis, A. T., Ludwig, R., Sterr, H., & Revilla Diez, J. (2012). Potential of remote sensing techniques for tsunami hazard and vulnerability analysis – a case study from Phang-Nga province, Thailand. *Natural Hazards and Earth System Sciences*, *12*(6), 2103-2126. https://doi.org/10.5194/nhess-12-2103-2012

Rosen, P. A., Hensley, S., Joughin, I. R., Li, F. K., Madsen, S. N., Rodriguez, E., & Goldstein, R. M. (2000). Synthetic aperture radar interferometry. *Proceedings of the IEEE*, *88*(3), 333-382. https://doi.org/10.1109/5.838084

Ruiz-Armenteros, A. M., Marchamalo-Sacristán, M., Lamas-Fernández, F., Hernández Cabezudo, Á., Delgado-Blasco, J. M., Bakon, M., Lazecky, M., Perissin, D., Papco, J., Mesa-Mingorance, J. L., Pachecho, A. da P., Jurado, J. M., & Sousa, J. (2023, julio 20). *Utilizing the land monitoring copernicus program as a regular method for observing dams, large ponds and surrounding areas*. International Geoscience and Remote Sensing Symposium(IGARSS), Pasadena (California).

Sadeghi, Z., Wright, T. J., Hooper, A. J., Jordan, C., Novellino, A., Bateson, L., & Biggs, J. (2021). Benchmarking and inter-comparison of Sentinel-1 InSAR velocities and time series. *Remote Sensing of Environment*, *256*, 112306. https://doi.org/10.1016/j.rse.2021.112306

Samieie-Esfahany, S., Hanssen, R. F., van Thienen-Visser, K., & Muntendam-Bos, A. (2009). On the effect of horizontal deformation on InSAR subsidence estimates. *ESA SP-677, March 2010*, 7.

Samsonov, S., d'Oreye, N., & Smets, B. (2013). Ground deformation associated with post-mining activity at the French–German border revealed by novel InSAR time series method. *International Journal of Applied Earth Observation and Geoinformation*, *23*, 142-154. https://doi.org/10.1016/j.jag.2012.12.008

Sang-Wan, K. (2010). *A Comparison of InSAR Techniques for Deformation Monitoring using Multi-temporal SAR*. *26*(2), 143-151.

Sharp, R. P., & Nobles, L. H. (1953). Mudflow of 1941 at Writghtwood, Southern California. *Geological Society of America Bulletin*, *64*(5), 547. https://doi.org/10.1130/0016-7606(1953)64[547:MOAWSC]2.0.CO;2

Singh Virk, A., Singh, A., & Mittal, S. K. (2018). Advanced MT-InSAR Landslide Monitoring: Methods and Trends. *Journal of Remote Sensing & GIS*, *07*(01). https://doi.org/10.4172/2469-4134.1000225

Sousa, J. J., Hooper, A. J., Hanssen, R. F., & Bastos, L. C. (2010). *Comparative Study of Two Different PS-InSAR Approaches: DEPSI vs. StaMPS*.

Tamayo Duque, J. S., Ruiz-Armenteros, A. M., Ávila Álvarez, G. E., Matiz, G., & Sousa, J. J. (2023). Study of Recent Deformations in the Bogotá Savanna and the City of Bogotá (Colombia) Using Multi-Temporal Satellite Radar Interferometry. *Remote Sensing*, *15*(21), 5249. https://doi.org/10.3390/rs15215249

Tzampoglou, P., Ilia, I., Karalis, K., Tsangaratos, P., Zhao, X., & Chen, W. (2023). Selected Worldwide Cases of Land Subsidence Due to Groundwater Withdrawal. *Water*, *15*(6), 1094. https://doi.org/10.3390/w15061094

UNDRR, A. G. (2015). *Transformar nuestro mundo: La Agenda 2030 para el Desarrollo Sostenible* (Resolución aprobada por la Asamblea General el 25 de Septiembre de 2015 A/RES/70/1; Septuagésimo período de sesiones, p. 40). Naciones Unidas.

UNISDR. (2009). *Terminología sobre reducción del Riesgo de Desastres*. Naciones Unidas. https://www.unisdr.org/files/7817_UNISDRTerminologySpanish.pdf

UNISDR. (2010). Reducción del riesgo de Desastres: Un Instrumento para alcanzar los Objetivos de Desarrollo del Milenio (S. Rodríguez, Egger, Trad.; Union Interparlamentaria). Unión Interparlamentaria.

UNISDR. (2022). *Sendai Framework for Disaster Risk Reduction 2015—2030*. The United Nations Office for Disaster Risk Reduction.

United Nations. (1994). Directrices para la Prevención de los Desastres Naturales, la Preparación para Casos de Desastre y la Mitigación de sus Efectos. *Informe de la Conferencia Mundial sobre la reducción de Riesgos naturales*, 17.

United Stated Geological Survey. (2018). *Seismic event: 11 km E of Nueva Concepción, Guatemala* [Seismic register]. USGS. https://earthquake.usgs.gov/earthquakes/map/

Vaides del Valle, V. D. (1973). *Mapa geológico Hoja 2059 I* (1ra ed.) [Map]. Instituto Geográfico Nacional.

Velásquez, E. (2018). *Estudio Hidrogeológico de los acuíferos aluviales del río Villalobos* (p. 21). EMPAGUA.

Wada, Y., Van Beek, L. P. H., Van Kempen, C. M., Reckman, J. W. T. M., Vasak, S., & Bierkens, M. F. P. (2010). Global depletion of groundwater resources. *Geophysical Research Letters*, *37*(20), 2010GL044571. https://doi.org/10.1029/2010GL044571

Wang, Y., Wang, C., Zhang, H., Dong, Y., & Wei, S. (2019). A SAR Dataset of Ship Detection for Deep Learning under Complex Backgrounds. *Remote Sensing*, *11*(7), 765. https://doi.org/10.3390/rs11070765

Ward, P. J., Blauhut, V., Bloemendaal, N., Daniell, J. E., De Ruiter, M. C., Duncan, M., Emberson, R., Jenkins, S. F., Kirschbaum, D., Kunz, M., Mohr, S., Muis, S., Riddell, G., Schäfer, A., Stanley, T., Veldkamp, T. I. E., & Winsemius, H. C. (2019). *Review article: Natural hazard risk assessments at the global scale* [Preprint]. Risk Assessment, Mitigation and Adaptation Strategies, Socioeconomic and Management Aspects. https://doi.org/10.5194/nhess-2019-403

Werner, C., Wegmuller, U., Strozzi, T., & Wiesmann, A. (2003). Interferometric point target analysis for deformation mapping. *IGARSS 2003. 2003 IEEE International Geoscience and Remote Sensing Symposium. Proceedings (IEEE Cat. No.03CH37477)*, *7*, 4362-4364. https://doi.org/10.1109/IGARSS.2003.1295516

Weyl, R. (1980). *Geology of Central America* (2d completely rev. ed). Gebr. Borntraeger.

Xue, L. (2015). *Investigations of fault zone behavior during earthquake cycles using hydrology and geodesy* [PhD Thesis]. University of California Santa Cruz.

Zebker, H. A., Rosen, P. A., & Hensley, S. (1997). Atmospheric effects in interferometric synthetic aperture radar surface deformation and

topographic maps. *Journal of Geophysical Research: Solid Earth*, *102*(B4), 7547-7563. https://doi.org/10.1029/96JB03804

Zheng, M., Deng, K., Fan, H., & Du, S. (2018). Monitoring and Analysis of Surface Deformation in Mining Area Based on InSAR and GRACE. *Remote Sensing*, *10*(9), 1392. https://doi.org/10.3390/rs10091392

Zhu, L., Gong, H., Li, X., Wang, R., Chen, B., Dai, Z., & Teatini, P. (2015). Land subsidence due to groundwater withdrawal in the northern Beijing plain, China. *Engineering Geology*, *193*, 243-255. https://doi.org/10.1016/j.enggeo.2015.04.020